

# THE BELL SYSTEM TECHNICAL JOURNAL

Volume 47

January 1968

Number 1

Copyright © 1968, American Telephone and Telegraph Company

## An Improved Design of Waveguide Band-Rejection Filters

By H. C. WANG

(Manuscript received August 16, 1967)

*The usual design technique for waveguide band-rejection filters uses narrow-band approximations and thus discrepancies generally exist between the designed and measured response, particularly in the fairly wide passband. Nevertheless, this design technique has been used because of its simplicity and because the filter configurations obtained are relatively simple. Lately, a new design technique using transmission line synthesis became available which, theoretically, would yield the desired response. However, the physical realization results in a complicated configuration which leads to certain practical problems. This paper presents a modified technique which simplifies the structure without sacrificing performance. With this modification the design procedure becomes very simple and many of the practical problems can be avoided. This paper gives precise design information and convenient design formulas. Furthermore, it shows that excellent agreement between the designed and measured response can be achieved.*

### I. INTRODUCTION

The microwave waveguide band-rejection filter (BRF) now used in many radio systems has many undesirable features. The designer finds that the actual bandwidth is consistently narrower than the designed value, and that the filter has a unique passband VSWR behavior which becomes worse as the frequency goes farther away from the

stopband. This becomes quite a severe problem in filters designed for the high frequency or low frequency channels of the band. (For example, in the 4 GHz band,\* the return loss of a filter with the stopband at 3710 MHz becomes progressively poorer as the frequency approaches 4190 MHz, and vice versa). In addition, the midband frequency of the VSWR curve and of the corresponding delay curve is found to differ from the midband frequency of the insertion loss curve at which the filter is tuned. The offset of a typical 3-cavity maximally flat BRF at the 4 GHz band with 3 dB points at  $\pm 17$  MHz can be as much as 2 MHz. Such an uncontrolled shift causes extreme difficulties in the delay equalization of a radio system.

The present BRF design is based on the lumped-element low-pass prototype filter design technique.<sup>1</sup> After making a proper frequency transformation, the loaded  $Q$  of each cavity can be computed. The cavities are then separated by waveguide lengths which give an effective spacing of an odd multiple of quarter wavelengths at the midband frequency, which is a standard technique to realize ladder filters in waveguide. It is desirable to keep the spacings as small as possible, but, in order to avoid higher order mode coupling between cavities, it has been determined that a three-quarter wavelength spacing is required.

In a recent investigation, it was determined that neglecting the frequency-dependent phase shift of the connecting lines results in both the narrower bandwidth and the problem of high VSWR in the passband. A rigorous analysis was carried out for a three-cavity BRF. The result shows that when the frequency dependence of the phase shift of the connecting lines is accounted for, an exact control of bandwidth is possible and the passband VSWR is improved; but the desired characteristic of the passband VSWR cannot be obtained as long as the present form of construction is retained.

Various techniques for the exact synthesis of transmission line filters have been available for many years.<sup>2</sup> However, they often are found to be not too practical for the design of waveguide filters because of the large number of changes of characteristic impedances usually required. There is already a sufficiently large number of discontinuities in a waveguide filter which are necessary to form the cavities. Additional discontinuities with their associated fringing susceptances, such as would be needed to change the characteristic impedance, would aggravate the practical realization difficulties. If these problems

---

\* 3.7 GHz to 4.2 GHz

could be overcome, the transmission line synthesis would offer the advantage of being exact.

The possibility of constructing a waveguide BRF using transmission line synthesis was mentioned by Schiffman and Matthaei.<sup>3</sup> Unfortunately, the form they suggest involves three impedance changes in each connecting line and therefore is not practical. This paper presents an improved form with only one impedance change in each connecting line. The susceptance discontinuity present at each impedance change is absorbed very naturally in the structure without causing any design difficulty. Design formulas for filters of up to five cavities are given in a very convenient form.

The problem of the midband frequency shift between the VSWR and the insertion loss was found to be the direct consequence of inaccurate correction for the connecting lines. The precise design procedure presented here guarantees the coincidence of the midband frequency of the VSWR and insertion loss characteristic.

An experimental model was built and tested, and the measured result agrees very well with the theoretical prediction. With this design technique, it is possible to achieve over 40 dB return loss across the passband and to control the exact bandwidth and the midband frequency. A pair of identical BRF were designed and in conjunction with two hybrids, a constant resistance channel separation network was built. Over 35 dB return loss across the band was observed; in addition, the delay distortion of the dropped channel was symmetrical with respect to the midband frequency. Channel separation networks built with BRFs designed with the old techniques always had unsymmetrical delay distortion for the dropped channel.

## II. BRF CONFIGURATIONS OBTAINED BY TRANSMISSION LINE FILTER SYNTHESIS

The easiest way to synthesize a transmission line filter is to use the known low-pass prototype filters as done by Schiffman and Matthaei.<sup>3</sup> The reactive elements of the prototype circuit are replaced by their equivalent transmission line stubs (all of the same length  $l$  and of the same propagation constant  $\beta$ ) using the frequency transformation:

$$\omega = A \tan \beta l \quad (1)$$

where  $\omega$  is the normalized frequency of the prototype circuit and  $A$  is a constant that determines the bandwidth of the filter. For a BRF,  $l$

can be chosen to be any odd multiple of a quarter wavelength of the midband frequency. Schiffman and Matthaei chose  $l = \lambda_{g0}/4$ . Then, the shunt susceptances and series reactances of the prototype filter transform as follows:

$$\omega C_i = C_i A \tan\left(\frac{\pi \lambda_{g0}}{2 \lambda_g}\right). \quad (2)$$

$$\omega L_i = L_i A \tan\left(\frac{\pi \lambda_{g0}}{2 \lambda_g}\right). \quad (3)$$

It is seen that the right side of (2) corresponds to the input susceptance of an open-circuited stub of characteristic admittance

$$Y_i = C_i A$$

and that the right side of (3) corresponds to the input reactance of a short-circuited stub of characteristic impedance

$$Z_i = L_i A.$$

As shown in Fig. 1, a three-element low-pass prototype filter becomes a transmission line with three stubs using the transformation (1). These stubs are connected to the main transmission line at the same point, which would be impossible in a physical realization. To solve this problem, connecting lines between stubs have to be inserted by making use of Kuroda's identity. This identity allows the inter-

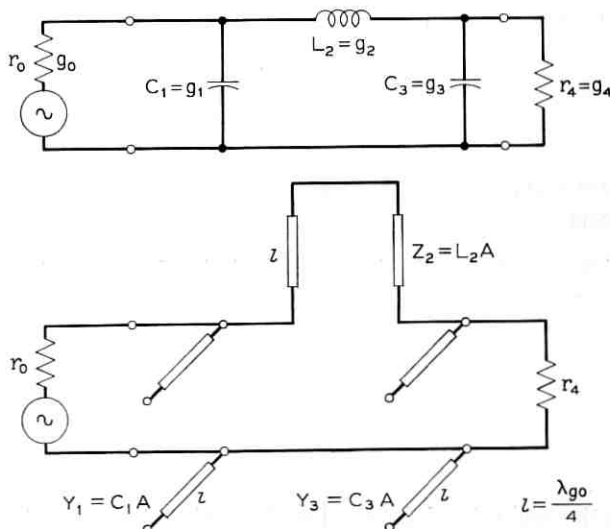


Fig. 1—The 3 element low pass prototype filter and its corresponding BRF with transmission line stubs.

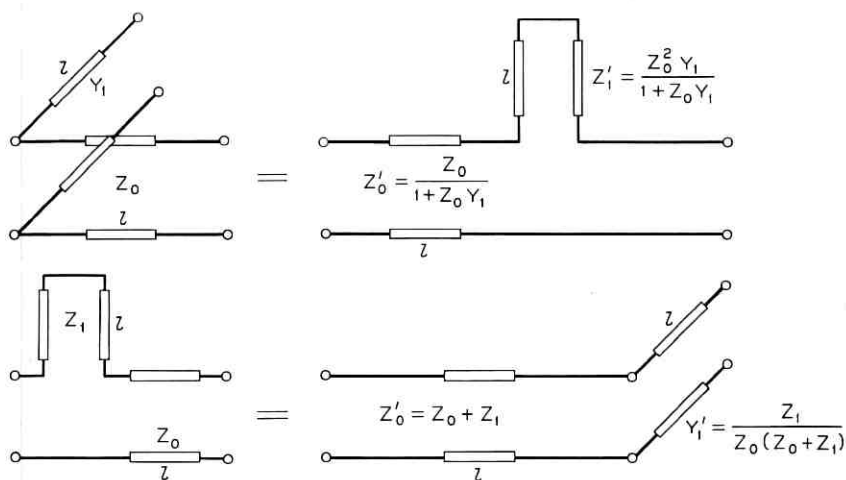


Fig. 2 — Kuroda's identity in transmission line form.

change of a stub and a connecting line (both of the same length  $l$ ) as shown in Fig. 2. Adding a section of transmission line of appropriate characteristic impedance on both ends of the filter (Fig. 1) as shown in Fig. 3(a), the circuit retains its amplitude response. Applying Kuroda's identity to the two shunt open-circuited stubs, one gets the desired form in Fig. 3(b). With a proper replacement of the three series stubs by rejection cavities (only an approximation), Fig. 3(b) forms three rejection cavities in cascade with quarter wavelength lines separation between the cavities.

For the most commonly used aperture-coupled rejection cavity, a quarter wavelength separation between the cavities would not be enough because of strong coupling resulting from higher order modes between the closely spaced discontinuities. It has been found, from past experience, that a three-quarter wavelength separation is necessary in most waveguide BRFs. For this reason, Schiffman and Matthaei treated the case of three-quarter wavelength separation between cavities. Following exactly the same technique as shown in Fig. 3, one can add three pieces of quarter wavelength line on both sides of the stubs, as seen in Fig. 4(a), without changing the amplitude response of the filter. Then, the final form of Fig. 4b is obtained by applying Kuroda's identity three times on each side. The characteristic impedances of the connecting line sections are tabulated for two and three cavity BRF,<sup>3</sup> but no test result has been given in the same reference.

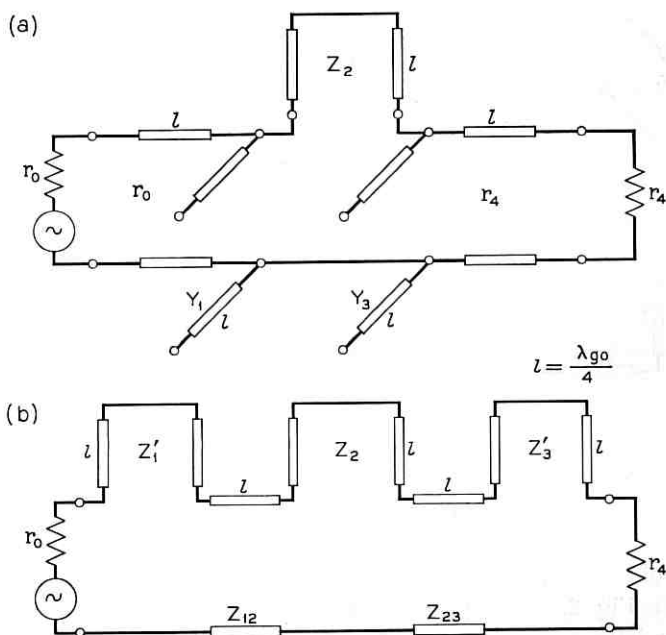


Fig. 3 — Practical realization of 3 stub transmission line BRF.

To realize the configuration of Fig. 4(b) in waveguide form, one would, usually, change the height to control the characteristic impedance such that the propagation constant  $\beta$  remains unchanged. A typical three cavity BRF would therefore assume the form shown in Fig. 5. Theoretically, one may be able to compensate for the discontinuity susceptances at each step by proper adjustment of the line length of each section. This, however, complicates the design procedure unduly, and it is not sure how good the result may be. As mentioned before, the higher order mode interaction between closely spaced discontinuities may degrade the performance of the filter. Since a better configuration, in every respect, is being proposed, no attention was paid to the practical problems associated with this suggested structure.

### III. PROPOSED NEW BRF CONFIGURATION

The only restriction which must be fulfilled in presently-available transmission line synthesis is that all the line sections must have the same length  $l$  and the same propagation constant  $\beta$  so that the frequency transformation (1) can be applied. To construct a BRF, one

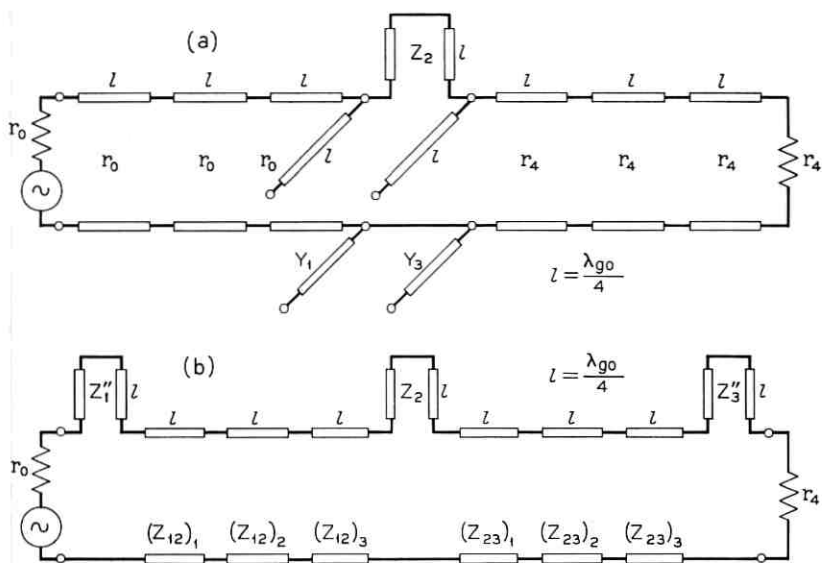


Fig. 4—Suggested 3 stub transmission line BRF to be realized in waveguide form.

may choose the length  $l$  to be any odd number of quarter wavelength of the midband frequency. For the waveguide BRF, it is convenient to choose  $l = 3\lambda_{g0}/4$ . Then the shunt susceptance and series reactance of the filter become

$$\omega C_i = C_i A \tan \left( \frac{3\pi}{2} \frac{\lambda_{g0}}{\lambda_g} \right) \quad (4)$$

$$\omega L_i = L_i A \tan \left( \frac{3\pi}{2} \frac{\lambda_{g0}}{\lambda_g} \right) \quad (5)$$

and the equivalence between prototype circuit and the transmission line stubs shown in Fig. 1 still holds except that the constant  $A$  is

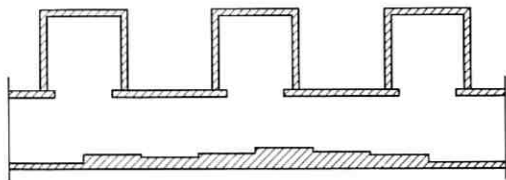


Fig. 5—Complicated form of a 3 cavity waveguide BRF.

changed due to the change of stub length  $l$ . The value of  $A$  may be computed from the given band edge attenuation specification; for example, from the 3 dB point for maximally flat filters or from the cutoff frequency for equal ripple filters. Let  $\omega_1$  be the edge frequency of the prototype filter and  $\lambda_{g1}$  be the corresponding waveguide wavelength, then

$$A = \omega_1 \cot \left( \frac{3\pi}{2} \frac{\lambda_{g0}}{\lambda_{g1}} \right). \quad (6)$$

After obtaining the characteristic impedances of all the stubs, one can apply Kuroda's identity to get the same form as Fig. 3(b), of course with  $l = 3\lambda_{g0}/4$ . This is almost the desired form for waveguide BRF except that the series stubs have to be replaced by cavities with the proper  $Q$  values. There are many ways to find the equivalence between stubs and cavities, all of which are approximations. Among them, one method is found to be particularly convenient. The input impedance of a short-circuited stub of  $3\lambda_{g0}/4$  length with characteristic impedance  $Z_0$  is

$$Z_{in} = jZ_0 \tan \left( \frac{3\pi}{2} \frac{\lambda_{g0}}{\lambda_g} \right) \quad (7)$$

By the well known partial fraction expansion of the tangent function, one gets:

$$Z_{in} = jZ_0 \frac{4}{\pi} \left( \frac{3\lambda_{g0}}{\lambda_g} \right) \sum_{k=1}^{\infty} \frac{1}{(2k-1)^2 - \left( \frac{3\lambda_{g0}}{\lambda_g} \right)^2} \quad (8)$$

In the vicinity of the resonance frequency ( $\lambda_{g0}/\lambda_g \approx 1$ ), it is clear that the  $k = 2$  term dominates (8). Then:

$$Z_{in} = jZ_0 \frac{4}{3\pi} \left[ \frac{\lambda_g}{\lambda_{g0}} - \frac{\lambda_{g0}}{\lambda_g} \right]^{-1} + \dots \quad (9)$$

Taking this approximation, it is clear that the equivalent cavity must possess a loaded  $Q$  of

$$Q_{\text{loaded}} = \frac{3\pi}{2Z_0}. \quad (10)$$

This approximation is found to be sufficiently accurate for frequencies close to the resonance frequency as is the case for most waveguide filters.

Most of the advantages of this new configuration are obvious. As seen in Fig. 6, a three-to-one reduction in the number of steps is

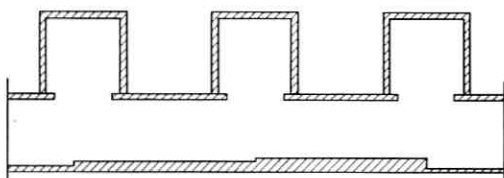


Fig. 6 — Improved form of a 3 cavity waveguide BRF.

obtained, which makes the design procedure much simpler. In addition, the spacing between discontinuities has become large, hence, one would expect less practical problems in realization (because of higher order mode interaction). One rather subtle practical advantage of this structure is that all the steps are located right under the center of the coupling apertures. For all inductive coupling apertures (the circular hole is one of them), a capacitive compensating stud is always required at the location of the hole, which in this structure happens to coincide with the location of the steps. Because of the capacitive step susceptance, the size of the compensating studs just has to be made slightly smaller. No additional compensation is needed for all the step susceptances.

#### IV. DESIGN INFORMATION

A convenient table for filters with two to five cavities is presented in this section which gives the  $Q$  values for each cavity and the characteristic impedance for each connecting line. The following symbols are used:

$n$  = number of cavities

$R_g$  = normalized generator impedance

$R_l$  = normalized load impedance

$Q_i$  = loaded  $Q$  value of  $i$ th cavity

$g_i$  = normalized values of the low pass prototype filter

$Z_{i,i+1}$  = normalized characteristic impedance of the connecting line between the  $i$ th and the  $(i + 1)$ th cavity

$A$  = bandwidth constant defined in (6)

$n = 2$

$$Q_1 = \frac{3\pi}{2R_g} \left( 1 + \frac{1}{Ag_0g_1} \right) \quad Z_{12} = R_g(1 + Ag_0g_1)^{-1}$$

$$Q_2 = \frac{3\pi}{2R_g} \frac{g_0}{Ag_2} \quad R_l = R_g \frac{1}{g_0g_3}$$

$n = 3$

$Q_1, Q_2, Z_{12}$  : same as  $n = 2$

$$Q_3 = \frac{3\pi g_0}{2R_v g_4} \left( 1 + \frac{1}{A g_3 g_4} \right) \quad Z_{23} = R_v \frac{g_4}{g_0} (1 + A g_3 g_4)^{-1}$$

$$R_l = R_v \frac{g_4}{g_0}$$

$n = 4$

$$Q_1 = \frac{3\pi}{2R_v} \left( 2 + \frac{1}{A g_0 g_1} \right) \quad Z_{12} = R_v \left( \frac{1 + A g_0 g_1}{1 + 2A g_0 g_1} \right)$$

$$Q_2 = \frac{3\pi}{2R_v} \left( \frac{1}{1 + A g_0 g_1} + \frac{g_0}{A g_2 (1 + A g_0 g_1)^2} \right)$$

$$Z_{23} = R_v g_0 \left( A g_2 + \frac{g_0}{1 + A g_0 g_1} \right)^{-1}$$

$$Q_3 = \frac{3\pi}{2R_v} \frac{1}{A g_0 g_3} \quad Z_{34} = R_v g_0 g_5 (1 + A g_4 g_5)^{-1}$$

$$Q_4 = \frac{3\pi}{2R_v} \frac{1}{g_0 g_5} \left( 1 + \frac{1}{A g_4 g_5} \right) \quad R_l = R_v g_0 g_5$$

$n = 5$

$Q_1, Q_2, Q_3, Z_{12}, Z_{23}$  : same as  $n = 4$

$$Q_4 = \frac{3\pi}{2R_v g_0} \left( \frac{1}{1 + A g_5 g_6} + \frac{g_6}{A g_4 (1 + A g_5 g_6)^2} \right),$$

$$Z_{34} = R_v g_0 \left( A g_4 + \frac{g_6}{1 + A g_5 g_6} \right)^{-1}$$

$$Q_5 = \frac{3\pi}{2R_v} \frac{g_6}{g_0} \left( 2 + \frac{1}{A g_5 g_6} \right) \quad Z_{45} = R_v \frac{g_0}{g_6} \left( \frac{1 + A g_5 g_6}{1 + 2A g_5 g_6} \right)$$

$$R_l = R_v \frac{g_0}{g_6}$$

To construct connecting lines for a given characteristic impedance, one may modify the heights  $b_i$  of waveguides according to

$$\frac{Z_1}{Z_2} = \frac{b_1}{b_2}. \quad (11)$$

Information on cavity design has been available for a long time. A set of curves was plotted of loaded  $Q$  vs aperture size for different

frequencies, of cavity length vs aperture size for different frequencies, and of stud length vs aperture size for different frequencies. Such frequencies were chosen that both the 4 GHz (3.7–4.2) and the 6 GHz (5.925–6.425) bands are covered.

The equivalent circuit of a properly compensated cavity of Fig. 7(a) is known (to the extent of the approximations used here) to be of the form shown in Fig. 7(b) referred to the reference plane  $T$ . Aside

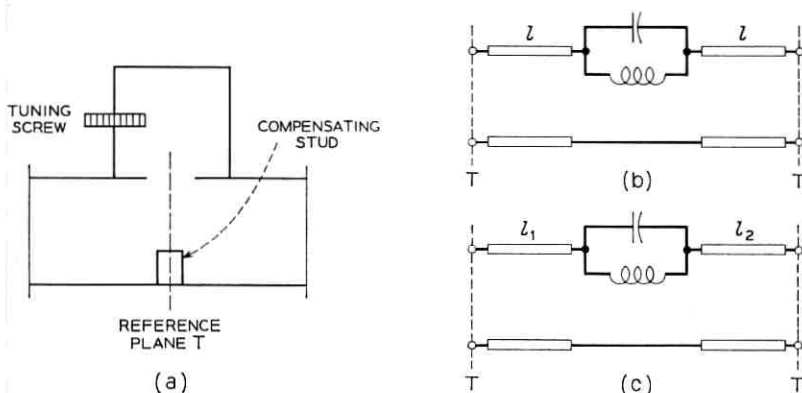


Fig. 7 — Waveguide rejection cavity and its equivalent circuits.

from the resonance circuit, an additional piece of transmission line of length  $l$  must be added at each side, in order to make the connecting line sections exactly  $3\lambda_{g0}/4$  and this line element must be taken into account accurately. It was found that the unpredictable midband frequency shift between VSWR and insertion loss response, which is one of the major problems of the previously designed BRF, is the direct consequence of an inaccurate correction for this line element. A theoretical study showed that any inaccuracy in the length of the connecting line may result in a shift in midband frequency of the VSWR response with respect to the insertion loss response.\* One typical 3-cavity 4 GHz BRF with  $\Delta f_{3dB} = \pm 17$  MHz was found to have a 2 MHz shift with a 35 mil error in each connecting line.

Because of its importance, an attempt was made to measure accurately the values of  $l$  for various sizes of coupling aperture. The first set of data based on the symmetrical equivalent circuit (Fig. 7b) was very disappointing since, for a simple measurement like this, the

\* Dissipation must be taken into account since this phenomenon does not exist in the lossless case.

widely spread measurement data was unexpected. It was found later that the symmetry of the structure is destroyed by the tuning screw on one side of the cavity (Fig. 7a); consequently, the symmetrical equivalent circuit 7(b) is no longer valid.

To make the equivalent circuit unsymmetrical, the circuit in Fig. 7(c), where the transmission lines on each side have different length, is introduced. This does not solve the problem, however, because both the length  $l_1$  and  $l_2$  depend strongly on the amount of tuning added to the cavity. A simple plot of  $l_1$  and  $l_2$  does not make sense unless one could specify a fixed amount of tuning. Fortunately, there is a quantity, mainly  $l_1 + l_2$ , which is very insensitive to the amount of tuning. As measured in the 4 GHz band, this quantity is accurate within a variation of 2 mils for a quite large tuning range. It is believed that this would be true for the other frequency bands, too. Hence, plots of  $(l_1 + l_2)/2$  vs hole diameter are presented in Figs. 8 and 9 for 4 and 6 GHz bands, respectively. For small tuning, it is true that  $l_1 \approx l_2 \approx (l_1 + l_2)/2$ . Furthermore, it was found that  $l_1$ , the length on the tuning screw side, is always larger than  $l_2$ , and that the difference,  $l_1 - l_2$ , may vary from zero to 20 mils depending on the tuning range for the sizes of apertures used in this study.

#### V. EXPERIMENTAL RESULTS

To verify the theoretical work discussed above and the available design data, a 3-cavity BRF was designed. Because of the approxima-

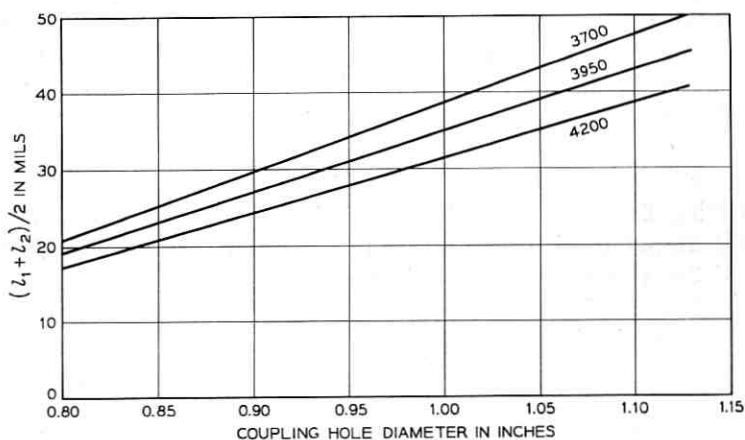


Fig. 8—Measured information on waveguide rejection cavities in the 4 GHz band.

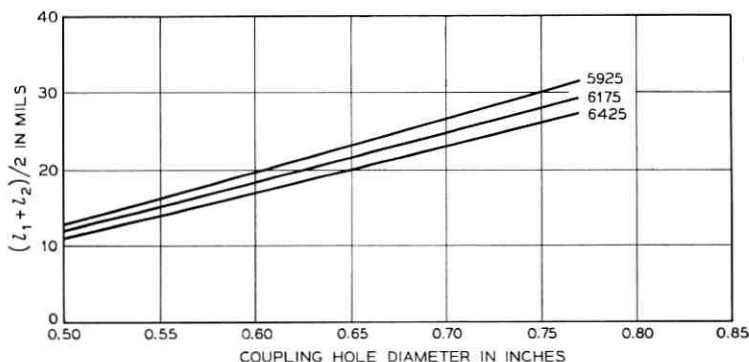


Fig. 9—Measured information on waveguide rejection cavities in the 6 GHz band.

tions involved in the equivalence between cavity and stub line, there might still be deviations from the expected performance at frequencies well removed from the center frequency. Therefore, the filter was purposely designed to operate in the highest frequency channel (4190 MHz) of the 4 GHz band. In this case, the passband extends almost 500 MHz below the midband frequency of the filter. Any severe discrepancy caused by the approximation should show up in this extreme case. The filter was designed to have a maximally flat response with the 3 dB points at  $\pm 17$  MHz, neglecting intrinsic losses. In order to convey some idea of the "exactness" of the filter performance, the measured results are compared with the computed theoretical response. This computed curve is the theoretical response of a transmission line filter of Fig. 3(b) ( $l = 3\lambda_{g0}/4$ ) with all line sections having an attenuation constant:

$$\alpha = 10^{-4} \text{ neper per inch.}$$

As seen in Figs. 10 and 11, the filter shows lower VSWR value in the vicinity of resonant frequency which is attributed to slightly higher intrinsic loss than the theoretical estimated value. However, over 40 dB return loss was obtained across the entire passband which is in very good agreement with the computed results.

Measured data were also taken from a channel-separating network constructed with two identical BRFs and two hybrid junctions. The channel separating network has over 35 dB return loss across the band. The delay distortion of the dropped channel was also measured, and the result shows that the delay distortion vs  $\Delta f$  curve is symmet-

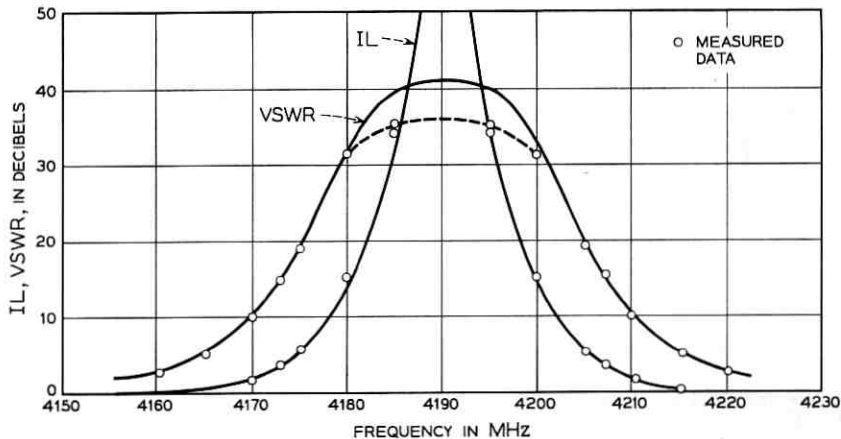


Fig. 10—Computed and measured stop band performance of a typical 3 cavity maximally flat BRF.

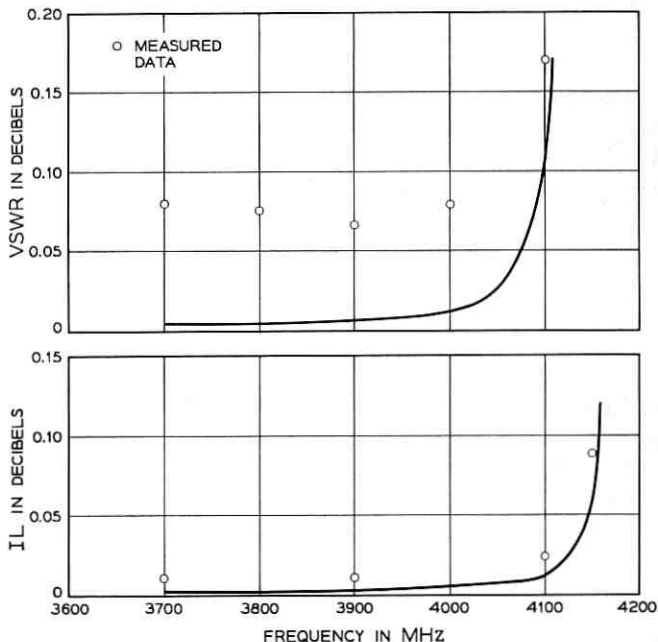


Fig. 11—Computed and measured passband performance of a typical 3 cavity maximally flat BRF

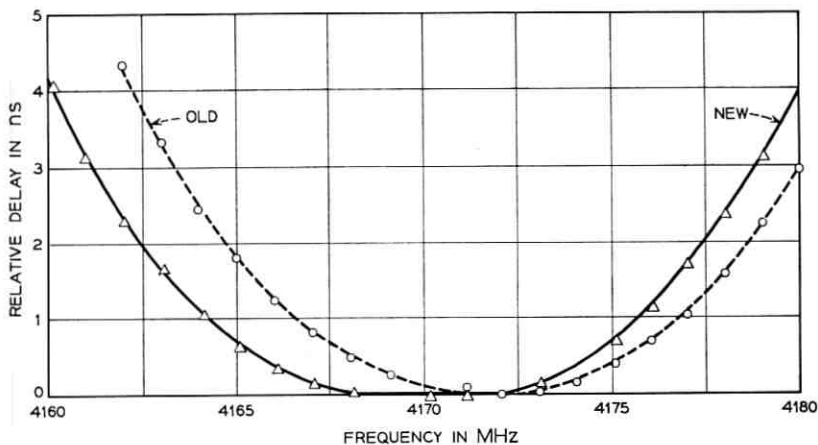


Fig. 12—Measured delay distortion of a channel separation network using present design techniques as compared with that using previous techniques.

rical with respect to the midband frequency. The measured data is shown in Fig. 12 where the delay distortion curve of the present existing channel separating network is plotted for comparison.

#### VI. ACKNOWLEDGMENT

The author wishes to thank F. G. Joyal for carrying out all of the measurements on the correction line lengths and on the filter performance.

#### REFERENCES

1. Young, L., Matthaei, G. L., and Jones, E. M. T., Microwave Bandstop Filters with Narrow Stop Band, *IRE Trans. on Microwave Theory and Techniques*, 10, November 1962, pp. 416-427.
2. For example, see A. I. Grayzel, A Synthesis Procedure for Transmission Line Networks, *IRE Trans. on Circuit Theory*, CT-5, September 1958, pp. 172-181.
3. Schiffman, B. M. and Matthaei, G. L., Exact Design of Bandstop Microwave Filters, *IEEE Trans. on Microwave Theory and Techniques*, 12, January 1964, pp. 6-15.



# Speech Synthesis by Rule: An Acoustic Domain Approach

By LAWRENCE RABINER

(Manuscript received August 30, 1967)

*A new approach to speech synthesis by rule has been formulated and evaluated. A discrete set of symbols (phonemes and stress marks) is converted to a continuous acoustic waveform by a two-step transformation. The first step involves conversion from phonemes to control signals capable of driving a terminal analog speech synthesizer. The second step is conversion from control signals to the acoustic waveform.*

*This paper presents a design for the terminal analog synthesizer and discusses the new features of this device. It discusses in detail the method of converting from phonemes to control signals. It places primary emphasis on determining the formant frequency control signals and the fundamental frequency contour, and presents models for determining these contours from the input data. The paper includes an experimental evaluation of the entire technique in terms of word intelligibility scores and consonant confusion matrices.*

## 1. INTRODUCTION

Speech synthesis by rule is the method of converting from a discrete representation of speech in linguistic units, that is, phonemes and stress marks, to a continuous acoustic waveform. Fig. 1 shows the technique for carrying out this transformation. The figure shows that the discrete input is converted to continuous control signals by the synthesis strategy. The synthesis strategy contains stored information about the phonemes and stored rules about the mutual effects of adjacent phonemes. The stored rules operate on the input sequence to produce the control signals for the synthesizer. The speech synthesizer converts the control signals to continuous speech. The synthesizer may be a terminal analog, a dynamic analog of the vocal tract, or a combination.

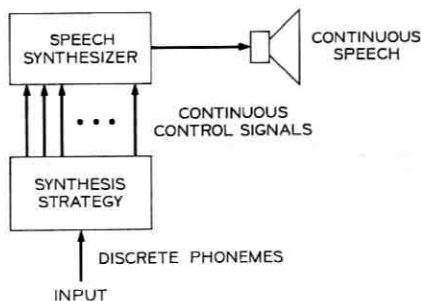


Fig. 1 — Technique of Speech Synthesis.

During the past ten years there have been many attempts at synthesis by rule. The primary goal of these attempts has been to produce natural sounding, intelligible speech. Of secondary importance has been the preservation, in some natural way, of the dynamics of speech production by embodying in the scheme the constraints imposed by the human vocal tract.

Previous methods of synthesis by rule are generally classified as either articulatory or acoustic domain approaches. An articulatory approach uses physiological parameters such as tongue-tip position, and lip opening as the control signals for the synthesizer. The stored data of the synthesis strategy are of the form of vocal tract configurations. An acoustic domain approach uses parameters such as formant values and fundamental frequency as control signals. The stored data include such information as target positions of formants and relative amplitudes of phonemes.

Articulatory domain approaches to synthesis by rule<sup>1, 2</sup> have been most successful in modelling the dynamics of the speech producing mechanism. Acoustic domain methods, such as the one presented here, can impose the natural constraints of the vocal tract only indirectly, that is, by rules which often lack a firm physiological basis. However, acoustic domain approaches have enjoyed the most success in producing intelligible, high quality speech<sup>3, 4, 5, 6</sup> thus justifying and motivating efforts along these lines. The technique for synthesis by rule, described in this paper, is an acoustic domain approach.

The next section gives a general description of the synthesizer. Terminal analog synthesizers of this type are common<sup>7, 8, 9</sup> and we discuss only the new features at any length.

## II. SYNTHESIZER

## 2.1 General Description

A terminal analog synthesizer models the speech-producing mechanism, which includes the vocal tract, excitation sources, and radiation impedance. The transfer function of the vocal tract can be reduced to either a cascade of complex conjugate pole and zero pair networks, or a parallel addition of complex pole pair networks. The cascade representation was used because it reduced the complexity of the synthesis strategy by reducing the number of synthesizer control parameters.

Fig. 2 is a block diagram of the synthesizer used in this work. The synthesizer was simulated on a computer at 20 kHz sampling frequency. There are two sources of excitation, a pitch impulse generator, and a frication (noise) generator. To produce voiced speech (vowels, nasals, voiced stops, and voiced fricatives) the pitch impulse generator output is gated by the switch to the upper arm of the synthesizer. The nasal network is included in the upper arm only for nasal consonants. To produce whispered or aspirated speech, the frication generator is gated by the switch to the upper arm of the synthesizer.

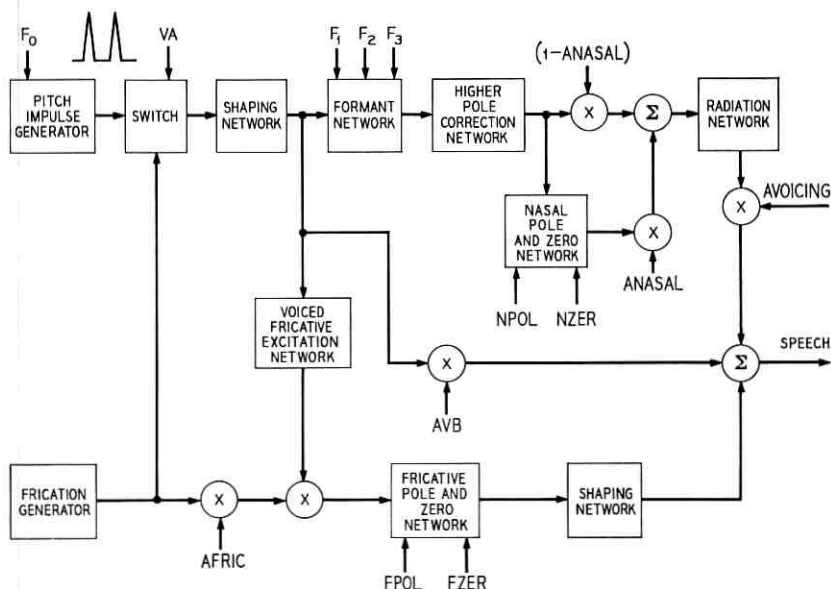


Fig. 2 — Synthesis used by author.

To produce a voiceless fricative or the unvoiced component of voiced fricatives, the frication generator excites the lower arm of the synthesizer. For a voiceless fricative, the output of the voiced fricative excitation network is constant. For a voiced fricative the output of the voiced fricative excitation network modulates the frication generator output. The details of this network are explained in Section 2.1 because this is an original design.

The higher pole correction network in the upper arm of the synthesizer compensates for the missing higher order poles.<sup>9, 10</sup> A new design for this network, based on the properties of sampled data systems, has been formulated and is discussed in Gold and Rabiner's paper.<sup>11</sup>

One last feature of the synthesizer is provision for generating a voice bar. (A voice bar is the quasi-periodic low frequency energy radiated from the region of the vocal cords during the closure interval of voiced stop consonants. During this interval the vocal cords are vibrating thus acting as the source of energy for the voice bar.) To produce a voice bar, the middle arm of the synthesizer is used with the switch gating the pitch impulse generator output to the shaping network. The voice bar has energy only at low frequency similar to voice bars of natural speech.

The outputs of the three arms of the synthesizer are added to produce the speech. The synthesizer control signals are indicated in Fig. 2 by arrows. These include four amplitude controls (avoicing, anasal, avb, afric); a derived amplitude control (1-anasal); 14 pole-zero controls (both center frequency and bandwidth of  $F_1$ ,  $F_2$ ,  $F_3$ , npol, nzer, fpol, fzer); a switch control (va); and a fundamental frequency control ( $F_0$ ).

## 2.2 Voiced Fricative Excitation Network

The network connecting the pitch impulse generator to the lower arm of the synthesizer is used to provide the excitation for the unvoiced component of voiced fricatives. Fig. 3 shows the relevant details of this network. (For clarity, certain components of the synthesizer have been omitted from Fig. 2.)

The output of the pulse generator is shaped to produce a suitable pitch pulse. A complex conjugate pole pair resonator was used, but any suitably chosen network could have been used. The pitch pulses excite a resonator tuned to the first formant of the fricative sound. A single resonance is the first order approximation to the transfer function of volume velocity (the signal of interest in Fig. 3) from the

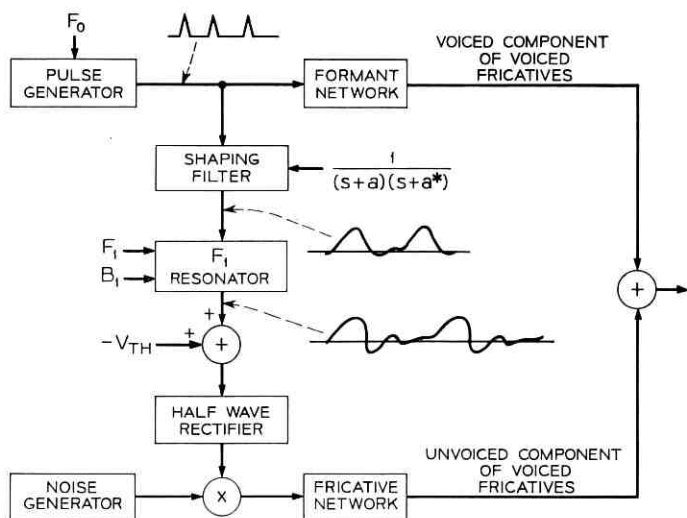


Fig. 3 — Excitation network for voiced fricatives.

glottis through the point of constriction of the vocal tract. A threshold level is subtracted from the output of the resonator and the result is half-wave rectified. These operations model the physical situation where turbulence is not produced until the volume velocity of the air-flow exceeds a threshold value. The output of the half-wave rectifier modulates the output of a noise generator, producing a pitch synchronous excitation for the unvoiced component of the fricative. The final unvoiced component is produced by exciting the fricative network by this excitation. The voiced component is produced in the standard manner, that is, by exciting the formant network by the pitch pulses.

Spectrograms of voiced fricatives produced by the above technique are quite similar to spectrograms from natural speech. Experimental evidence presented later shows that the synthetic fricatives are highly intelligible.

### III. SYNTHESIS STRATEGY

Since formant contours are crucial to speech intelligibility (see pages 220-234 of Ref. 9), the first step in transforming a discrete set of input symbols to the synthesizer control signals is to generate the formant contours. The method is explained in Sections 3.1, 3.2, and 3.3.

Once the formant contours are specified, the remaining control parameter contours are determined by delimiting certain characteristic times along the formant contours. At these times, motion of the other parameters is initiated or terminated. The techniques for generating these contours are discussed in Section 3.4.

Part IV treats the generation of a fundamental frequency contour. Table I shows international phonetic alphabet symbols and the letter equivalents used in the following sections.

### 3.1 *Static Phoneme Characterizations*

In order to generate the formant contours from the phoneme input sequence, certain information must be supplied. Corresponding to

TABLE I—LETTER EQUIVALENTS OF INTERNATIONAL  
PHONETIC ALPHABET

Letter Symbol	IPA Symbol
IY	<i>i</i>
I	<i>I</i>
E	<i>e</i>
AE	<i>ae</i>
UH	$\Lambda$
A	<i>a</i>
OW	$\text{ɔ}$
U	<i>U</i>
OO	<i>u</i>
ER	<i>ɜ</i>
W	<i>w</i>
L	<i>l</i>
R	<i>r</i>
Y	<i>y</i>
B	<i>b</i>
D	<i>d</i>
G	<i>g</i>
P	<i>p</i>
T	<i>t</i>
K	<i>k</i>
M	<i>m</i>
N	<i>n</i>
NG	<i>ŋ</i>
F	<i>f</i>
TH	<i>θ</i>
S	<i>s</i>
SH	<i>ʃ</i>
V	<i>v</i>
THE	$\text{ð}$
Z	<i>z</i>
ZH	<i>ʒ</i>
CH	<i>tʃ</i>
J	<i>dʒ</i>

each possible phoneme there must be data on formant target positions. These data, along with other data, are included in a phoneme characterization table. Certain durational data are necessary, such as for stressed vowels. Finally a technique for generating formant transitions must be supplied.

Each phoneme has a characterization independent of adjacent phonemes. The characterization includes formant information, source characteristics in the production of the phoneme, a description of whether it is nasal or fricative, and a set of frequency regions surrounding the formant positions.

The formant information is a set of target positions for both center frequency and bandwidth of formants one, two and three. The source characteristics describe the condition of the vocal cords during the production of the phoneme. If the vocal cords are vibrating the sound is voiced. The frequency regions of a phoneme represent the degree to which certain acoustic parameters must approximate the target values of these parameters in the context of connected speech. In an articulatory analog, the corresponding concept would be the extent to which a given vocal tract configuration must approximate the target configuration for the phoneme.

The frequency regions represent a compromise between choosing a single characterization for a phoneme and considering it inviolate, and the realization that there are many acceptable characterizations for a phoneme—especially in the context of connected speech.

Table II shows the phoneme characterizations we have used. The first three columns list the formant target positions of the phonemes. The second three columns show the frequency regions of the phonemes. (The figures represent both  $\pm$  values.) The final three columns describe nasality, fricative, and voicing characteristics of the phonemes. A + in any column indicates the presence of the feature and a - indicates its absence. The voicing condition of the voiced fricatives *z* and *zh* is  $\pm$  indicating the two sources used to produce these sounds on the synthesizer. The bandwidths of  $F_2$  and  $F_3$  are held fixed at 100 Hz and 120 Hz for all phonemes. The bandwidth of  $F_1$  is 60 Hz except for nasals where it is 150 Hz. When a + appears in the nasality or fricative columns, a table look-up procedure is used to specify pole-zero locations.\*

---

\* All data referred to but not included in this paper are available in the author's Ph.D. thesis which is available from the MIT library. (See Ref. 12.)

TABLE II—PHONEME CHARACTERIZATION

Phoneme	F1	F2	F3	$\Delta 1$	$\Delta 2$	$\Delta 3$	Nasal	Fricative	Voiced
IY	270	2290	3010	75	75	150	—	—	+
I	390	1990	2550	75	75	110	—	—	+
E	530	1840	2480	75	80	110	—	—	+
AE	660	1720	2410	75	75	110	—	—	+
UH	520	1190	2390	75	75	75	—	—	+
A	730	1090	2440	37	75	115	—	—	+
OW	570	840	2410	75	75	115	—	—	+
U	440	1020	2240	75	75	90	—	—	+
OO	300	870	2240	75	80	90	—	—	+
ER	490	1350	1690	75	80	100	—	—	+
W	300	610	2200	25	40	150	—	—	+
L	380	880	2575	25	80	150	—	—	+
R	420	1300	1600	30	80	100	—	—	+
Y	300	2200	3065	25	110	200	—	—	+
B	0	800	1750	50	75	120	—	—	+
D	0	1700	2600	30	50	160	—	—	+
G	0	2350	2000	15	50	100	—	—	+
M	280	900	2200	17	17	40	+	—	+
N	280	1700	2600	17	17	100	+	—	+
NG	280	2300	2750	17	17	100	+	—	+
P	0	800	1750	50	40	80	—	—	—
T	0	1700	2600	30	30	100	—	—	—
K	0	2350	2000	10	30	70	—	—	—
F	175	900	2400	30	50	120	—	+	—
TH	200	1400	2200	30	40	100	—	+	—
S	200	1300	2500	30	40	70	—	+	—
SH	175	1800	2000	30	100	150	—	+	—
V	175	1100	2400	30	50	120	—	+	+
THE	200	1600	2200	30	40	100	—	+	+
Z	200	1300	2500	30	40	70	—	+	±
ZH	175	1800	2000	30	100	150	—	+	±

(The data for  $\Delta 1$ ,  $\Delta 2$ ,  $\Delta 3$  were determined experimentally.)

### 3.2 Duration and Amplitude

Vowel duration is specified only for stressed vowels. The durations of unstressed vowels are determined by the methods illustrated in Section 3.3. The duration of a stressed vowel is modified by its following phoneme. The longest vowels are those followed by voiced fricative consonants; the shortest are followed by voiceless stop consonants.<sup>13</sup>

For certain consonants maximum durations are specified. Consonant duration (as measured from human speech) is not a fixed quantity but is very dependent on context. (For example, initial consonants are much longer than medial consonants.) The synthesis strategy generates consonants whose duration is variable within certain limits. Maximum durations are specified to prevent the consonant from being unnaturally long, hence objectionable.

Maximum stop gap durations are specified for stops; aspiration duration, as a function of the succeeding phoneme, is specified for voiceless stop consonants. Values of amplitude control signals are specified for all phonemes. Rates of change of control signals are specified for various phoneme classes (that is, vowels, nasals, fricatives, and stops).

### 3.3 Formant Motion

The technique for generating formant transitions (and hence formant contours) is a new one. We present it in detail because the entire synthesis strategy is built around it.

As we stated, the motion of formants is one of the most significant factors contributing to the intelligibility of speech. Smooth, continuous formant transitions are generally observed on spectrograms of real speech. To match these characteristics, we used the solution to a critically-damped second degree differential equation to describe the transitions of formants. We chose a second degree equation because it provided a good fit to data on formant transitions. We used a critically-damped solution because it was completely specified from a single time constant. Values of time constants were determined from examining formant transitions for real speech on spectrograms.

The input to the differential equation represents the formant target position appropriate for the current phoneme. Since the current phoneme changes its value discretely, the input to the differential equation changes in a steplike manner. The formant motion, in response to this step input, is smooth and continuous. Thus motion from steady state value  $A_i$  to target value  $A_f$ , beginning at time  $t = 0$  is of the form:

$$x(t) = A_f + (A_i - A_f)(1 + t/\tau) \exp(-t/\tau)$$

where  $\tau$  is the time constant of motion and  $x(t)$  the formant position at time  $t$ .

In general, motion between target positions does not proceed from a steady state condition; that is, there are initial conditions. Motion to a target whose formant value is  $A_f$  from an initial formant position  $A_i$  with an initial formant velocity  $V_i = dx/dt|_{0-}$  is of the form:

$$x(t) = A_f + (A_i - A_f) \exp(-t/\tau) + \left[ V_i + \frac{(A_i - A_f)}{\tau} \right] t \exp(-t/\tau); \quad t \geq 0.$$

At times when the input to the differential equation is changed discretely, both the output value *and* slope are continuous. Thus the concept of smooth, continuous formant transitions is realized in all cases.

The time constants of the differential equation are functions of the individual formant *and* the pair of phonemes between which the transition is being made. Hence, for each possible pair of phonemes, and each formant, a time constant is specified. Certain simplifying approximations reduce (by an order of magnitude) the number of time constants that have to be specified.

The inputs to the differential equations change discretely in time in a steplike manner. However, provision is made for delaying, to any formant, the steplike change in formant target position. Thus, in the most general case, formants move independently of each other with unequal time constants of motion. This delay feature was found necessary for only a few cases.

The phonemic goals change discretely in time. The decision of when to make the discrete changes, that is, when to initiate motion to new sets of formant targets, is based on the criterion that the formants must first be within the phoneme frequency regions of the targets, and then satisfy durational requirements of the phoneme, if there are any.

Formants, in general, are in motion towards target values appropriate for the phonemes to be generated. Their motion is characterized by the solution to a differential equation. The time constant of motion is a function of the phoneme from which motion began and the phoneme which is being generated. Each formant moves with its own time constant and there is provision for delay in time of initiation of the motion of formants. When all formants are within the frequency regions of the target, a decision is made. If a stressed vowel is being generated, then a table look-up procedure determines the correct vowel duration and motion continues for the specified time. Once a vowel of proper duration has been generated, motion towards target positions characteristic of the next phoneme is begun. If the current phoneme is not a stressed vowel, motion towards the new phoneme targets is initiated as soon as all the formants are within their specified frequency regions.

The decision to start motion to new target values results in three separate operations. First, new time constants for each formant are inserted into the respective difference equations. Second, the forcing functions (input) to the difference equations are changed in a step-

like manner indicating the changes in target positions. Finally, the initial conditions of the difference equation are set to preserve continuity of formant values and formant velocities. If the motion of any formant is to be delayed, the changes in the difference equation for that formant are delayed appropriately.

Fig. 4 shows a typical cycle of events. Initially formants one and two (we shall neglect formant three in this example) are at target positions appropriate for phoneme 1. At time  $t_1$  motion is initiated to phoneme 2. Formants one and two begin motion simultaneously (no delay is used here) with time constants  $\tau_{12}^1$  and  $\tau_{12}^2$  respectively.  $\tau_{12}^1$  is much smaller than  $\tau_{12}^2$  so formant one moves more rapidly to its target value than formant two. Periodically the formant values are tested to see whether they are within the specified frequency regions of the targets. (The frequency regions are indicated by  $\Delta 1$ ,  $\Delta 2$  in Fig. 4.) If they are not, the formants continue their motion, thus moving closer to target. For the example in Fig. 4, formant one enters its frequency region prior to formant two. Until formant two enters its frequency region at time  $t_2$ , formant one moves closer to its target position. At time  $t_2$  both formants are within the specified frequency regions and so a check is made on whether phoneme 2 is a stressed vowel or not. In this example phoneme 2 is not a stressed vowel, so motion to phoneme 3 is initiated at  $t_2$ . However, we now have the

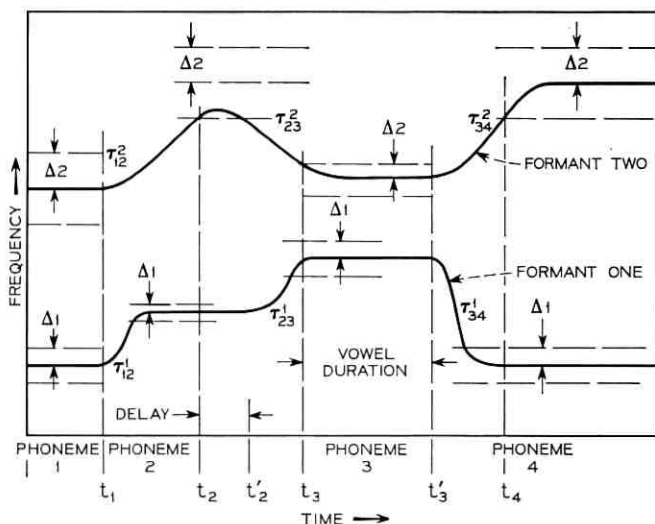


Fig. 4 — Simplified example of formant motion.

case when the time of initiation of motion of formant one is delayed. Hence at  $t_2$  the target value and time constant for formant two is changed, but formant one's target is unchanged. At time  $t'_2$  the delay is terminated and formant one begins its motion.

Phoneme 3 of Fig. 4 is a stressed vowel. So at time  $t_3$ , when both formants are within the frequency regions for phoneme 3, motion to targets for phoneme 3 continues for the specified vowel duration. At time  $t'_3$ , following the vowel duration, motion begins toward targets for phoneme 4. New time constants and targets are again inserted in the equations of motion. The process continues in this manner until all the input phonemes have been generated.

### 3.4 Remaining Synthesizer Controls

The motion of the remaining synthesizer control parameters (that is, nasal and fricative poles, and zeros and source amplitudes) is time-locked to the formant motion. The source amplitudes (avoicing, anasal, afric, avb) begin to switch approximately one time constant after the discrete phoneme goal is changed. The amplitudes change linearly at predetermined rates. The nasal and fricative poles and zeros initiate motion at the time the phoneme goal is changed. The motion is linear and the slopes are arranged so that the poles and zeros just reach their targets at the time the source amplitudes are switched. The target positions are specified in a table.

For nonnasal sounds, the target positions of the nasal zero and pole are set to 1400 Hz. Thus the pole and zero will cancel each other in these cases. Furthermore, for nasal sounds, the bandwidth of formant one (nominally 60 Hz) is changed linearly to 150 Hz for the duration of the nasal. The bandwidth begins to change 50 msec before the amplitudes switch and is linearly changed back to its nominal value in 50 msec after the nasal. For nonfricative sounds the fricative pole and zero target positions are set to 1500 Hz.

## IV. FUNDAMENTAL FREQUENCY

Our model for generating fundamental frequency data is based on the assumption that these data can be derived from data on laryngeal tension (LT) and subglottal pressure (Ps). A description of an utterance in terms of these variables is then used to produce the desired fundamental frequency data.

The model is based on that of P. Lieberman, in which the breath-group is defined as an underlying phonetic feature of American Eng-

lish.<sup>14</sup> The unmarked breath-group is characteristic of a simple, declarative sentence, whereas the marked breath-group characterizes a simple interrogative sentence.

The feature breath-group is converted to a global description of an utterance in terms of Ps and LT. Fig. 5 shows the archetypal Ps contour, as suggested by Lieberman's data. Ps increases over the first 300 msec of the utterance, and then remains constant until the last 300 msec of the breath-group, at which point it decreases rapidly to zero. The LT contour for an unmarked breath-group is constant, whereas for a marked breath-group it is characterized by a steady increase over the last 175 msec of phonation. Fundamental frequency is linearly proportional to both Ps and LT. Since the archetypal Ps contour falls at the end of a marked breath-group, the increase in LT must compensate for the decrease in Ps to give fundamental frequency a rising terminal contour. A slope of 0.6 Hz/msec, for the last 175 msec of phonation, was assigned to the LT contour. This resulted in a terminal rise of 60 Hz in fundamental frequency for a question.

The subglottal pressure contour is modified by both consonants and vowels. Two levels of stressed vowels are adopted. One level is referred to as emphasis and only one vowel in a breath-group is emphasized. The emphasized vowel provides the highest peak in the Ps contour. All other stressed vowels are treated similarly. When a vowel is stressed, there is an increase in subglottal pressure for a pe-

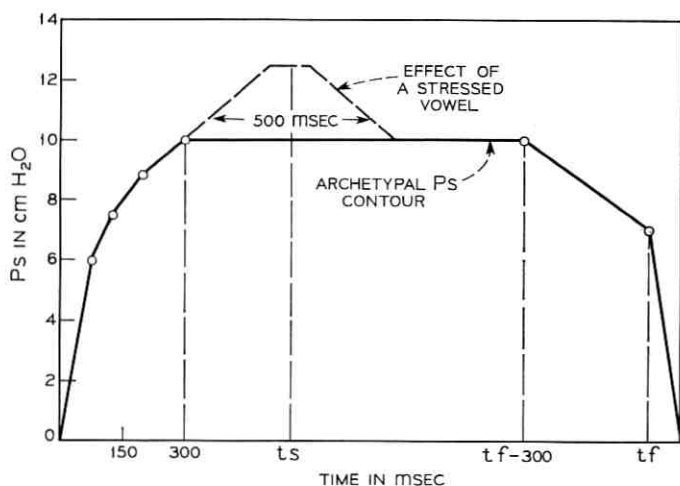


Fig. 5—Archetypal subglottal pressure contour showing effects of vowel stress.

riod of 500 msec, centered on the vowel. Fig. 5 shows an example of this effect. The dashed curve shows the effects of placing stress on a vowel at the beginning of the breath-group. There is a rise in  $P_s$  early in the breath-group and the increase is centered at  $t_s$ , the midpoint of the vowel steady state. If the stressed vowel had been the emphasized one, the only difference in Fig. 5 would be the amplitude of the increased  $P_s$ . It would have been 2.5 cm  $H_2O$  as compared to 1.0 cm  $H_2O$ .

The effects of consonants on subglottal pressure have also been included in our scheme. For a voiceless consonant, subglottal pressure automatically increases whereas subglottal pressure automatically decreased for voiced consonants. Thus the consonants introduce local perturbations to the  $P_s$  contour. The change in  $P_s$  for consonants is  $\pm 1.0$  cm  $H_2O$ , and this change occurs over a period of 150 msec centered on the consonant.

#### V. TYPICAL INPUT SEQUENCES

All vowels are unstressed except those followed by the symbol *strss*. The symbol *strss1* signifies the emphasized vowel. Word boundaries are signified by the symbol *space* and pauses by the symbol *pause*. A question is signified by the symbol *ques*. The sentence boundary is indicated by the symbol *end*. The examples are:

- (i) This is an olive.  
THE I *strss* S *space* I Z *space* AE N *space* A *strss1* L I V *end*.
- (ii) Why are you sad?  
W A *strss1* IY *space* A R *space* Y OO *space* S AE *strss* D *end*.
- (iii) We sang all day.  
W IY *space* S AE *strss1* NG *space* OW L *space* D E IY *strss* *end*.

Whenever a word boundary (*space* in our code) occurs, consonants on either side of the word boundary are affected. In this strategy an initial consonant is lengthened by about 20 percent, whereas a final consonant is shortened by a similar amount. A word boundary has no effect on phonemes which do not lie on either side of the word boundary.

#### VI. EVALUATION TESTS

Intelligibility tests were conducted to evaluate the scheme. To test the rules in a limited environment, consonant intelligibility tests were run. One test was intended to test perception of consonants in pre-

stressed position. The schwa vowel UH always preceded the consonant and was used as a perceptual cue for stop consonants because it provided a basis for perceiving the stop gap. The second test was intended to test perception of consonants in post-stressed position. The schwa vowel UH always followed the final consonant—again providing a basis for perceiving stop gap duration, bursts, and aspiration for stops.

Sixteen consonants were used: B, D, G, P, T, K, M, N, F, TH, S, SH, V, THE, Z, and ZH. Five vowels (besides schwa) were used: IY, AE, A, OW, and OO. For each test there were 80 possible stimuli. Twenty additional stimuli were used, ten initiating the test and ten concluding it, giving a total of 100 stimuli per test. Only the middle 80 were used for evaluation, and these were presented in random order.

Three subjects were tested. Their results are summarized in the two confusion matrices shown in Table III. In prestressed position (UH-C-V), 73 percent were correct; in post-stressed position (V-C-UH), 77 percent were correct. If F, TH and V, THE responses are pooled, as is often done, then the correct percentages increase to 79 in prestressed position and 81 in post-stressed position. Ten prestressed consonants were identified correctly more than 75 percent of the time: B, D, P, T, N, TH, S, SH, Z, and ZH. The post-stressed consonants identified correctly more than 75 percent of the time were B, P, T, K, TH, S, SH, Z, and SH. The consonants which were identified incorrectly most often were G, M, D, and K.

An examination of the errors in the confusion matrices of Table III shows:

- (i) The voiced stop G was often confused with T and K; and D in post-stressed position was often confused with G.
- (ii) The unvoiced stop K was often confused with T in prestressed position.
- (iii) The nasal M was often confused with B and V.
- (iv) The fricative pairs V, THE and F, TH were often confused.

These errors were the major confusions in the tests. The stop confusions primarily were caused by errors in frication burst positions. The fricative pair errors were anticipated because of the acute acoustic similarities between these particular fricatives. The cause for the confusions between M and other phonemes is unknown. Further work remains to be done in this area.

A second series of tests, using sentences as test material, were run.

One test contained simple declarative, interrogative and imperative sentences. A second test contained sentences chosen from a list of sentences used often in intelligibility tests.<sup>15</sup>

The sentences were presented to listeners who wrote down what they heard. They were told to guess whenever in doubt. The sentences were played a second time and the listeners were allowed to make changes. The tests were scored on the number of words which were correctly identified (excluding only *the* and *a* as words). The results of the tests are as follows. For the test using simple sentences, eight listeners had an average of 92 percent of the words correct after one try, and 95 percent after the second try. For the test using the longer

TABLE III—CONSONANT CONFUSION MATRICES

		CONSONANT RECEIVED																								
		B	D	G	P	T	K	M	N	F	TH	S	SH	V	THE	Z	ZH									
C O N S O N A N T  S E N T	B	13															2									
	D		15																							
	G			1	3	2	6	3																		
	P					13	2																			
	T						1	14																		
	K							2	7	6																
	M		2														4									
	N																	12								
	F																		10							
	TH																			2						
	S																				12					
	SH																					1				
	V																						15			
	THE																							15		
	Z																								7	
	ZH																									2
																										8
																									6	
																									15	
																									15	

UH-C-V MATRIX  
(3 SUBJECTS)

## CONSONANT RECEIVED

	B	D	G	P	T	K	M	N	F	TH	S	SH	V	THE	Z	ZH	?
B	12												3				
D		7	8														
G			6		1	8											
P				14		1											
T				1	14												
K				1	2	12											
M	4						4	3					4				
N			6					9									
F									11	3	1						
TH										12	3						
S											15						
SH												15					
V	3						1						10	1			
THE													4	11			
Z																15	
ZH																	15

V-C-UH MATRIX  
(3 SUBJECTS)

standard sentences four listeners had an average of 83 percent of the words correct after one try; and 86 percent after the second try.

As shown above, the percent intelligibility scores for sentences were significantly higher than for isolated syllables, primarily because of the context of speech in a meaningful utterance. However, the longer the utterance, the less intelligible it became. This is because rhythm and timing are much more important for a long sentence than for a short, simple one.

## VII. SPECTROGRAPHIC EXAMPLES OF SYNTHETIC SPEECH

Fig. 6a shows wideband spectrograms of the utterance "Larry and Bob are here." The spectrogram in the upper half of the figure is the

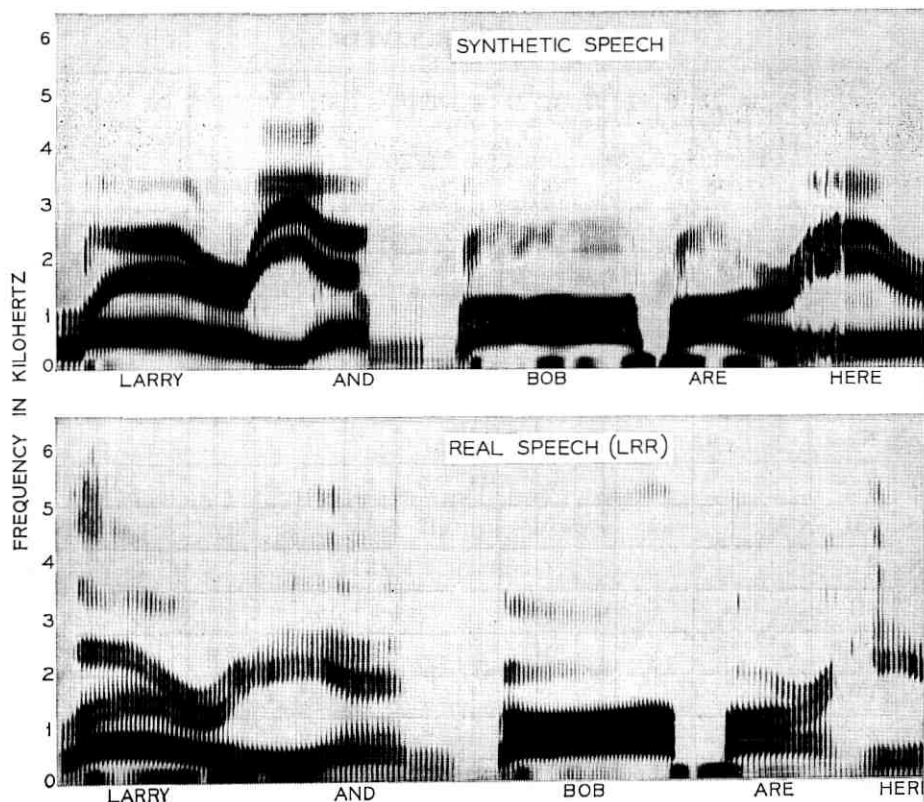


Fig. 6a—Wideband spectrograms of synthetic (top) and natural versions of "Larry and Bob are here."

synthetic version. The lower spectrogram was made from the author's speech. (The synthetic utterance was in no way modelled after or modified by the natural utterance.) Fig. 6b shows narrowband spectrograms of both the synthetic and natural versions of this utterance.

This is a high degree of similarity between the spectrograms of the real and synthetic speech. The durations of both the synthetic and natural utterances are comparable. Fig. 6a shows that the variation of the formants for both versions is quite similar. Even the fundamental frequency contours for these utterances are quite similar. As Fig. 6b shows, both contours are peaked during the stressed vowels A in BOB and I in HERE. A careful examination of the narrowband spectrograms shows the decrease of fundamental frequency, for both utterances, during the initial and final B of BOB.

The stressed vowels of this utterance can easily be identified from either the long steady state duration of Fig. 6a or the peak in the fundamental frequency contour of Fig. 6b.

#### VIII. FURTHER WORK

The results of the consonant intelligibility tests showed that most consonants were reproduced accurately. The sentence intelligibility tests also produced good intelligibility scores, indicating a high degree of success for the major goal of this project.

Many of the listeners made informal comments concerning the machine-like quality of the speech, but no formal tests were run to measure the naturalness or quality of the synthetic speech. Current studies

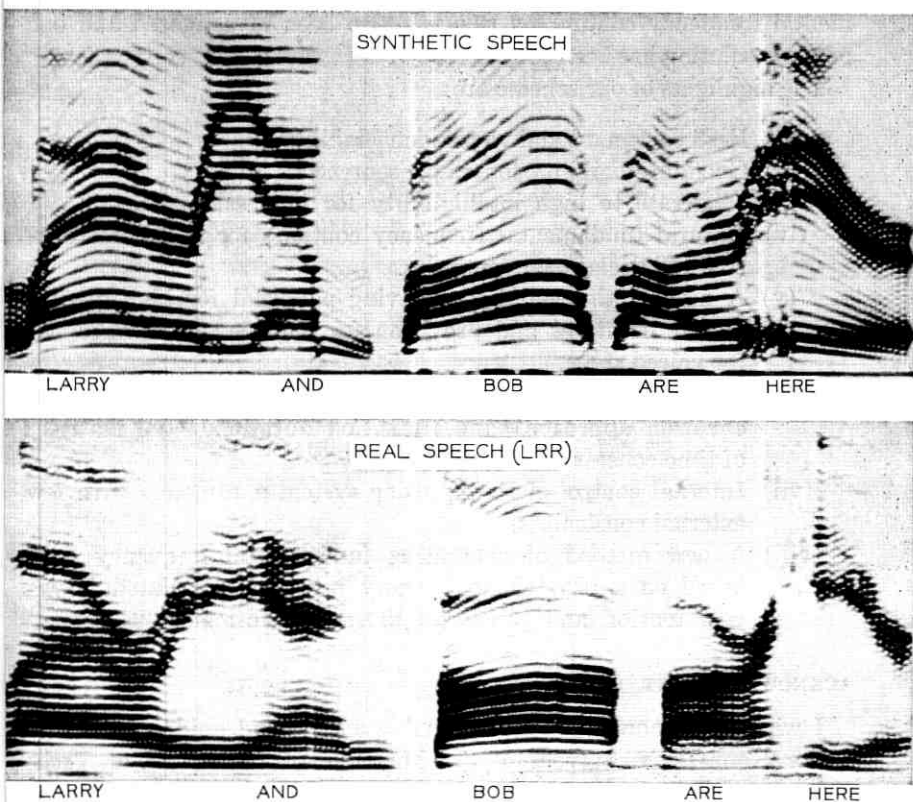


Fig. 6b — Narrowband spectrograms of synthetic (top) and natural versions of "Larry and Bob are here."

about the characteristics of the source of voiced speech are expected to produce valuable information about the determinants of synthetic speech quality.

Among the topics that will be considered for future work are the effects of stress and rhythm on timing of an utterance, the inclusion of more than one breath-group in an utterance, and studies of further correlates of word boundaries.

#### IX. SUMMARY

An acoustic domain approach to speech synthesis by rule has been formulated and programmed on a digital computer. Samples of speech have been generated using our scheme and their intelligibility has been measured. The problem of automatically generating a fundamental frequency contour by rule has also been investigated and one possible solution has been found.

The highlights of our scheme are:

- (i) High consonant and vowel identifiability.
- (ii) Good intelligibility for simple sentences.
- (iii) Moderate to high intelligibility for long sentences.
- (iv) Natural fundamental frequency contours for both interrogative and declarative sentences.
- (v) A new synthesizer design having potential for high quality voiced fricatives and provision for inclusion of a voice bar for voiced stops.
- (vi) A new method of handling formant transitions (a differential equation approach) and transition durations (the matrices of time constants).
- (vii) Internal control of timing using system parameters with few external constraints.
- (viii) A new method of generating fundamental frequency data based on a physiological theory involving simulated laryngeal tension and subglottal pressure information.

#### ACKNOWLEDGMENT

I wish to acknowledge the invaluable advice and guidance of Professor Kenneth N. Stevens of the Massachusetts Institute of Technology and Doctor James L. Flanagan of the Bell Telephone Laboratories. I would also like to thank Doctors Harry Levitt and Peter Brady for valuable comments and criticisms of this manuscript.

## REFERENCES

1. Henke, W., Dynamic Articulatory Model of Speech Production Using Computer Simulation, Ph.D. thesis, Massachusetts Institute of Technology, 1966.
2. Coker, C. H. and Fujimura, O., Model for Specification of the Vocal Tract Area Function, *J. Acoust. Soc. Amer.* 40, 1966, p. 1271, (A).
3. Holmes, J., Mattingly, I. and Shearme, J., Speech Synthesis by Rule, *Language and Speech*, 7, 1964, pp. 127-143.
4. Cooper, F., Liberman, A., Lisker, L. and Gaitenby, J., Speech Synthesis by Rules, Speech Communication Seminar, Stockholm, August 29 to September 1, 1962, Paper F2
5. Liberman, A., Ingemann, F., Lisker, L., Delattre, P., and Cooper, F., Minimal Rules for Synthesizing Speech. *J. Acoust. Soc. Amer.* 31, 1959, pp. 1490-1499.
6. Peterson, G., Wang, W., and Sivertsen, E., Segmentation Techniques in Speech Synthesis. *J. Acoust. Soc. Amer.* 30, 1958, pp. 739-742.
7. Fant, G., and Martony, J., Speech Synthesis. *Speech Transmission Laboratory, Quarterly Progress Report* Univ. of Stockholm, 1962.
8. Tomlinson, R. S., SPASS—An Improved Terminal-Analog Speech Synthesizer, *J. Acoust. Soc. Amer.*, 1965, 38, p. 940.
9. Flanagan, J. L., *Speech Analysis Synthesis and Perception*, Academic Press, Inc., New York, 1965.
10. Fant, G., *Acoustic Theory of Speech Production*, 's-Gravenhage: 1960 Mouton and Co.
11. Gold, B. and Rabiner, L., Analysis of Digital and Analog Formant Synthesizers. Paper presented at 1967 Conference on Speech Communication and Processing, Massachusetts Institute of Technology, and accepted for publication in *IEEE Trans. Audio and Elec.*, March 1968.
12. Rabiner, L., Speech Synthesis by Rule: An Acoustic Domain Approach, Ph.D. thesis, Massachusetts Institute of Technology, 1967.
13. House, A., On vowel duration in English, *J. Acoust. Soc. Amer.*, 33, 1961, pp. 1174-1178.
14. Lieberman, P., Intonation, Perception and Language, Research Monograph 38, MIT Press, Cambridge, Mass., 1967.
15. Beranek, L., *Acoustic Measurements*, John Wiley and Sons, Inc., New York, 1949, pp. 773-777.



# Unified Matrix Theory of Lumped and Distributed Directional Couplers

By M. A. MURRAY-LASSO

(Manuscript received September 12, 1967)

*This paper presents the theory of directional couplers using matrix formulation for lumped, distributed, or any linear time-invariant black-box. The starting point is the matrix theory of uniform multiple coupled transmission lines in terms of which are brought in the concepts of characteristic impedance matrix, propagation matrix, reflection matrix, and scattering matrix. Next, we use the results obtained with the theory of multiple coupled transmission lines to derive expressions for the loading impedance and voltage ratios for distributed directional couplers. We do this using the spectral properties of the matrices. Then we generalize the concepts of characteristic impedance matrix and propagation matrix for a class of black-boxes with the aid of the  $A, B, C, D$  transmission matrix. We give conditions for the loading impedance and expressions for the voltage ratios, using the spectral theory of the transmission matrix. We discuss the physical significance of the directional coupler effect at all frequencies in a vector-matrix framework and analyse in detail some lumped directional couplers. Finally we discuss hybrid (lumped and distributed) directional couplers.*

## I. INTRODUCTION

The directional coupler is an important device in many transmission systems. The theory for the electrical design of certain types of distributed-parameter directional couplers is well established through the contributions of a number of researchers.<sup>1-7</sup>

The purpose of this paper is to present the theory of transmission-line symmetric directional couplers in matrix form and then extend that theory to arbitrary lossless reciprocal circuits. There are many notational and conceptual advantages in using a matrix formulation which give further insight for the synthesis of different types of directional couplers.

The starting point is to examine the coupled-line directional coupler as a particular application of multiple coupled transmission line theory and then to use the concepts of characteristic impedance matrix and propagation matrix to examine the whole problem, rather than one line at a time or one mode at a time. By using a matrix approach the fundamental properties of the modes become more evident and thus physical intuition and mathematical reasoning blend to give a clearer picture of the situation. For instance, when the lines are no longer identical it is the eigenvectors of the matrices which provide the information of how to extend the mode concept.

## II. MULTIPLE COUPLED TRANSMISSION

### 2.1 Propagation and Characteristic Impedance Matrices

Several researchers<sup>8-10</sup> have analyzed the behavior of a set of multiple coupled transmission lines. For reference in subsequent sections of this paper we present a brief account of this theory. For simplicity the discussion is restricted to two identical lines operating in the TEM mode. Fig. 1 shows schematically a differential section of two lines and a ground plane. The circuit of which Fig. 1 is a differential section obeys the following vector differential equations\* in the steady state

$$\frac{d\mathbf{V}}{dx} = -\mathbf{Z}\mathbf{I}, \quad (1)$$

$$\frac{d\mathbf{I}}{dx} = -\mathbf{Y}\mathbf{V}, \quad (2)$$

where

$$\mathbf{V} = \begin{bmatrix} V_1(x) \\ V_2(x) \end{bmatrix}, \quad \mathbf{I} = \begin{bmatrix} I_1(x) \\ I_2(x) \end{bmatrix},$$

$$\mathbf{Z} = \begin{bmatrix} Z_{11} & Z_{12} \\ Z_{12} & Z_{22} \end{bmatrix}, \quad \mathbf{Y} = \begin{bmatrix} Y_1 + Y_m & -Y_m \\ -Y_m & Y_2 + Y_m \end{bmatrix}.$$

By solving for  $\mathbf{I}$  in (1) and substituting its value in (2), or solving for  $\mathbf{V}$  in (2) and substituting its value in (1) the following are obtained:

$$\frac{d^2\mathbf{V}}{dx^2} = \mathbf{Z}\mathbf{Y}\mathbf{V}, \quad (3)$$

\* The matrices  $\mathbf{V}$ ,  $\mathbf{I}$ ,  $\mathbf{Z}$ ,  $\mathbf{Y}$  are all functions of frequency. For simplicity in the notation this dependency is not explicitly indicated.

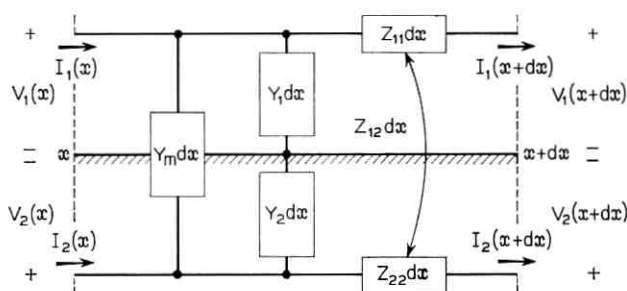


Fig. 1—Differential section of two coupled lines above a ground plane.

$$\frac{d^2 \mathbf{I}}{dx^2} = \mathbf{Y} \mathbf{Z} \mathbf{I}. \quad (4)$$

Define the matrices  $\mathbf{\Gamma}$ ,  $\mathbf{Y}_0$  and  $\mathbf{Z}_0$  as follows:

$$\mathbf{\Gamma} \triangleq \sqrt{\mathbf{Z} \mathbf{Y}}, \quad (5)$$

$$\mathbf{Y}_0 \triangleq \mathbf{Z}^{-1} \mathbf{\Gamma}, \quad (6)$$

$$\mathbf{Z}_0 \triangleq \mathbf{Y}_0^{-1}. \quad (7)$$

In terms of the matrices defined, the solution of (3) and (4) is\*

$$\mathbf{V}(x) = e^{-\mathbf{\Gamma} x} \mathbf{v}_+ + e^{\mathbf{\Gamma} x} \mathbf{v}_-, \quad (8)$$

$$\mathbf{I}(x) = \mathbf{Y}_0 (e^{-\mathbf{\Gamma} x} \mathbf{v}_+ - e^{\mathbf{\Gamma} x} \mathbf{v}_-), \quad (9)$$

where the 2-vectors  $\mathbf{v}_+$  and  $\mathbf{v}_-$  are arbitrary constants (dependent on frequency) which depend on the boundary conditions. Their interpretation is very similar to the one of single line theory,  $\mathbf{v}_+$  may be called the forward wave and  $\mathbf{v}_-$  the reflected wave.

Equations (3), (8) and (9) have the same form as the single transmission line equations. For this reason the matrices  $\mathbf{\Gamma}$ ,  $\mathbf{Y}_0$ ,  $\mathbf{Z}_0$ , are called propagation matrix, characteristic admittance matrix, and characteristic impedance matrix, respectively. Many properties of the single transmission line hold for the multiple case. In particular, if the set of lines is terminated in a network whose open circuit impedance matrix is equal to the characteristic impedance matrix of the set of lines, a vector of incident voltage waves traveling down the lines will experience no reflection. The manner in which the voltages and currents

\* In evaluating  $\sqrt{\mathbf{Z} \mathbf{Y}}$  to calculate  $\mathbf{\Gamma}$  the convention is made to associate with  $\mathbf{\Gamma}$  eigenvalues whose real part are positive and with  $-\mathbf{\Gamma}$  the ones with negative real part.

in the lines interact is best understood by examining the matrix functions  $e^{-\Gamma x}$  and  $e^{\Gamma x}$ . (See Appendix.)

## 2.2 Reflection and Scattering Matrices

In single transmission line theory the voltage reflection coefficient  $\Gamma_R$  at a discontinuity is defined as

$$v_- = \Gamma_R v_+, \quad (10)$$

where  $v_+$  is the incident voltage and  $v_-$  is the reflected voltage. The expression for  $\Gamma_R$  in terms of the characteristic admittance  $Y_0$  of the line and the input impedance  $Z_L$  at the discontinuity is

$$\Gamma_R = \frac{Z_L Y_0 - 1}{Z_L Y_0 + 1}. \quad (11)$$

The concept of reflection coefficient can be generalized very simply for the case of a multiple set of lines. Consider Fig. 2 depicting a pair of coupled lines of length  $l$  and matrices  $\Gamma$ , and  $Y_0$  terminated at  $x = 0$  in a device of open circuit impedance matrix  $Z_L$ . According to (8) and (9) for  $x = 0$

$$\mathbf{V}(0) = \mathbf{v}_+ + \mathbf{v}_-, \quad (12)$$

$$\mathbf{I}(0) = \mathbf{Y}_0(\mathbf{v}_+ - \mathbf{v}_-). \quad (13)$$

The box marked  $Z_L$  obeys

$$\mathbf{V}(0) = \mathbf{Z}_L \mathbf{I}(0). \quad (14)$$

Substitution of  $\mathbf{V}(0)$  and  $\mathbf{I}(0)$  from (12) and (13) into (14) gives

$$\mathbf{v}_+ + \mathbf{v}_- = \mathbf{Z}_L \mathbf{Y}_0 (\mathbf{v}_+ - \mathbf{v}_-), \quad (14b)$$

from which solving for  $\mathbf{v}_-$

$$\mathbf{v}_- = (\mathbf{Z}_L \mathbf{Y}_0 + \mathbf{I})^{-1} (\mathbf{Z}_L \mathbf{Y}_0 - \mathbf{I}) \mathbf{v}_+. \quad (15)$$

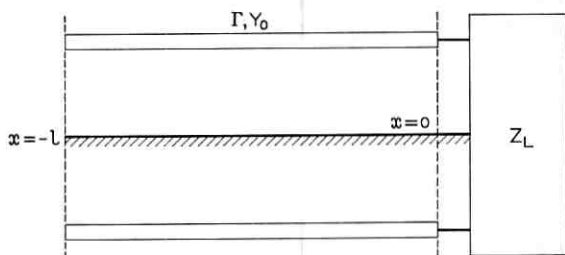


Fig. 2—Pair of coupled lines terminated in a circuit of impedance matrix  $Z_L$ .

Thus, defining the *reflection matrix*  $\Gamma_R$  as a generalization of (10) according to

$$\mathbf{v}_- = \Gamma_R \mathbf{v}_+, \quad (16)$$

it follows from (15) that

$$\Gamma_R = (\mathbf{Z}_L \mathbf{Y}_0 + \mathbf{I})^{-1} (\mathbf{Z}_L \mathbf{Y}_0 - \mathbf{I}), \quad (17)$$

which is the generalization to multiple lines of (11).

The *scattering matrix*  $\mathbf{S}$  is a reflection matrix in which the incident and reflected voltages are normalized.\* It is defined by

$$\hat{\mathbf{v}}_- = \mathbf{S} \hat{\mathbf{v}}_+; \quad (18)$$

where

$$\hat{\mathbf{v}}_+ = \mathbf{Y}_0^\dagger \mathbf{v}_+, \quad \hat{\mathbf{v}}_- = \mathbf{Y}_0^\dagger \mathbf{v}_-, \quad (19)$$

$$\hat{\mathbf{V}} = \mathbf{Y}_0^\dagger \mathbf{V}, \quad \hat{\mathbf{I}} = \mathbf{Z}_0^\dagger \mathbf{I}. \quad (20)$$

From (14b) it follows that

$$\mathbf{Z}_0^\dagger (\hat{\mathbf{v}}_+ + \hat{\mathbf{v}}_-) = \mathbf{Z}_L \mathbf{Y}_0 [\mathbf{Z}_0^\dagger (\mathbf{v}_+ - \mathbf{v}_-)]. \quad (21)$$

Defining the normalized load impedance matrix  $\hat{\mathbf{Z}}_L$  according to

$$\hat{\mathbf{Z}}_L = \mathbf{Y}_0^\dagger \mathbf{Z}_L \mathbf{Y}_0^\dagger, \quad (22)$$

equation (21) may be rearranged as follows:

$$\hat{\mathbf{v}}_- = (\hat{\mathbf{Z}}_L + \mathbf{I})^{-1} (\hat{\mathbf{Z}}_L - \mathbf{I}) \hat{\mathbf{v}}_+. \quad (23)$$

Comparison of (23) and (18) gives

$$\mathbf{S} = (\hat{\mathbf{Z}}_L + \mathbf{I})^{-1} (\hat{\mathbf{Z}}_L - \mathbf{I}). \quad (24)$$

From either (17) or (24) it is clear that if the load has an open circuit impedance matrix equal to  $\mathbf{Z}_0$  of the lines the reflected wave is zero since both the reflection matrix  $\Gamma_R$  and the scattering matrix  $\mathbf{S}$  vanish.

The complex power in terms of the normalized variables is given by

$$P = \hat{\mathbf{V}}^\dagger \hat{\mathbf{V}} = \hat{\mathbf{I}}^\dagger \hat{\mathbf{I}}. \quad (25)$$

(The superscript  $\dagger$  denotes transposed conjugate of a matrix.) For a lossless device the incident power must be equal to the reflected power,

\* In the literature on the scattering matrix the variables are normalized with respect to a diagonal matrix (usually a real matrix). Here the matrix may be complex and not necessarily diagonal. This derivation provides the physical interpretation for a scattering matrix normalized with respect to a complex nondiagonal matrix.

hence, from (18)

$$P = \hat{v}_-^+ \hat{v}_- = \hat{v}_+^+ \mathbf{S}^+ \mathbf{S} \hat{v}_+ = \hat{v}_+^+ \hat{v}_+, \quad (26)$$

which means that

$$\mathbf{S}^+ \mathbf{S} = \mathbf{I}, \quad (27)$$

that is, the scattering matrix is unitary.

### 2.3 Terminal Matrices of a Set of Lines

Viewed from its terminal behavior the two coupled lines and ground of Fig. 3 can be studied as a four port which may be characterized by, among others, an impedance matrix  $\zeta$  or a transmission  $\mathbf{E}$  matrix. (The  $\mathbf{E}$  matrix is the extension to  $2N$  ports of the concept of the  $A$ ,  $B$ ,  $C$ ,  $D$  parameter matrix of two ports. See Ref. 11.)

The  $\zeta$  matrix may be written in partitioned form as follows:

$$\zeta = \left[ \begin{array}{c|c} \coth(\Gamma \cdot l) Z_0 & (\operatorname{csch}[\Gamma \cdot l] Z_0)' \\ \operatorname{csch}(\Gamma \cdot l) Z_0 & \coth(\Gamma \cdot l) Z_0 \end{array} \right]. \quad (28)$$

(The prime indicates the transpose matrix.) The  $\mathbf{E}$  matrix, written in partitioned form, is

$$\mathbf{E} = \left[ \begin{array}{c|c} \mathbf{A} & \mathbf{B} \\ \mathbf{C} & \mathbf{D} \end{array} \right] = \left[ \begin{array}{c|c} \cosh \Gamma \cdot l & \sinh(\Gamma \cdot l) Z_0 \\ Y_0 \sinh \Gamma \cdot l & \cosh \Gamma \cdot l \end{array} \right]. \quad (29)$$

If the two lines in Fig. 3 are identical then  $\Gamma$  is symmetric and hence  $\Gamma' = \Gamma$  so that in (29),  $\mathbf{A} = \mathbf{D}$ . Furthermore, for this case all the matrices  $Z_0$ ,  $Y_0$ ,  $\Gamma$ ,  $\mathbf{A}$ ,  $\mathbf{B}$ ,  $\mathbf{C}$ ,  $\mathbf{D}$  and their analytic functions commute and therefore may be treated unambiguously as ordinary numbers. For instance (29) may be written

$$\mathbf{E} = \left[ \begin{array}{c|c} \cosh \Gamma \cdot l & Z_0 \sinh \Gamma \cdot l \\ \frac{1}{Z_0} \sinh \Gamma \cdot l & \cosh \Gamma \cdot l \end{array} \right]. \quad (30)$$

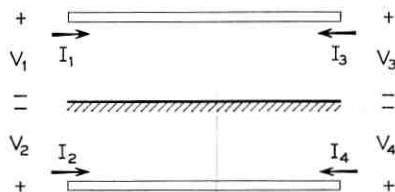


Fig. 3—Two coupled lines above a ground plane forming a four-port.

The analogy between the  $\mathbf{E}$  matrix of (30) and the  $A, B, C, D$  parameter matrix of a single transmission line considered as a two port is now complete.

### III. SYMMETRICAL TRANSMISSION DIRECTIONAL COUPLERS

#### 3.1 Derivation of Matching Impedances

A symmetric matched directional coupler is a four port device whose scattering matrix is of the form of  $\mathbf{S}$  of (31) when the ports are adequately numbered.  $\beta$  and  $\delta$  are, in general, frequency dependent. It is well known in microwave circuits that, given any lossless reciprocal 4-port, if all ports are matched, then the device is a directional coupler.<sup>12</sup> By properly numbering the ports it may be assumed that the directional coupler has the following scattering matrix

$$\mathbf{S} = \begin{bmatrix} 0 & \beta & \delta & 0 \\ \beta & 0 & 0 & \delta \\ \delta & 0 & 0 & \beta \\ 0 & \delta & \beta & 0 \end{bmatrix}. \quad (31)$$

For the case of two identical lossless coupled lines equally loaded at the four ports all that is necessary to obtain a directional coupler is to match one of the ports. This results from the great symmetry.

Fig. 4 shows two identical lines loaded at ports 2, 3, and 4 with equal resistances,  $R$ . To calculate the driving point impedance at port 1 the following procedure can be used. Consider Fig. 5. The equation

$$\mathbf{Z} = \frac{RA + B}{RC + D} = \begin{bmatrix} Z_{11} & Z_{12} \\ Z_{21} & Z_{22} \end{bmatrix} \quad (32)$$

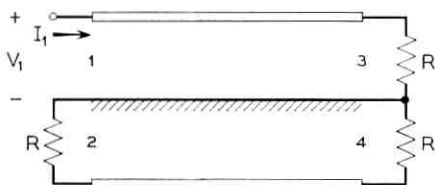


Fig. 4 — Two-terminal circuit formed by a pair of coupled lines above a ground plane loaded with resistances at three ports.

is the matrix version of the well known formula for calculating the driving point impedance at one port of a two-port when the other port is loaded. In (32)  $Z$  is the open circuit impedance matrix of the two-port at the left in Fig. 5,  $A, B, C, D$  are the matrices given by (29).

Once the  $Z$  of (32) is known the resistor  $R$  may be connected to port 2 as shown in Fig. 6 and the driving point impedance at port 1 calculated by a second application of (32) although now, instead of matrices,  $A, B, C, D$  are scalars. The matrices in (32) are all of the form

$$K = \begin{bmatrix} \alpha & \beta \\ \beta & \alpha \end{bmatrix}, \quad (33)$$

hence the methods of the appendix are applicable. Using (30) and (32)

$$Z = R_1 p + R_2 q = \left[ \begin{array}{c|c} \frac{1}{2}(p+q) & \frac{1}{2}(p-q) \\ \hline \frac{1}{2}(p-q) & \frac{1}{2}(p+q) \end{array} \right], \quad (34)$$

where  $R_1$  and  $R_2$  form the spectral set of  $Z$  and are

$$R_1 = \begin{bmatrix} \frac{1}{2} & \frac{1}{2} \\ \frac{1}{2} & \frac{1}{2} \end{bmatrix}, \quad R_2 = \begin{bmatrix} \frac{1}{2} & -\frac{1}{2} \\ -\frac{1}{2} & \frac{1}{2} \end{bmatrix}, \quad (35)$$

and  $p$  and  $q$  are the eigenvalues of  $Z$  and are

$$p = R \frac{\cosh \gamma^+ l + \frac{Z_0^+}{R} \sinh \gamma^+ l}{\frac{R}{Z_0^-} \sinh \gamma^+ l + \cosh \gamma^+ l}, \quad (36)$$

$$q = R \frac{\cosh \gamma^- l + \frac{Z_0^-}{R} \sinh \gamma^- l}{\frac{R}{Z_0^-} \sinh \gamma^- l + \cosh \gamma^- l}. \quad (37)$$

The symbols  $\gamma^+, \gamma^-$  denote the eigenvalues of  $\Gamma$ ; and  $Z_0^+, Z_0^-$  the eigenvalues of  $Z_0$ .

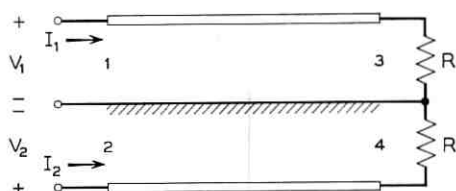


Fig. 5—Intermediate circuit for calculating the driving point impedance at port 1 of the circuit in Fig. 4.

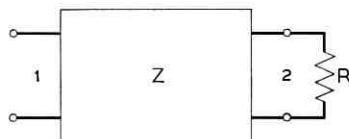


Fig. 6.—Second intermediate circuit for calculating the driving point impedance at port 1 of the circuit in Fig. 4.

To transform the  $Z_{i,j}$  of (32) to **A**, **B**, **C**, **D** matrices the well known formulas:

$$\mathbf{A} = \mathbf{Z}_{11}\mathbf{Z}_{21}^{-1}, \quad (38)$$

$$\mathbf{B} = \mathbf{Z}_{11}\mathbf{Z}_{21}^{-1}\mathbf{Z}_{22} - \mathbf{Z}_{12}, \quad (39)$$

$$\mathbf{C} = \mathbf{Z}_{21}^{-1}, \quad (40)$$

$$\mathbf{D} = \mathbf{Z}_{21}^{-1}\mathbf{Z}_{22}, \quad (41)$$

which hold for matrices (and hence for scalars considering them as  $1 \times 1$  matrices) may be used. The second application of (32) with the aid of (38)–(41) gives

$$z = \frac{(p+q)R + 2pq}{2R + p + q}. \quad (42)$$

For port 1 to be matched  $z$  must equal  $R$ , hence, the condition for directional coupler effect is

$$R = \frac{(p+q)R + 2pq}{2R + p + q},$$

which reduces to

$$R = \sqrt{pq}. \quad (43)$$

When the values given by (36) and (37) are substituted in (43), after some algebra, the following equation results:

$$\left(\frac{Z_0^+ Z_0^-}{R^2} - \frac{R^2}{Z_0^+ Z_0^-}\right) \sinh \gamma^+ l \sinh \gamma^- l + \left(\frac{Z_0^-}{R} - \frac{R}{Z_0^-}\right) \sinh \gamma^- l \cosh \gamma^+ l \\ + \left(\frac{Z_0^+}{R} - \frac{R}{Z_0^+}\right) \sinh \gamma^+ l \cosh \gamma^- l = 0. \quad (44)$$

If a matched directional coupler at all frequencies is desired, (44) must be satisfied at all frequencies. Some possible mathematical solutions are the following:

(i) Make the three terms in parentheses in (44) vanish. This happens if

$$Z_0^+ = Z_0^- = R. \quad (45)$$

(ii) A second possibility is to make

$$\gamma^+ = \gamma^- = \gamma. \quad (46)$$

Then (44) reduces to

$$\left( \frac{Z_0^+ Z_0^-}{R^2} - \frac{R^2}{Z_0^+ Z_0^-} \right) \sinh^2 \gamma l + \left( \frac{Z_0^+}{R} + \frac{Z_0^-}{R} - \frac{R}{Z_0^+} - \frac{R}{Z_0^-} \right) \sinh \gamma l \cosh \gamma l = 0. \quad (47)$$

To make the quantities in the parentheses in (47) vanish,  $R$  is given by

$$R = \sqrt{Z_0^+ Z_0^-}. \quad (48)$$

Equation (45) or (46) and (48) give possible conditions for directional coupler effect at all frequencies. If a narrow band directional coupler is desired one may match the coupler at the discrete frequencies which satisfy (47). Since (47) is a transcendental equation it is not unreasonable to expect an infinity of roots. For instance, suppose (46) holds, and  $l$  is made so that

$$\sinh \gamma l = 0. \quad (49)$$

Then the device will be a directional coupler at the frequencies that are roots of (49).

Some explicit relationships for two identical lossless lines of inductance per unit length  $L_{11}$ , mutual inductance per unit length  $L_{12}$ , capacitance per unit length of one line alone  $C$ , and capacitance between the two lines per unit length  $C_M$ , are:

$$\gamma^+ = j \sqrt{(L_{11} + L_{12})C} \omega, \quad (50)$$

$$\gamma^- = j \sqrt{(L_{11} - L_{12})(C + 2C_M)} \omega, \quad (51)$$

$$Z_0^+ = \frac{(L_{11} + L_{12})}{\sqrt{(L_{11} + L_{12})C}}, \quad (52)$$

$$Z_0^- = \frac{(L_{11} - L_{12})}{\sqrt{(L_{11} - L_{12})(C + 2C_M)}}. \quad (53)$$

The condition expressed by (45) implies, equating (52) and (53)

$$-\frac{L_{11}}{L_{12}} = \frac{C + C_M}{C_M}, \quad (54)$$

$$R = \sqrt{\frac{L_{11}}{C + C_M}}. \quad (55)$$

While the condition expressed by (46) implies

$$\frac{L_{11}}{L_{12}} = \frac{C + C_M}{C_M}, \quad (56)$$

and (48) reads

$$R = \sqrt{\frac{L_{11}}{C + C_M}},$$

which is the same as (55). Equation (54) implies that the lines have negative mutual inductance, which is not achievable with parallel lines. This condition can, however, be satisfied with counter-wound lumped elements.

If (56) holds, which implies (46) then (49) implies

$$\omega_k = \frac{k\pi}{l\sqrt{L_{12}C_M - L_{11}(C + C_M)}}, \quad k = 0, 1, 2, \dots \quad (57)$$

That is, for the frequencies given by (57), independent of the value of the loads (as long as they are all equal) the lines will be matched and will exhibit directional coupler effect.

### 3.2 Frequency Dependency of the Coupling Between the Ports

Equations (54) and (55) or alternatively (56) and (55) are not frequency-dependent. This means that the resulting circuit will be matched for all frequencies. Therefore, the directional coupler effect will exist for all frequencies, meaning that the coupling between uncoupled ports is zero at all frequencies. However, the coupling between coupled ports is frequency-dependent. This dependency is derived as follows.

Considering the coupled transmission lines as the load to four uncoupled lines, each of characteristic impedance  $R$  as shown in Fig. 7, the scattering matrix of the load is calculated according to (24) and (22) with

$$Y_0 = \begin{bmatrix} \frac{1}{R} & 0 & 0 & 0 \\ 0 & \frac{1}{R} & 0 & 0 \\ 0 & 0 & \frac{1}{R} & 0 \\ 0 & 0 & 0 & \frac{1}{R} \end{bmatrix} \quad (58)$$

and  $Z_L$  given by  $\zeta$  of (28). Applying the methods of the appendix the matrix  $\zeta$  may be expressed as follows:

$$\zeta = R_a \lambda_{fa} + R_b \lambda_{fb} + R_c \lambda_{fc} + R_d \lambda_{fd}, \quad (59)$$

where  $R_a, R_b, R_c, R_d$  are the spectral set of  $\zeta$  and they are given by (165)–(168) of the appendix and  $\lambda_{fa}, \lambda_{fb}, \lambda_{fc}, \lambda_{fd}$  are the eigenvalues of  $\zeta$  and are given by

$$\lambda_{fa} = \coth(\gamma^+ l) Z_0^+ + \operatorname{cosech}(\gamma^+ l) Z_0^+, \quad (60)$$

$$\lambda_{fb} = \coth(\gamma^+ l) Z_0^+ - \operatorname{csch}(\gamma^+ l) Z_0^+, \quad (61)$$

$$\lambda_{fc} = \coth(\gamma^- l) Z_0^- + \operatorname{csch}(\gamma^- l) Z_0^-, \quad (62)$$

$$\lambda_{fd} = \coth(\gamma^- l) Z_0^- - \operatorname{csch}(\gamma^- l) Z_0^-. \quad (63)$$

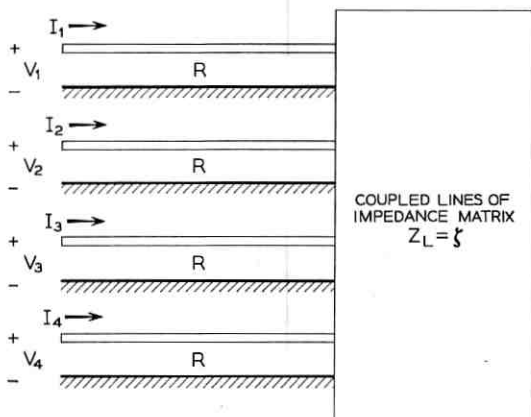


Fig. 7—Two coupled lines above a ground plane of impedance matrix given by equation (28) serve as load to four uncoupled lines of characteristic impedance  $R$  for calculation of scattering matrix of coupled lines.

The matrix  $\mathbf{S}$  may be written

$$\mathbf{S} = \mathbf{R}_a \lambda_{S_a} + \mathbf{R}_b \lambda_{S_b} + \mathbf{R}_c \lambda_{S_c} + \mathbf{R}_d \lambda_{S_d}, \quad (64)$$

where the eigenvalues of  $\mathbf{S}$  are

$$\lambda_{S_a} = \frac{\lambda_{f_a} - R}{\lambda_{f_a} + R}, \quad (65)$$

$$\lambda_{S_b} = \frac{\lambda_{f_b} - R}{\lambda_{f_b} + R}, \quad (66)$$

$$\lambda_{S_c} = \frac{\lambda_{f_c} - R}{\lambda_{f_c} + R}, \quad (67)$$

$$\lambda_{S_d} = \frac{\lambda_{f_d} - R}{\lambda_{f_d} + R}. \quad (68)$$

If the values of  $\lambda_{f_a}$ ,  $\lambda_{f_b}$ ,  $\lambda_{f_c}$ ,  $\lambda_{f_d}$  are substituted in (65)–(68) and those are in turn substituted into (64) while the conditions indicated by (46) and (48) are imposed, the following result is obtained after some algebra

$$\mathbf{S} = \begin{bmatrix} 0 & S_{12} & S_{13} & 0 \\ S_{12} & 0 & 0 & S_{13} \\ S_{13} & 0 & 0 & S_{12} \\ 0 & S_{13} & S_{12} & 0 \end{bmatrix}; \quad (69)$$

where

$$S_{12} = \frac{\left( \sqrt{\frac{Z_0^+}{Z_0}} - \sqrt{\frac{Z_0^-}{Z_0}} \right) \sinh \gamma l}{2 \cosh \gamma l + \left( \sqrt{\frac{Z_0^+}{Z_0}} + \sqrt{\frac{Z_0^-}{Z_0}} \right) \sinh \gamma l}, \quad (70)$$

$$S_{13} = \frac{2}{2 \cosh \gamma l + \left( \sqrt{\frac{Z_0^+}{Z_0}} + \sqrt{\frac{Z_0^-}{Z_0}} \right) \sinh \gamma l}; \quad (71)$$

where

$$\gamma = j\omega \sqrt{(L_{11} + L_{12})C}, \quad (72)$$

$$Z_0^+ = \sqrt{\frac{L_{11} + L_{12}}{C}}, \quad (73)$$

$$Z_0^- = \frac{L_{11} - L_{12}}{\sqrt{C(L_{11} + L_{12})}}. \quad (74)$$

If, instead of the condition of (46), the one of (45) is imposed plus (48) then the following result is obtained

$$\mathbf{S} = \begin{bmatrix} 0 & 0 & S_{13} & S_{14} \\ 0 & 0 & S_{14} & S_{13} \\ S_{13} & S_{14} & 0 & 0 \\ S_{14} & S_{13} & 0 & 0 \end{bmatrix}; \quad (75)$$

where

$$S_{13} = \frac{\frac{1}{2}}{\cosh \gamma^+ l + \sinh \gamma^+ l} + \frac{\frac{1}{2}}{\cosh \gamma^- l + \sinh \gamma^- l}, \quad (76)$$

$$S_{14} = \frac{\frac{1}{2}}{\cosh \gamma^+ l + \sinh \gamma^+ l} - \frac{\frac{1}{2}}{\cosh \gamma^- l + \sinh \gamma^- l}; \quad (77)$$

where

$$Z_0 = \sqrt{\frac{L_{11}}{C + C_M}}, \quad (78)$$

$$\gamma^+ = \frac{j\omega(L_{11} + L_{12})}{Z_0}, \quad (79)$$

$$\gamma^- = \frac{j(L_{11} - L_{12})\omega}{Z_0}. \quad (80)$$

The matrices of (69) and (75) with the aid of (70)–(74) and (76)–(80) give the frequency dependency of the coupling between the ports for the two types of directional couplers derived (matched at all frequencies)

#### IV. EXPLANATION OF THE EFFECT

Two sets of conditions have been derived for obtaining the directional coupler effect at all frequencies for transmission lines. Fig. 8 represents a pair of lossless lines  $c, d$  which are coupled from  $x = -l$  to  $x = 0$ . The coupled lines are connected to four (uncoupled) lossless transmission lines  $a, b, e, f$ , each of characteristic impedance  $R$  and each terminated in  $R$ . The matrix  $Z_0$  is the characteristic impedance matrix of the set of coupled lines ( $c$  and  $d$  in Fig. 8) and  $\Gamma$  its propagation matrix.

Consider a case in which the eigenvalues of the matrix  $Z_0$  of the lines  $c, d$  satisfy

$$R = Z_0^+ = Z_0^-,$$

which implies

$$Z_0 = RI^*,$$

where  $I$  is the unit matrix. Assume that a pulse travelling down line  $a$  occupies at time  $t_1$  the position shown in Fig. 8. Lines  $a$  and  $b$  together may be considered as a particular case of a set of multiple lines, in which both  $(Z_0)_{ab}$  and  $(\Gamma)_{ab}$ —the characteristic impedance and propagation matrices of lines  $a$ ,  $b$ —are diagonal because lines  $a$  and  $b$  are uncoupled. Thus it is convenient to think of the pulse traveling down line  $a$  as a vector of pulses traveling down the two lines  $a$ ,  $b$ ; the second component of the vector which corresponds to line  $b$  being zero. When the vector of pulses arrives at the position  $x = -l$ , indicated by  $M$  in Fig. 8, the vector of pulses continue "seeing" the same characteristic

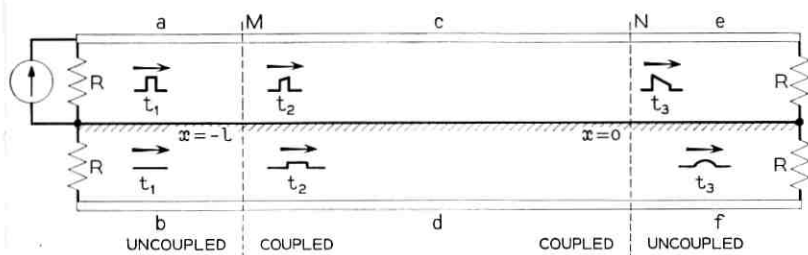


Fig. 8—Pair of coupled lossless lines  $c$  and  $d$  above a ground plane which has uncoupled terminated lines  $a$ ,  $b$ ,  $e$ ,  $f$  of characteristic impedances  $R$ . This shows the progress of a pulse to explain the directional coupler effect in physical terms for a coupler with diagonal characteristic impedance matrix.

impedance matrix  $RI$  as before and hence no reflection of the vector is created at  $M$ .

In a vector formulation one speaks of reflections in a multidimensional sense. The voltage on line  $a$  may give rise to a reflected voltage on line  $a$  [self reflection] or to a reflected voltage on line  $b$  [mutual reflection]. If all the lines are self matched and mutually matched there will be no reflections whatever. Often a line might be self matched but not mutually matched; then no self reflection will occur, but a mutual reflection will.

At time  $t_2$  the second component of the vector pulse is no longer zero because the pulse on line  $c$  which is coupled to line  $d$  induces a pulse on line  $d$  as shown in Fig. 8. These component pulses will be

\* Although for simplicity in the explanations, parallel lines are assumed, this kind of coupler requires negative mutual inductances which are in general achieved with counter-wound helices.

distorted because continually varying portions of them travel at different speeds on the lines  $c$  and  $d$ .<sup>\*</sup> When they reach  $x = 0$  marked by  $N$  in Fig. 8, the vector again continues to see the same characteristic impedance matrix and hence no reflections are caused at  $N$ . Finally the pulses travel out on lines  $e$  and  $f$  and are dissipated at the resistances  $R$ .

From this it is clear that the two ports at  $M$  are uncoupled and also the two ports at  $N$  are uncoupled. However a port at  $M$  is coupled to both ports at  $N$  and vice versa. All the ports are self matched. This explanation suggests a simple way of determining the conditions for a nonsymmetric coupler realized with transmission lines. Assume lines  $c$  and  $d$  are no longer identical but that the characteristic impedance matrix of the set is still diagonal

$$\mathbf{Z}_0 = \begin{bmatrix} (Z_0)_{11} & 0 \\ 0 & (Z_0)_{22} \end{bmatrix}$$

while the propagation matrix  $\Gamma$  is not. If the lines  $a$  and  $e$  have characteristic impedance  $(Z_0)_{11}$  and lines  $b$  and  $f$  have characteristic impedance  $(Z_0)_{22}$  and  $a, b, e, f$  are properly terminated, the coupled lines  $c, d$  will constitute a matched nonsymmetric directional coupler since the discussion above holds for this case without modification.

A physical account of the directional coupler satisfying

$$\begin{aligned} \gamma^+ &= \gamma^- = \gamma, \\ R &= \sqrt{\frac{L_{11}}{C + 2C_M}}, \end{aligned}$$

is as follows.

Fig. 9 shows the same arrangement as Fig. 8. A pulse traveling to the right on line  $a$  is shown at  $t = t_1$ . The second component of the incident pulse corresponding to line  $b$  is zero since lines  $a$  and  $b$  are uncoupled. As the vector of pulses reaches the position  $M$ , the vector of voltage is reflected according to a reflection matrix because for this case, the vector no longer sees the same characteristic impedance matrix in the transition from lines  $a, b$  to lines  $c, d$ . However, because line  $a$  matches line  $c$  there is no self reflection; only a mutual reflection appears on line  $b$ . Besides the reflected pulse, an identical transmitted pulse appears on line  $d$  at time  $t_2$  as indicated in Fig. 9. The appearance

<sup>\*</sup> The propagation matrix should not have equal eigenvalues, otherwise it will be diagonal which, together with a diagonal characteristic impedance, implies uncoupled lines.

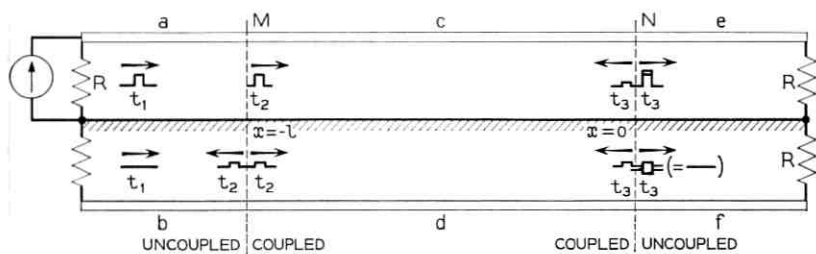


Fig. 9—Same structure as in Fig. 8 showing the progress of a pulse for a coupler with scalar propagation matrix.

of the mutual reflection indicates that the two ports at  $M$  are coupled.

After  $t_2$ , as the two forward pulses travel along lines  $c$  and  $d$  they do so at the same speed, without distortion and do not interact with each other since the propagation matrix is diagonal. As the two pulses arrive at point  $N$  they encounter a reflection matrix of opposite sign to the one they encountered at  $M$ . This means that the pulse on line  $c$  passes through  $N$  undisturbed but creates on lines  $d$  and  $f$  reflected and transmitted pulses identical to the ones created at  $M$  but of opposite sign. Likewise, the incident pulse on line  $d$  goes right through  $N$  (since each individual line is matched) creating transmitted and reflected pulses on lines  $e$  and  $c$ , but being cancelled on line  $f$  by the transmitted pulse created by the incident pulse on line  $c$ ; thus, nothing comes out of line  $f$ .

At time  $t_3$  right after the reflection at  $N$  the situation is depicted in Fig. 9. After  $t_3$  the reflected pulses are traveling to the left at the same speed undisturbed and undistorted on lines  $c$  and  $d$ . As they arrive from the right at point  $M$  the pulse on line  $d$  goes out line  $b$  undisturbed but creating transmitted and reflected pulses on lines  $a$  and  $c$ . Likewise the pulse on line  $c$  goes out line  $a$  undisturbed creating transmitted and reflected pulses on lines  $b$  and  $d$ , but being cancelled on line  $a$  by the transmitted pulse created by the incident pulse on line  $d$ . This eliminates any delayed reflections on line  $a$  to the original incident pulse. The process continues in the same manner, the outgoing pulses on lines  $a$  and  $f$  always being such that they cancel. This means that the ports associated with lines  $a$  and  $f$  are uncoupled, but the ports of lines  $a$ ,  $b$  and  $e$  are coupled.

It is clear that what is necessary for directional coupler effect on this type of coupler is: all ports self matched, equal propagation velocities without attenuation or distortion. Hence it should be possible to realize a nonsymmetrical directional coupler of this type whose propaga-

tion matrix is a scalar matrix\* by self matching its ports. This may be useful for interconnecting lines  $a$  and  $b$  of different characteristic impedances.

Because the reasoning above was made in the time domain with pulses of arbitrary shape, the results hold for all frequencies. This is an example of the gain in insight owing to the vector-matrix formulation.

## V. EXTENSION OF THE THEORY

### 5.1 Matrices for a $2N$ -Port

Let us generalize several concepts introduced in Section 2.1. Consider a  $(2N + 1)$ -terminal network in which terminal  $2N + 1$  will be grounded and ports from terminals 1 through  $2N$  to ground will be considered. Ports 1 to  $N$  will be considered input ports and Ports  $N + 1$  to  $2N$  output ports. Suppose the  $2N$ -port is characterized by  $\mathbf{A}$ ,  $\mathbf{B}$ ,  $\mathbf{C}$ ,  $\mathbf{D}$   $N \times N$  matrices. (Extensions to  $2N$ -ports of the  $A$ ,  $B$ ,  $C$ ,  $D$  parameters of a two-port). Assume the circuit is such that

$$\mathbf{A} = \mathbf{D}, \quad (81)$$

$$\mathbf{A}^2 - \mathbf{BC} = \mathbf{I}, \quad (82)$$

where  $\mathbf{I}$  is the  $N \times N$  unit matrix and  $\mathbf{A}$ ,  $\mathbf{B}$ ,  $\mathbf{C}$  are  $N \times N$  symmetric matrices which commute.

By analogy with a multiple transmission line the characteristic impedance matrix  $\mathbf{Z}_0$  and the propagation matrix  $\mathbf{\Gamma}$  are defined so that they satisfy the following equations:

$$\mathbf{A} = \cosh \mathbf{\Gamma}, \quad (83)$$

$$\mathbf{B} = \sinh \mathbf{\Gamma}, \quad (84)$$

$$\mathbf{C} = \mathbf{Z}_0^{-1} \sinh \mathbf{\Gamma}. \quad (85)$$

Solving for  $\mathbf{\Gamma}$  and  $\mathbf{Z}_0$

$$\mathbf{\Gamma} = \cosh^{-1} \mathbf{A} = \sinh^{-1} \mathbf{B}, \quad (86)$$

$$\mathbf{Z}_0 = \sqrt{\mathbf{BC}^{-1}}. \quad (87)$$

The  $N \times N$  matrices  $\mathbf{\Gamma}$  and  $\mathbf{Z}_0$  will also be symmetric and commute. The matrix  $\mathbf{Z}_0$  is the open circuit impedance matrix of that network which, when connected to the output ports  $N + 1$  through  $2N$  of

\* A scalar matrix is the unit matrix multiplied by a scalar.

the circuit whose  $\mathbf{A}$ ,  $\mathbf{B}$ ,  $\mathbf{C}$  matrices are those of (86) and (87), will result in an open circuit impedance matrix of  $\mathbf{Z}_0$  when the circuit is viewed at its ports 1 through  $N$ . This property is analogous to the one of the characteristic impedance matrices of a set of multiple coupled transmission lines. The matrix  $\mathbf{\Gamma}$ , has virtually the same properties of the matrix  $\mathbf{\Gamma}l$  of a set of coupled lines (although the single quantity  $l$  loses its significance as a length in case the  $2N$ -port is a lumped circuit). For instance, if  $n$  identical  $2N$ -ports are cascaded the resulting  $2N$ -port has a propagation matrix equal to  $n\mathbf{\Gamma}$ .

The matrices  $\mathbf{\Gamma}$  and  $\mathbf{Z}_0$  may be expressed in terms of the  $2N \times 2N$  impedance matrix  $\mathbf{Z}$  of the  $2N$ -port with the aid of (38) through (41)

$$\mathbf{\Gamma} = \cosh^{-1} (\mathbf{Z}_{11}\mathbf{Z}_{21}^{-1}), \quad (88)$$

$$\mathbf{Z}_0 = \sqrt{\mathbf{Z}_{11}^2 - \mathbf{Z}_{12}^2}; \quad (89)$$

where the  $\mathbf{Z}$  matrix is partitioned as follows:

$$\mathbf{Z} = \left[ \begin{array}{c|c} \mathbf{Z}_{11} & \mathbf{Z}_{12} \\ \hline \mathbf{Z}_{21} & \mathbf{Z}_{22} \end{array} \right], \quad (90)$$

the submatrices  $\mathbf{Z}_{11}$ ,  $\mathbf{Z}_{12}$ ,  $\mathbf{Z}_{21}$ ,  $\mathbf{Z}_{22}$  are  $N \times N$  symmetric matrices and commute with each other. The characteristic impedance matrix may also be expressed in terms of the so-called open and short impedance matrices. If the  $N$ -vector  $\mathbf{V}_1$  and  $\mathbf{I}_1$  denote the voltages and currents at the  $N$  input ports and  $\mathbf{V}_2$  and  $\mathbf{I}_2$  denote the voltages and currents at the output ports, then if  $\mathbf{I}_2 = \mathbf{0}$ , that is, the terminals on the output ports are open then

$$\mathbf{V}_1 = \mathbf{A}\mathbf{V}_2, \quad (91)$$

$$\mathbf{I}_1 = \mathbf{C}\mathbf{V}_2. \quad (92)$$

Solving for  $\mathbf{V}_2$  in (92) and substituting in (91)

$$\mathbf{V}_1 = \mathbf{A}\mathbf{C}^{-1}\mathbf{I}_1. \quad (93)$$

which shows that the  $N \times N$  impedance matrix  $\mathbf{Z}_{0c}$  seen at the input ports is

$$\mathbf{Z}_{0c} = \mathbf{A}\mathbf{C}^{-1}. \quad (94)$$

Now, if the output ports are shorted, that is  $\mathbf{V}_2 = \mathbf{0}$  then

$$\mathbf{V}_1 = \mathbf{B}\mathbf{I}_2, \quad (95)$$

$$\mathbf{I}_1 = \mathbf{A}\mathbf{I}_2, \quad (96)$$

from which

$$\mathbf{V}_1 = \mathbf{B}\mathbf{A}^{-1}\mathbf{I}_1. \quad (97)$$

That is the  $N \times N$  impedance matrix with the output terminals shorted  $\mathbf{Z}_{s_e}$  is

$$\mathbf{Z}_{s_e} = \mathbf{B}\mathbf{A}^{-1}. \quad (98)$$

From Eqs. (94) and (98) it is seen that

$$\mathbf{Z}_0 = \sqrt{\mathbf{Z}_{s_e}\mathbf{Z}_{0e}}. \quad (99)$$

Equation (99) gives an experimental method of determining  $\mathbf{Z}_0$  if it is known that the network satisfies equations (81) and (82), and the symmetry and commutativity conditions.

### 5.2 Multiport Circuits and Multiple Transmission

It is often convenient to analyze some lumped or distributed (or combinations of lumped and distributed) systems as though they were multiple transmission lines using such concepts as reflection matrix and incident voltage.

Consider the connection shown in Fig. 10. Each network is an  $(2N+1)$ -terminal network in which ports from each terminal to ground are made. Ports 1 through  $N$  and  $1'$  through  $N'$  are considered input ports. Ports  $N+1$  through  $2N$  and  $(N+1)'$  through  $(2N)'$  are considered output ports. The voltage vector at the junction  $B$  whose components are the voltages of nodes  $N+1, N+2, \dots, 2N$  to ground is denoted by  $\mathbf{V}_B$ .

The vectors  $\mathbf{v}_+, \mathbf{v}_-, \mathbf{i}_+, \mathbf{i}_-$ , called incident voltage, reflected voltage, incident current, and reflected current at the junction  $B$  (assuming the direction of propagation from left to right), are defined to satisfy

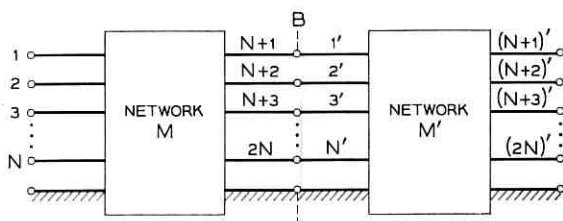


Fig. 10—Connection of two  $2N$  ports in cascade used to define the reflection matrix.

$$\mathbf{V}_B = \mathbf{v}_+ + \mathbf{v}_-, \quad (100)$$

$$\mathbf{I}_B = \mathbf{i}_+ - \mathbf{i}_-, \quad (101)$$

$$\mathbf{i}_+ = \mathbf{Z}^{-1}\mathbf{v}_+, \quad (102)$$

$$\mathbf{i}_- = \mathbf{Z}^{-1}\mathbf{v}_-; \quad (103)$$

where  $\mathbf{I}_B$  is the  $N$ -vector whose components are the currents flowing out of terminals  $N+1, N+2, \dots, 2N$  and into terminals  $1', 2', \dots, N'$ ;  $\mathbf{Z}$  is the  $N \times N$  open-circuit impedance matrix of network  $M$  seen from the ports  $N+1, N+2, \dots, 2N$  with network  $M'$  disconnected.

The reflection matrix  $\Gamma_{MM'}$  is defined according to

$$\mathbf{v}_+ = \Gamma_{MM'}\mathbf{v}_-. \quad (104)$$

The matrix  $\Gamma_{MM'}$  satisfies the following relationship:

$$\Gamma_{MM'} = (\mathbf{Z}'\mathbf{Z}^{-1} + \mathbf{I})^{-1}(\mathbf{Z}'\mathbf{Z}^{-1} - \mathbf{I}), \quad (105)$$

where  $\mathbf{Z}'$  is the  $N \times N$  open-circuit impedance matrix of network  $M'$  as seen from ports  $1', 2', \dots, N'$  with network  $M$  disconnected.  $\mathbf{I}$  is the  $N \times N$  unit matrix. The indices  $MM'$  on  $\Gamma_{MM'}$  indicate the direction of propagation from  $M$  to  $M'$ . If the indices are reversed the roles of  $\mathbf{Z}'$  and  $\mathbf{Z}$  are reversed, that is

$$\Gamma_{M'M} = (\mathbf{Z}(\mathbf{Z}')^{-1} + \mathbf{I})(\mathbf{Z}(\mathbf{Z}')^{-1} - \mathbf{I}). \quad (106)$$

The transmission matrix  $\mathbf{T}_{MM'}$  is defined by

$$\mathbf{V}_B = \mathbf{T}_{MM'}\mathbf{v}_+. \quad (107)$$

Hence  $\mathbf{T}_{MM'}$  satisfies

$$\mathbf{T}_{MM'} = \mathbf{I} + \Gamma_{MM'}. \quad (108)$$

### 5.3 Directional Coupler Equations

Taking advantage of the derivations done for transmission line directional couplers and the analogies introduced in Sections 5.1 and 5.2, it is possible to write without further work, the equations of a directional coupler having the same mathematical symmetry of a multiple transmission line directional coupler but which may have lumped components or combinations of lumped and distributed components. Suppose a four-port is characterized by its  $\mathbf{E}$  matrix whose  $2 \times 2$  submatrices  $\mathbf{A}, \mathbf{B}, \mathbf{C}, \mathbf{D}$  have the form of the matrix  $\mathbf{K}$  of equation (1) of the Appendix and satisfy equations (81) and (82). Without any further work it can be stated that if the load impedance  $z$  and the

four port satisfy for some frequency the equation

$$z = Z_0^+ = Z_0^-, \quad (109)$$

the device will be a directional coupler for that frequency.

This result is deduced from equation (45). Likewise from equation (46) it may be deduced that if the four port is such that

$$\gamma^+ = \gamma^-, \quad (110)$$

and

$$z = \sqrt{Z_0^+ Z_0^-}, \quad (111)$$

then the device will also be a directional coupler for those frequencies for which (110) and (111) are satisfied.

It is convenient at this point to exemplify with a simple lumped circuit.

Consider the four-port lumped circuit shown in Fig. 11. The E matrix of the circuit of Fig. 11 may be calculated by cascading 3 sections, the first and third containing only capacitors and the second containing the inductors and mutuals. By proceeding carefully much labor can be saved using the spectral sets given in the Appendix. The results are

$$\mathbf{E} = \left[ \frac{\mathbf{I}}{\mathbf{Y}} \middle| \frac{\mathbf{0}}{\mathbf{I}} \right] \left[ \frac{\mathbf{I}}{\mathbf{0}} \middle| \frac{\mathbf{Z}}{\mathbf{I}} \right] \left[ \frac{\mathbf{I}}{\mathbf{Y}} \middle| \frac{\mathbf{0}}{\mathbf{I}} \right] = \left[ \frac{\mathbf{I} + \mathbf{ZY}}{(\mathbf{YZ} + 2\mathbf{I})\mathbf{Y}} \middle| \frac{\mathbf{Z}}{\mathbf{YZ} + \mathbf{I}} \right]; \quad (112)$$

where

$$\mathbf{Y} = \mathcal{S} \begin{bmatrix} C + C_M & -C_M \\ -C_M & C + C_M \end{bmatrix},$$

$$\mathbf{Z} = \mathcal{S} \begin{bmatrix} L_{11} & L_{12} \\ L_{12} & L_{11} \end{bmatrix}.$$

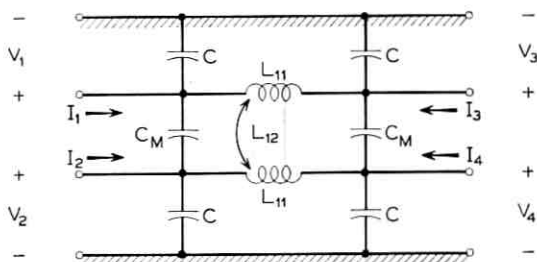


Fig. 11 — Four-port lumped circuit that can be used as a directional coupler.

From (86) the hyperbolic sine and cosine of the propagation matrix is

$$\begin{aligned} \cosh \Gamma &= \frac{1}{2} \begin{bmatrix} 1 & 1 \\ 1 & 1 \end{bmatrix} [1 + S^2 C(L_{11} + L_{12})] \\ &+ \frac{1}{2} \begin{bmatrix} 1 & -1 \\ -1 & 1 \end{bmatrix} [1 + S^2(C + 2C_M)(L_{11} - L_{12})], \end{aligned} \quad (113)$$

$$\sinh \Gamma = \frac{1}{2} \begin{bmatrix} 1 & 1 \\ 1 & 1 \end{bmatrix} S(L_{11} + L_{12}) + \frac{1}{2} \begin{bmatrix} 1 & -1 \\ -1 & 1 \end{bmatrix} S(L_{11} - L_{12}). \quad (114)$$

From (87) the characteristic impedance matrix is found to be

$$\begin{aligned} \mathbf{Z}_0 &= \frac{1}{2} \begin{bmatrix} 1 & 1 \\ 1 & 1 \end{bmatrix} \left( \frac{(L_{11} + L_{12})}{[S^2 C(L_{11} + L_{12}) + 2]C} \right)^{\frac{1}{2}} + \frac{1}{2} \begin{bmatrix} 1 & -1 \\ -1 & 1 \end{bmatrix} \\ &\cdot \left( \frac{(L_{11} - L_{12})}{[S^2(C + 2C_M)(L_{11} - L_{12}) + 2](C + 2C_M)} \right)^{\frac{1}{2}} \end{aligned} \quad (115)$$

The condition expressed by (109) is, for this case,

$$\begin{aligned} z &= \left( \frac{L_{11} + L_{12}}{[S^2 C(L_{11} + L_{12}) + 2]C} \right)^{\frac{1}{2}} \\ &= \left( \frac{L_{11} - L_{12}}{[S^2(C + 2C_M)(L_{11} - L_{12}) + 2](C + 2C_M)} \right)^{\frac{1}{2}}. \end{aligned} \quad (116)$$

The second and third members of (116) imply

$$\begin{aligned} [S^2(L_{11}^2 - L_{12}^2)(C + 2C_M) + 2(L_{11} + L_{12})](C + 2C_M) \\ = [S^2 C(L_{11}^2 - L_{12}^2) + 2(L_{11} - L_{12})]C. \end{aligned} \quad (117)$$

If this condition is to be satisfied at all frequencies then

$$(L_{11}^2 - L_{12}^2)(C + 2C_M)^2 = (L_{11}^2 - L_{12}^2)C^2, \quad (118)$$

$$2(L_{11} + L_{12})(C + 2C_M) = 2(L_{11} - L_{12})C. \quad (119)$$

Both (118) and (119) are satisfied for the following choice:  $L_{11} = -L_{12}$ ,  $C = 0$ . Thus the circuit of Fig. 11 with  $C = 0$  and  $L_{11} = -L_{12}$  (perfectly coupled counterwound inductors) is a directional coupler at all frequencies, provided it is loaded at all ports with the impedance

$$z = \left( \frac{L_{11}}{4L_{11}C_M S^2 + 2C_M} \right)^{\frac{1}{2}}. \quad (120)$$

The impedance  $z$  is frequency dependent. The voltage ratios will be given by (76) and (77),\* that is

$$S_{13} = \frac{1}{2} \left( 1 + \frac{1}{4C_M L_{11} S^2 + 1} \right), \quad (121)$$

$$S_{14} = \frac{1}{2} \left( 1 - \frac{1}{4C_M L_{11} S^2 + 1} \right). \quad (122)$$

#### 5.4 Equations in Terms of $\mathbf{A}$ , $\mathbf{B}$ , $\mathbf{C}$ , $\mathbf{D}$ Matrices

It is often convenient to express the equations of a directional coupler in terms of the  $\mathbf{A}$ ,  $\mathbf{B}$ ,  $\mathbf{C}$ ,  $\mathbf{D}$  matrices directly instead of the  $\mathbf{Z}_0$  and  $\mathbf{\Gamma}$  matrices. For this purpose assume a lossless reciprocal four-port is characterized in terms of its  $\mathbf{A}$ ,  $\mathbf{B}$ ,  $\mathbf{C}$ ,  $\mathbf{D}$  matrices which are of the form of the matrix  $\mathbf{K}$  of equation (150) of the Appendix. Assume  $\mathbf{A} = \mathbf{D}$ . The condition  $\mathbf{A}^2 - \mathbf{BC} = \mathbf{I}$  is automatically satisfied if the circuit is reciprocal.  $\mathbf{A}$ ,  $\mathbf{B}$ ,  $\mathbf{C}$ ,  $\mathbf{D}$  commute, since they have the same eigenvectors. Because all matrices commute they may be treated without ambiguity as scalars. The open circuit impedance matrix is

$$\zeta = \left[ \begin{array}{c|c} \mathbf{AC}^{-1} & \mathbf{C}^{-1} \\ \mathbf{C}^{-1} & \mathbf{AC}^{-1} \end{array} \right]. \quad (123)$$

Suppose the ports are loaded with equal impedance  $z$ . The impedance matrix  $\zeta$  normalized with respect to the matrix  $z\mathbf{I}$  is

$$\zeta_n = \left[ \begin{array}{c|c} \mathbf{AC}^{-1}z^{-1} & \mathbf{C}^{-1}z^{-1} \\ \mathbf{C}^{-1}z^{-1} & \mathbf{AC}^{-1}z^{-1} \end{array} \right]. \quad (124)$$

The eigenvalues of  $\zeta_n$  are

$$\lambda_a = \frac{A^+ + 1}{zC^+}, \quad (125)$$

$$\lambda_b = \frac{A^+ - 1}{zC^+}, \quad (126)$$

$$\lambda_c = \frac{A^- + 1}{zC^-}, \quad (127)$$

$$\lambda_d = \frac{A^- - 1}{zC^-}; \quad (128)$$

where  $A^+$ ,  $A^-$ ,  $C^+$ ,  $C^-$  are the eigenvalues of  $\mathbf{A}$  and  $\mathbf{C}$  associated with the sum and difference modes. (See Appendix.) The reflection matrix

\* Because for lumped elements  $\mathbf{\Gamma}$  corresponds to  $\mathbf{\Gamma}l$  in using the formulas derived for distributed elements for circuits with lumped elements one should take  $l = 1$ .

(or scattering matrix) is

$$\Gamma_R = (\zeta_n - I)(\zeta_n + I)^{-1}, \quad (129)$$

which may be written

$$\Gamma_R = R_a \frac{\lambda_a - 1}{\lambda_a + 1} + R_b \frac{\lambda_b - 1}{\lambda_b + 1} + R_c \frac{\lambda_c - 1}{\lambda_c + 1} + R_d \frac{\lambda_d - 1}{\lambda_d + 1}; \quad (130)$$

where  $R_a, R_b, R_c, R_d$  are the members of the spectral set of  $\zeta_n$  and which are given by equations (165) to (168) of the appendix.

To find the condition for self match at port 1 (which because of the symmetry gives the condition of self match at any port) the eigenvalues given by equations (125) to (128) are substituted in (130) and the upper left corner of  $\Gamma_R$  is equated to zero. After some algebra this yields

$$\begin{aligned} & [(A^- + zC^-)^2 - 1][(A^+)^2 - (zC^+)^2 - 1] \\ & + [(A^+ + zC^+)^2 - 1][(A^-)^2 - (zC^-)^2 - 1] = 0. \end{aligned} \quad (131)$$

Equation (131) is a quartic in  $z$  which may be rewritten

$$\begin{aligned} & z^4(C^+C^-) + z^3(C^+A^- + C^-A^+) \\ & - z(A^+B^- + B^+A^-) - B^+B^- = 0 \end{aligned} \quad (132)$$

The solutions of Equation (118) give the values of the impedances which will match the four ports in terms of the eigenvalues of the matrices  $A, B, C$ . Although a quartic algebraic equation can be solved in terms of the coefficients, the solution is extremely cumbersome algebraically and it would be very difficult to see the effect of varying the quantities  $A^+, A^-, B^+, B^-, C^+, C^-$ . A sounder approach is probably to look at particular simple cases. For instance if

$$C^+ = 0 \quad \text{and} \quad B^- = 0, \quad (133)$$

Equation (132) reduces to

$$z^3(C^-A^+) - z(B^+A^-) = 0,$$

whose solutions are

$$z = 0 \quad \text{and} \quad z = \sqrt{\frac{B^+A^-}{C^-A^+}}. \quad (134)$$

A second possibility is

$$C^+ = 0, \quad A^+ = 0. \quad (135)$$

Eq. (132) then reduces to

$$-z(B^+ A^-) - B^+ B^- = 0,$$

whose solution is

$$z = -\frac{B^-}{A^-}. \quad (136)$$

Obviously there are many possibilities. Some of the solutions are not immediately apparent. For instance from equations (46) and (48) if

$$A^+ = A^-, \quad (137)$$

then

$$z = \sqrt[4]{\frac{B^+ B^-}{C^+ C^-}} \quad (138)$$

is a root of equation (132). This fact can only be seen after a good deal of algebra, for this reason it is convenient to express (132) in different ways so that different possibilities may be "seen." With this in mind equation (129) may be written

$$\Gamma_R = \mathbf{I} - 2(\zeta_n + \mathbf{I})^{-1}. \quad (139)$$

Using the spectral set of  $\zeta_n$  the following alternative expression for the condition for the self-match of all ports is obtained

$$\begin{aligned} \frac{1}{4} \frac{2}{\frac{A^+ + 1}{zC^+} + 1} + \frac{1}{4} \frac{2}{\frac{A^+ - 1}{zC^+} + 1} \\ + \frac{1}{4} \frac{2}{\frac{A^- + 1}{zC^-} + 1} + \frac{1}{4} \frac{2}{\frac{A^- - 1}{zC^-} + 1} = 1, \end{aligned}$$

which after some algebra may be written

$$\frac{(A^+ + zC^+)zC^+}{(A^+ + zC^+)^2 - 1} + \frac{(A^- + zC^-)zC^-}{(A^- + zC^-)^2 - 1} = 1. \quad (140)$$

It is simpler (although not trivial) to verify that the conclusions associated with equations (137) and (138) are true from (140) than from (132).

The reflected voltages caused by an incident voltage at port 1 may be obtained from equation (130).

$$\frac{V_{2-}}{V_{1+}} = \frac{(A^+)^2 - (zC^+)^2 - 1}{2[(A^+ + zC^+)^2 - 1]} - \frac{(A^-)^2 - (zC^-)^2 - 1}{2[(A^- + zC^-)^2 - 1]}, \quad (141)$$

$$\frac{V_{3-}}{V_{1+}} = \frac{zC^+}{(A^+ + zC^+)^2 - 1} + \frac{zC^-}{(A^- + zC^-)^2 - 1}, \quad (142)$$

$$\frac{V_{4-}}{V_{1+}} = \frac{zC^+}{(A^+ + zC^+)^2 - 1} - \frac{zC^-}{(A^- + zC^-)^2 - 1}. \quad (143)$$

Equations (123) through (143) all are good for any four-port, whether lumped, distributed, or made with combinations of lumped and distributed elements.

### 5.5 A Degenerate Situation:

Consider the circuit of Fig. 12. Notice the structure is not physically symmetrical. The **A**, **B**, **C**, **D** matrices of the circuit are

$$\begin{bmatrix} \mathbf{A} & \mathbf{B} \\ \mathbf{C} & \mathbf{D} \end{bmatrix} = \begin{bmatrix} \mathbf{I} & \mathbf{0} \\ \mathbf{Y} & \mathbf{I} \end{bmatrix} \begin{bmatrix} \mathbf{I} & \mathbf{Z} \\ \mathbf{0} & \mathbf{I} \end{bmatrix} = \begin{bmatrix} -\mathbf{I} & \mathbf{Z} \\ \mathbf{Y} & \mathbf{YZ} + \mathbf{I} \end{bmatrix} \quad (144)$$

where

$$\mathbf{Z} = \begin{bmatrix} 1 & 1 \\ 1 & 1 \end{bmatrix} 2SL_{11}, \quad \mathbf{Y} = \begin{bmatrix} 1 & -1 \\ -1 & 1 \end{bmatrix} 2SC_M$$

Although in equation (144) **A** and **D** are apparently not equal, it turns out that **Y** and **Z** are orthogonal and therefore **YZ** = **0**. Thus (144) reads

$$\begin{bmatrix} \mathbf{A} & \mathbf{B} \\ \mathbf{C} & \mathbf{D} \end{bmatrix} = \begin{bmatrix} \mathbf{I} & \mathbf{Z} \\ \mathbf{Y} & \mathbf{I} \end{bmatrix}. \quad (145)$$

The matrices **A**, **B**, **C**, **D** commute and satisfy equations (81) and (82). Thus, although the structure is not physically symmetrical, it is electrically symmetrical. When one attempts to use equation (87) to determine **Z**<sub>0</sub> one finds that the matrix **C**<sup>-1</sup> does not exist because **C** = **Y** is singular. Since **Z**<sub>0</sub> does not exist, equations (48), (70), and

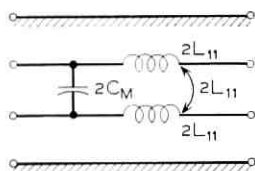


Fig. 12 — Lumped directional coupler which, when connected to a resistive load, exhibits directional coupler effect of all frequencies.

(71) cannot be used. Equation (132) can be used instead. The eigenvalues of **A**, **B**, **C** are:

$$\begin{aligned} A^+ &= 1, & A^- &= 1 \\ B^+ &= 4SL_{11}, & B^- &= 0 \\ C^+ &= 0, & C^- &= 4SC_M \end{aligned}$$

Thus (132) reads

$$4SC_M z^3 - 4SL_{11}z = 0,$$

the solutions of which are

$$z_1 = 0, \quad z_2 = \sqrt{\frac{L_{11}}{C_M}}, \quad z_3 = -\sqrt{\frac{L_{11}}{C_M}}. \quad (146)$$

The load impedances are frequency invariant, which indicates that the circuit may be matched with a constant at all frequencies and should exhibit directional coupler effect at all frequencies when loaded with a positive resistance of value  $\sqrt{L_{11}/C_M}$ . Using equations (141)–(143) the voltage ratios are found to be

$$\frac{V_{2-}}{V_{1+}} = \frac{2S\sqrt{L_{11}C_M}}{1 + 2S\sqrt{L_{11}C_M}}, \quad (147)$$

$$\frac{V_{3-}}{V_{1+}} = \frac{1}{1 + 2S\sqrt{L_{11}C_M}}, \quad (148)$$

$$\frac{V_{4-}}{V_{1+}} = 0. \quad (149)$$

Equation (149) corroborates that the coupler exhibits directional coupler effect at all frequencies. This example illustrates the use of the directional coupler equations in terms of the **A**, **B**, **C**, **D** matrices.

### 5.6 Lumped and Distributed Elements

The formulation that has been developed allows the handling of circuits with both lumped and distributed elements without any changes because the formulas are good for "black boxes." For example, for the circuit shown in Fig. 13, the total **E** matrix is found by multiplying the individual **E** matrices of the sections. The **E** matrix of section *P* or *T* is given by equation (145) while that of *Q* is given by equation (29). Once the total **E** matrix is known, it is partitioned into **A**, **B**, **C**, **D** matrices and equation (132) applied to determine the proper *z* for terminating the coupler. When the coupler is thus terminated, equations (141)–(143) yield the voltage ratios.

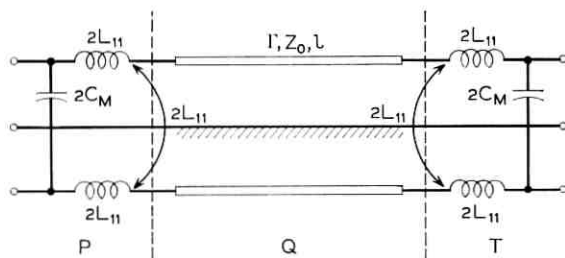


Fig. 13—Directional coupler configuration containing both lumped and distributed elements.

In general, the algebra will get quite unmanageable and one will have to resort to numerical calculations on a digital computer at discrete frequencies.<sup>13</sup> The  $z$  may be found by numerically solving the quartic equation (132) at a set of discrete frequencies and then realizing it as a driving point impedance through successive approximations, or some similar procedure. The processes of normalizing the impedance  $z$  and of making frequency transformations can be used very effectively in the realization of directional couplers of this sort.

## VI. CONCLUSIONS

Although strictly speaking all physical devices are distributed in space and thus, in general, have transcendental transfer functions for certain frequency regions, it might be possible to model the devices accurately enough with conventional ideal lumped elements, or more generally with elements having given frequency curves, which may be given analytically or numerically. In this paper we give a matrix theory for lumped and distributed circuits, keeping this fact in mind.

By using matrix formulation and treating the circuits as black boxes, it is possible to extend the classic theory of stripline directional couplers to more general circuits while still keeping many of the concepts (such as even and odd characteristic impedance) that have been found useful.

The paper makes evident the fact that the concepts of odd and even mode arise because of the special symmetry of the matrices and that they correspond to their eigenvectors and eigenvalues. We indicate in the appendix that when such special symmetry is lost, the odd and even modes are also lost and it might be necessary to introduce one set of modes for the currents and another for the voltages. This fact is not simple to see without the matrix formulation.

By thinking in vector-matrix terms, we explain the directional coupler

effect and gain considerable insight which is useful for realizing directional couplers lacking double symmetry.

We have given general equations for analyzing and designing black-box directional couplers in terms of the characteristic impedance and propagation matrices, and in terms of the transmission **A**, **B**, **C**, **D** matrices. The latter may be necessary to analyze circuits whose characteristic impedance matrix (hence even or odd characteristic impedances) does not exist but which have a scattering matrix.

The topic of the actual design of directional couplers with lumped or with lumped and distributed elements, and more specifically the design of multisection directional couplers using computer aids, is not treated because it is the subject of a forthcoming paper.

#### APPENDIX

Here are some spectral properties of the principal matrices in the paper for ease of reference.<sup>14</sup>

The symmetric matrix

$$\mathbf{K} = \begin{bmatrix} k_{11} & k_{12} \\ k_{12} & k_{11} \end{bmatrix} \quad (150)$$

has eigenvalues

$$\lambda_1 = k_{11} + k_{12} \quad (151)$$

$$\lambda_2 = k_{11} - k_{12} \quad (152)$$

and normalized eigenvectors

$$\mathbf{U}_1 = \frac{1}{\sqrt{2}} \begin{bmatrix} 1 \\ 1 \end{bmatrix}, \quad \mathbf{U}_2 = \frac{1}{\sqrt{2}} \begin{bmatrix} 1 \\ -1 \end{bmatrix}. \quad (153)$$

This can be seen by verifying the following identity

$$\frac{1}{\sqrt{2}} \begin{bmatrix} 1 & 1 \\ 1 & -1 \end{bmatrix} \begin{bmatrix} k_{11} + k_{12} & 0 \\ 0 & k_{11} - k_{12} \end{bmatrix} \begin{bmatrix} 1 & 1 \\ 1 & -1 \end{bmatrix} \frac{1}{\sqrt{2}} \equiv \begin{bmatrix} k_{11} & k_{12} \\ k_{12} & k_{11} \end{bmatrix} \quad (154)$$

The spectral set of **K** is:

$$\mathbf{R}_1 = \mathbf{U}_1 \mathbf{U}_1'; \quad \mathbf{R}_1 = \frac{1}{2} \begin{bmatrix} 1 & 1 \\ 1 & 1 \end{bmatrix} \quad (155)$$

$$\mathbf{R}_2 = \mathbf{U}_2 \mathbf{U}_2'; \quad \mathbf{R}_2 = \frac{1}{2} \begin{bmatrix} 1 & -1 \\ -1 & 1 \end{bmatrix} \quad (156)$$

Hence an analytic function  $f$  of the matrix  $\mathbf{K}$  may be written

$$f(\mathbf{K}) = \mathbf{R}_1 f(\lambda_1) + \mathbf{R}_2 f(\lambda_2) \quad (157)$$

For example

$$\cosh \begin{bmatrix} k_{11} & k_{12} \\ k_{12} & k_{11} \end{bmatrix} = \begin{bmatrix} \frac{1}{2}[\cosh(k_{11}+k_{12}) + \cosh(k_{11}-k_{12})] & \frac{1}{2}[\cosh(k_{11}+k_{12}) - \cosh(k_{11}-k_{12})] \\ \frac{1}{2}[\cosh(k_{11}+k_{12}) - \cosh(k_{11}-k_{12})] & \frac{1}{2}[\cosh(k_{11}+k_{12}) + \cosh(k_{11}-k_{12})] \end{bmatrix}.$$

The quantities associated with the vector  $\mathbf{U}_1$  are called the "even mode" or "sum mode." The quantities associated with the vector  $\mathbf{U}_2$  are called the "odd mode" or "difference mode."

In our main paper, the eigenvalues of the matrices  $\mathbf{Z}_0$  and  $\mathbf{\Gamma}$  which are in the form of equation (1), are denoted by  $Z_0^+$  and  $\gamma^+$  for the sum mode and  $Z_0^-$  and  $\gamma^-$  for the difference mode.

The partitioned matrix

$$\mathbf{M} = \left[ \begin{array}{c|c} \mathbf{M}_{11} & \mathbf{M}_{12} \\ \hline \mathbf{M}_{12} & \mathbf{M}_{11} \end{array} \right], \quad (158)$$

where  $\mathbf{M}_{11}$  and  $\mathbf{M}_{12}$  are the following  $2 \times 2$  symmetric matrices

$$\mathbf{M}_{11} = \begin{bmatrix} \alpha & \beta \\ \beta & \alpha \end{bmatrix}, \quad \mathbf{M}_{12} = \begin{bmatrix} \gamma & \delta \\ \delta & \gamma \end{bmatrix}, \quad (159)$$

has the following eigenvalues

$$\lambda_a = (\alpha + \beta) + (\gamma + \delta), \quad (160)$$

$$\lambda_b = (\alpha + \beta) - (\gamma + \delta), \quad (161)$$

$$\lambda_c = (\alpha - \beta) + (\gamma - \delta), \quad (162)$$

$$\lambda_d = (\alpha - \beta) - (\gamma - \delta), \quad (163)$$

and the corresponding eigenvectors

$$\mathbf{U}_a = \frac{1}{2} \begin{bmatrix} 1 \\ 1 \\ 1 \\ 1 \end{bmatrix}, \quad \mathbf{U}_b = \begin{bmatrix} 1 \\ 1 \\ -1 \\ -1 \end{bmatrix}, \quad \mathbf{U}_c = \begin{bmatrix} 1 \\ -1 \\ 1 \\ -1 \end{bmatrix}, \quad \mathbf{U}_d = \begin{bmatrix} 1 \\ -1 \\ -1 \\ 1 \end{bmatrix}. \quad (164)$$

This can be verified by a matrix multiplication similar to that of equation (154).

The spectral set of  $\mathbf{M}$  is

$$\mathbf{R}_a = \mathbf{U}_a \mathbf{U}'_a = \frac{1}{4} \begin{bmatrix} 1 & 1 & 1 & 1 \\ 1 & 1 & 1 & 1 \\ 1 & 1 & 1 & 1 \\ 1 & 1 & 1 & 1 \end{bmatrix}, \quad (165)$$

$$\mathbf{R}_b = \mathbf{U}_b \mathbf{U}'_b = \frac{1}{4} \begin{bmatrix} 1 & 1 & -1 & -1 \\ 1 & 1 & -1 & -1 \\ -1 & -1 & 1 & 1 \\ -1 & -1 & 1 & 1 \end{bmatrix}, \quad (166)$$

$$\mathbf{R}_c = \mathbf{U}_c \mathbf{U}'_c = \frac{1}{4} \begin{bmatrix} 1 & -1 & 1 & -1 \\ -1 & 1 & -1 & 1 \\ 1 & -1 & 1 & -1 \\ -1 & 1 & -1 & 1 \end{bmatrix}, \quad (167)$$

$$\mathbf{R}_d = \mathbf{U}_d \mathbf{U}'_d = \frac{1}{4} \begin{bmatrix} 1 & -1 & -1 & 1 \\ -1 & 1 & 1 & -1 \\ -1 & 1 & 1 & -1 \\ 1 & -1 & -1 & 1 \end{bmatrix}. \quad (168)$$

Any analytic function  $f$  of  $\mathbf{M}$  may be written

$$f(\mathbf{M}) = \mathbf{R}_a f(\lambda_a) + \mathbf{R}_b f(\lambda_b) + \mathbf{R}_c f(\lambda_c) + \mathbf{R}_d f(\lambda_d). \quad (169)$$

Concerning the so-called "modes of propagation" of a set of two coupled lines, when the  $\mathbf{\Gamma}$  matrix of the two lines has the double symmetry exhibited by the matrix  $\mathbf{K}$  of equation (1), the eigenvectors of the matrix are those given by equation (4). Since the matrix is symmetrical, the eigenvectors of the transposed matrix  $\mathbf{\Gamma}'$  are the same; therefore, one may speak of the "sum mode voltages and currents" and "difference mode voltages and currents." However, it might happen that  $\mathbf{\Gamma}$  does not have the form of  $\mathbf{K}$  in equation (1). Then the concept of sum and difference modes disappear because the eigenvectors that will result will not be quite so simple. If he wishes, one may then speak of "first mode" and "second mode," associating each mode with each eigenvector.

If the matrix  $\Gamma$  is symmetrical the voltage and current modes will coincide. However, if  $\Gamma$  is not symmetrical then the eigenvectors of  $\Gamma'$  will not be the same as those of  $\Gamma$ . It will be necessary to speak of "first voltage mode," "second voltage mode," "first current mode," and "second current mode" because the voltage modes will differ from the current modes if  $\Gamma$  is not symmetrical. The eigenvalues of a matrix and its transpose are always the same, hence no distinction is necessary for the propagation constants of the voltage and current modes.

## REFERENCES

1. Firestone, W. L., Analysis of Transmission Line Directional Couplers, *Proc. IRE*, 42, October 1954, pp. 1529-1538.
2. Oliver, B. M., Directional Electromagnetic Couplers, *Proc. IRE*, 42, November 1954, pp. 1686-1692.
3. Shimizu, J. K. and Jones, E. M. T., Coupled Transmission Line Directional Couplers, *IRE Trans. PGMTT-6*, October 1958, pp. 403-410.
4. Jones, E. M. T. and Bolljahn, J. T., Coupled Strip Transmission Line Filters and Directional Couplers, *IRE Trans. PGMTT-4*, April 1956, pp. 75-81.
5. Fel'dshstein, A. L., Synthesis of Stepped Directional Couplers, *Radiotekhnika i Elektronika*, 6, No. 2, February 1961, pp. 234-240; English translation, Pergamon Press, New York, 1961, pp. 75-85.
6. Young, L., The Analytical Equivalence of TEM-Mode Directional Couplers and Transmission-Line Stepped-Impedance Filters, *Proc. IEEE*, 110, February 1963, pp. 275-281.
7. Levy, R., General Synthesis of Asymmetric Multi-Element Coupled-Transmission-Line Directional Couplers, *IEEE Trans. PTGMTT-11*, July 1963, pp. 226-237.
8. Carson, J. R. and Hoyt, R. S., Propagation of Periodic Currents Over a System of Parallel Wires, *B.S.T.J.*, 6, 1927, pp. 495-545.
9. Rice, S. O., Steady State Solutions of Transmission Line Equations, *B.S.T.J.*, 20, No. 2, April 1941, pp. 131-178.
10. Pipes, L. A., Matrix Theory of Multiconductor Transmission Lines, *Phil. Mag.*, Series 7, 24, July 1937, pp. 97-113.
11. Huelsman, L. P., *Circuits, Matrices and Linear Vector Spaces*, McGraw-Hill Book Company, Inc., New York, 1963.
12. Montgomery, C. G., Dicke, R. H., and Purcell, E. M., *Principles of Microwave Circuits*, McGraw-Hill Book Company, Inc., New York, 1948.
13. Murray-Lasso, M. A., A Digital Computer Simulation of a Class of Lumped and/or Distributed Four-Ports, *Proc. SHARE-A.C.M. Design Automation Workshop*, Los Angeles, Calif., June 19-22, 1967.
14. Frazer, R. A., Duncan, W. J., and A. R. Collar, *Elementary Matrices*, Cambridge University Press, Cambridge, 1963.



# A Statistical Analysis of On-Off Patterns in 16 Conversations

By PAUL T. BRADY

(Manuscript received September 14, 1967)

*This is a summary of data from an extensive analysis of on-off speech patterns in 16 experimental telephone conversations. The on-off patterns are determined by a fixed threshold speech detector having certain rules for rejecting noise and for filling in short gaps (for example, from stop consonants). Distributions are obtained for ten events, including talkspurts, pauses, double talking (simultaneous speech from both parties), mutual silence, etc. Particular emphasis is placed on events surrounding interruptions. The entire analysis is performed for three speech detector thresholds, since most of the data are strongly influenced by choice of threshold. Observations are made about the influence of threshold on the data, properties of speech invariant with choice of threshold, and differences between male and female speech patterns.*

## I. INTRODUCTION

A statistical analysis of the on-off speech patterns of 16 recorded conversations has been obtained by a computer program written by Mrs. N. W. Shrimpton in 1963, and recently modified by the author. The data can serve the following purposes.

(i) They can illustrate the effect of variation of threshold setting on the resulting speech data. This problem has been plaguing virtually all researchers who have attempted to arrive at the "basic" talkspurt-pause patterns, that is, patterns which represent the subjective on-off behavior, either as intended by the speaker or as perceived by the listener. (There is, of course, no certainty that such on-off classification actually occurs during normal talking and listening.)

(ii) They can guide the design of voice operated devices, such as conventional echo suppressors<sup>1</sup> or an adaptive transversal filter echo canceller,<sup>2</sup> both of which have critical timing problems in the intervals surrounding interruptions.

(iii) They can provide material for building stochastic models of speech patterns in conversations. Several studies have already used basic models (such as Markov processes) to approximate talkspurt and pause durations.<sup>3, 4</sup> These models could be useful in predicting conversational behavior over special circuits, such as those containing transmission delay.

Applicability of the data to the above-mentioned purposes is influenced by the source and nature of the speech material and by the speech detector used to obtain on-off patterns. Section II is a description of the speech material, and Section III contains a description of the speech detector. This detector tries to yield patterns as close as possible to the original waveform, while making certain corrections to make the pattern representative of perceived speech patterns. These corrections, requiring two arbitrary parameters, include rejection of impulse noise operation and bridging of gaps caused by stop consonants. The third parameter, threshold, has such an effect on the data that the analysis is performed for a range of thresholds. In other respects however, the detector preserves fine details of timing of events; for example, the attack and release times are less than 5 msec.

Characterization of speech for speech detectors in the telephone system is a different problem from characterization of speech for modeling conversational speech patterns. The data of the present study are not intended to provide a basis for characterizing speech for telephone system speech detectors. Within the constraints of the corrections described in the preceding paragraph, however, the data can be extended to predict the behavior of certain speech detectors as explained in Section 5.2.

## II. THE CONVERSATIONS

### 2.1 *Source*

Of the 16 conversations, eight, obtained from four male pairs and four female pairs, lasted about 7 minutes each and were documented in a previous paper.<sup>5</sup> The remaining eight, also four male and four female pairs, lasted about 10 minutes each. The subjects talked over a 4-wire circuit such as illustrated in Fig. 1. The losses were typical of a long distance call, and there were no degrading factors such as noise, echo, or delay. The voices were recorded at the zero transmission level points (0 TLP), determined to be 6 dB "away from" the transmitters. The 0 TLP is an arbitrary reference level used to establish relative levels in a telephone circuit.)

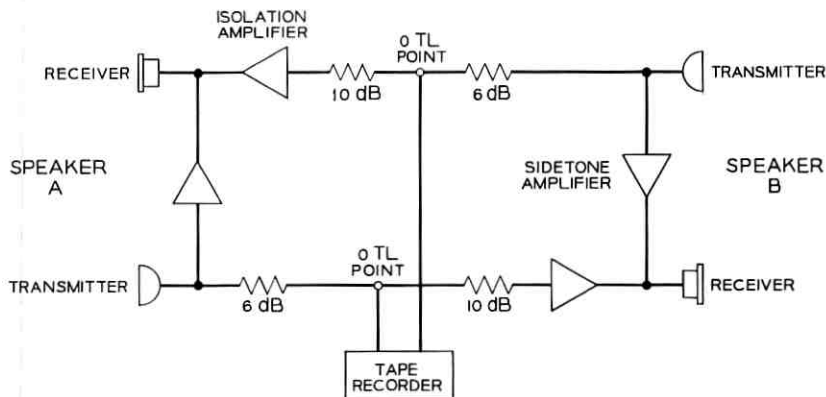


Fig. 1 — Circuit over which subjects talked.

The members of each pair were close friends; we have found that conversation between strangers can be restrained and halting. Their instructions were as follows.

“Your task in this experiment will be to converse with each other for approximately 10 minutes. You may talk about anything you wish, but keep in mind that you will be recorded. The recording will be kept private and will be used for computer analysis of speech. We ask that you *both* talk frequently; if only one person talks the conversation will be of almost no value to us.”

This method seemed to produce natural conversational speech which was not restrained by the subjects' knowledge that they were being recorded.

## 2.2 Scope of the Conversations

Since the experimental conversations do not represent a random sample of calls in a telephone office, they cannot provide documentation of speech patterns on subscriber circuits. They are, however, of interest in their own right and even possess advantages over customer calls.

(i) The experimental calls are recorded, and can be studied for contextual material, etc.

(ii) The subjects are indeed conversing, rather than momentarily setting the phone down, or even switching off to other persons. In short, in the experimental calls, the subjects and tasks are known.

(iii) Interest in transmission work is often centered on those parts

of a call with active interchange, as our experimental calls generally had. This is especially true in echo suppressor<sup>1</sup> and speakerphone<sup>6</sup> studies.

### III. THE SPEECH DETECTOR

The technique of obtaining on-off speech patterns, although already documented,<sup>5</sup> is summarized as follows. A flip-flop is set any time speech (full-wave rectified and unfiltered) from speaker *A* crosses a threshold. This flip-flop is examined and cleared every 5 milliseconds, with the output being a 1 if the threshold was crossed, 0 otherwise. The resulting string of 1s (spurts) and 0s (gaps) is examined for short spurts; all spurts  $\leq 15$  msec\* are erased. After this is done, all gaps  $\leq 200$  msec are filled in to account for momentary interruptions, such as those due to stop consonants. The resulting on-off pattern consists, by definition used here, of *talkspurts* and *pauses*. An identical procedure is used for speaker *B*.

Three thresholds have been chosen:  $-45$  dBm0† (most sensitive),  $-40$ , and  $-35$ . These values seemed to bracket the range between excessive noise operation and insufficient speech operation. The average peak level (apl)‡ for all 32 speakers was  $-18.9$  dBm re 0 TLP, 26.1 dB above the most sensitive threshold. If one prefers VUs, a previous study<sup>7</sup> showed that VUs obtained by Miss K. L. McAdoo (an experienced VU meter reader) are roughly 6 dB below the apIs, hence, the average VU for that observer would have been near  $-25$  dBm.

### IV. DATA

#### 4.1 Approximation in the Medians

Although all means reported here are exact (in that they equal the total time in an event divided by the number of event occurrences) the medians are not exact because the measuring intervals are arbitrarily categorized. For example, the median talkspurt at the  $-45$  dBm threshold is somewhere between 750 and 800 msec, and is reported at 775 msec, the interval midpoint. The measuring intervals are roughly proportional to the lengths of events; the intervals are as short as 10 msec for events  $\leq 200$  msec and as long as 1 second for events  $\geq 6$  seconds.

\* This was originally 10 msec, but 15 msec seems to be required for good impulse noise rejection.

†  $-45$  dBm measured at the 0 TLP.

‡ Average peak level is a measure of speech level based on the average log rectified speech voltage.<sup>7</sup>

#### 4.2 Percent of Time Spent in Different States

Table I shows three measures made per person or per conversation:

(i) Percent of time each person talked, averaged over 32 persons, obtained for each person by dividing his total speech time by the length of his conversation.

(ii) Percent of time in double-talking, averaged over 16 conversations.

(iii) Percent of time in mutual silence, averaged over 16 conversations.

Table II shows two measures made on the entire sample of 137.4 minutes of conversation: the percent of time in double talking, and the percent of time in mutual silence. Notice that mutual silence is the complement of the event that one or both speakers are talking.

#### 4.3 Categorized Events

Ten events were defined and measured. Figs. 2 through 11 are cumulative distribution plots of the events. The arrows show which event is being measured. For example, in Fig. 2, which shows the talkspurt cumulative distribution, there are three events illustrated and indicated by the arrows.

The defined events are:

(i) Talkspurt—defined in Section III.

(ii) Pause—defined in Section III.

(iii) Double talk—a time when speech is present from both *A* and *B*.

(iv) Mutual silence—a time when silence is present from both *A* and *B*.

TABLE I—PERCENT OF TIME IN DIFFERENT STATES\*

State	-45 dBm		-40 dBm		-35 dBm	
	Mean	$\sigma$	Mean	$\sigma$	Mean	$\sigma$
Talking (per person)	43.53	9.10	39.5	8.37	35.00	8.31
Double talking (per conversation)	6.58	3.47	4.49	2.41	3.10	1.81
Mutual silence (per conversation)	18.97	6.55	25.01	7.28	32.55	9.77

\* Average of 32 persons or 16 conversations.

TABLE II—PERCENT OF TIME IN STATES FOR ENTIRE SAMPLE\*

State	-45 dBm	-40 dBm	-35 dBm
Double talking	6.78	4.62	3.22
Mutual silence	19.07	24.99	32.37

\* 137.4 minutes, including all 16 conversations.

(v) Alternation silence—the period of mutual silence between the end of one speaker's talkspurt and the beginning of the other's. Event 5 is a subset of 4. If a speaker alternation results from an interruption so that there is no mutual silence period, then an alternation silence has not occurred. (There are no negative alternation silences.)

(vi) Pause in isolation—a pause in which the other speaker is silent throughout the pause. Event 6 is a subset of both 2 and 4.

(vii) Solitary talkspurt—a talkspurt which occurs entirely within the other speaker's silence. Event 7 is a subset of 1.

(viii) Interruption—if *A* interrupts *B*, the time at which *A*'s talkspurt begins determines the start of an interruption. The interruption terminates at the end of *A*'s talkspurt, unless *B* stops and then interrupts *A*, in which case *A*'s interruption terminates upon *B*'s counter interruption.

(ix) Speech after interruption—if *A* interrupts *B*, the remainder

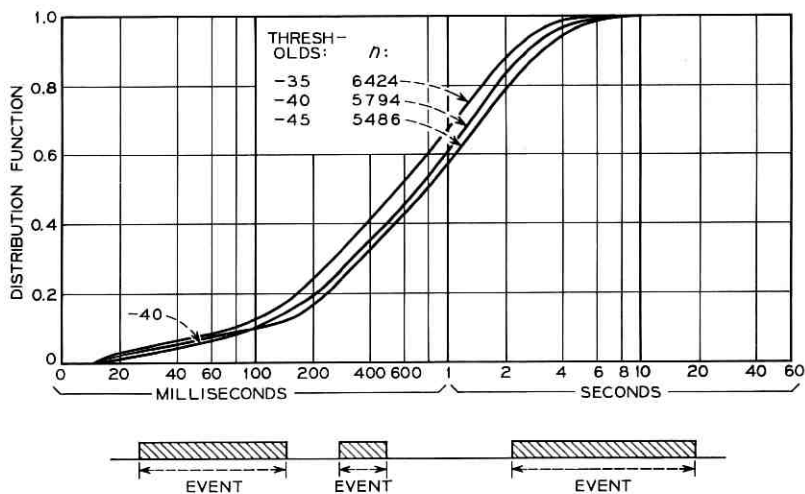


Fig. 2 — Talkspurts for 32 speakers.

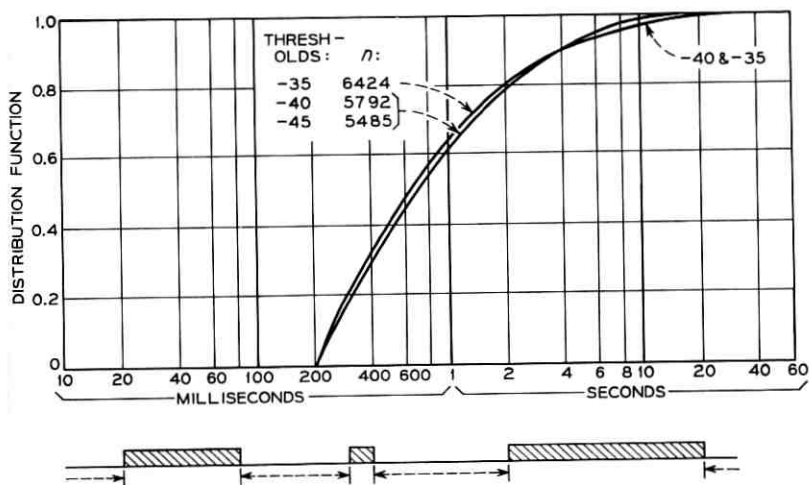


Fig. 3 — Pauses for 32 speakers.

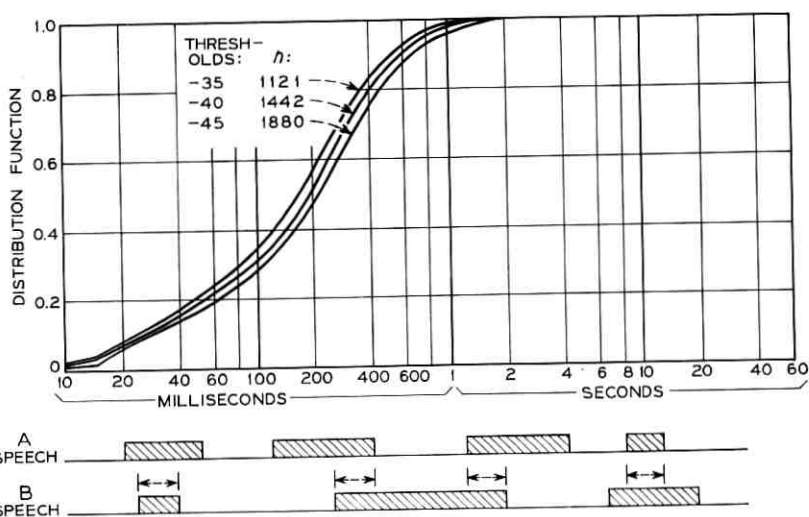


Fig. 4 — Doubletalk for 16 conversations.

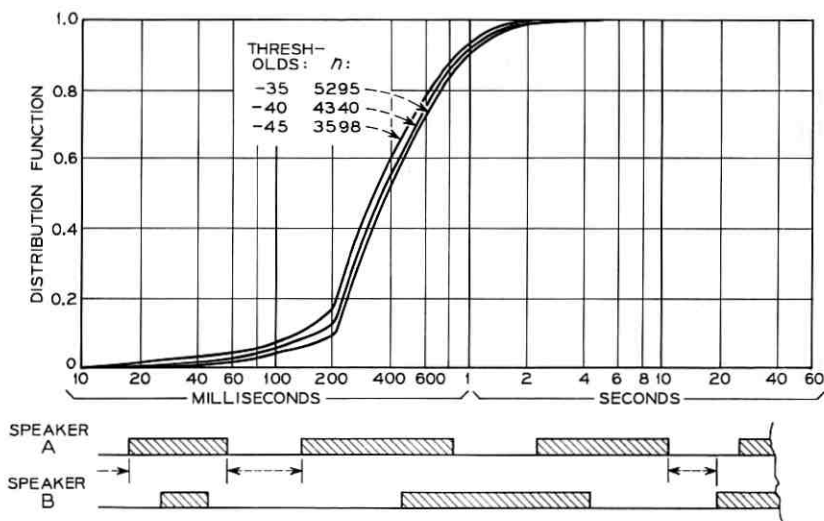


Fig. 5 — Mutual silence for 16 conversations.

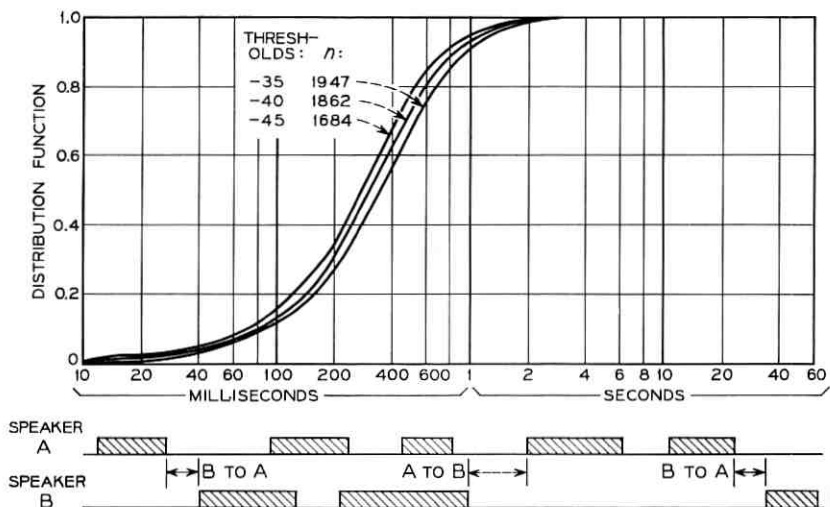


Fig. 6 — Alternation silences for 32 subjects. A to B and B to A have been combined.

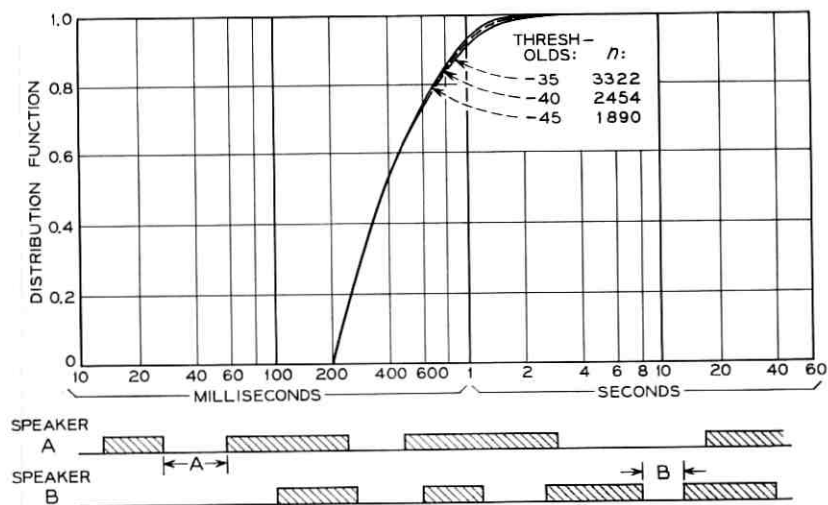


Fig. 7—Pauses in isolation for 32 subjects. Events from *A* and *B* have been combined.

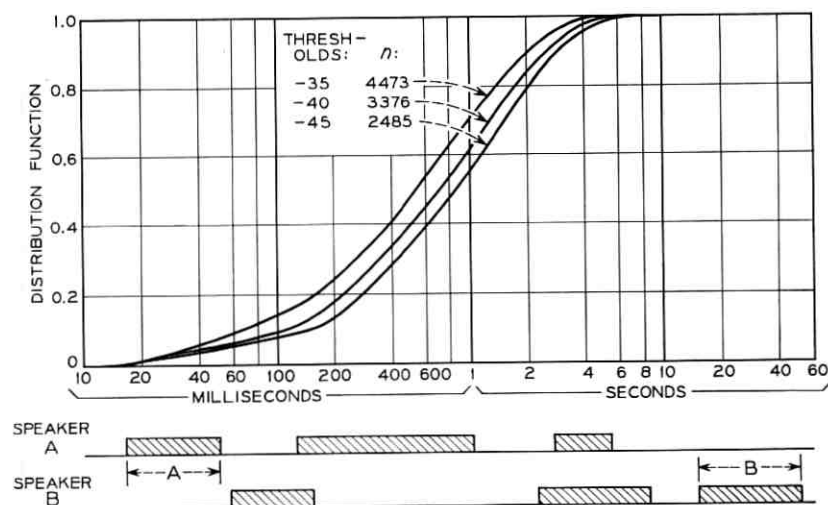


Fig. 8—Solitary talkspurts for 32 speakers. Events from *A* and *B* have been combined.

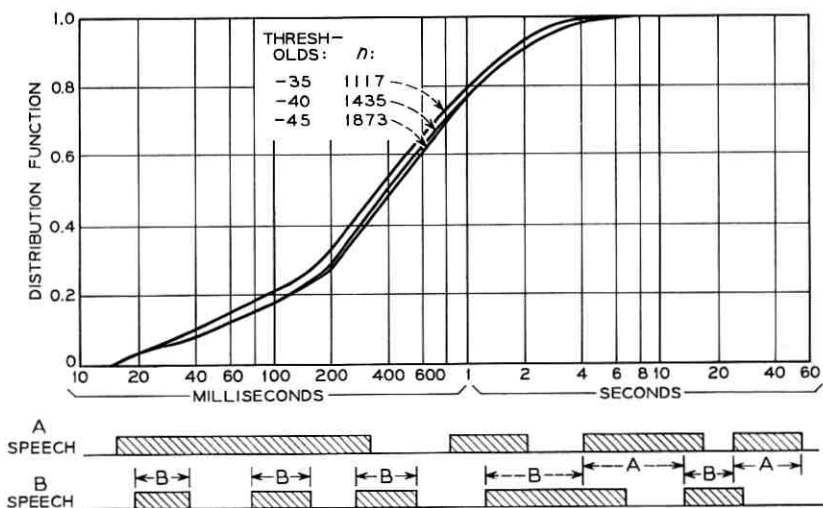


Fig. 9—Interruptions for 32 speakers. Events from *A* and *B* have been combined.

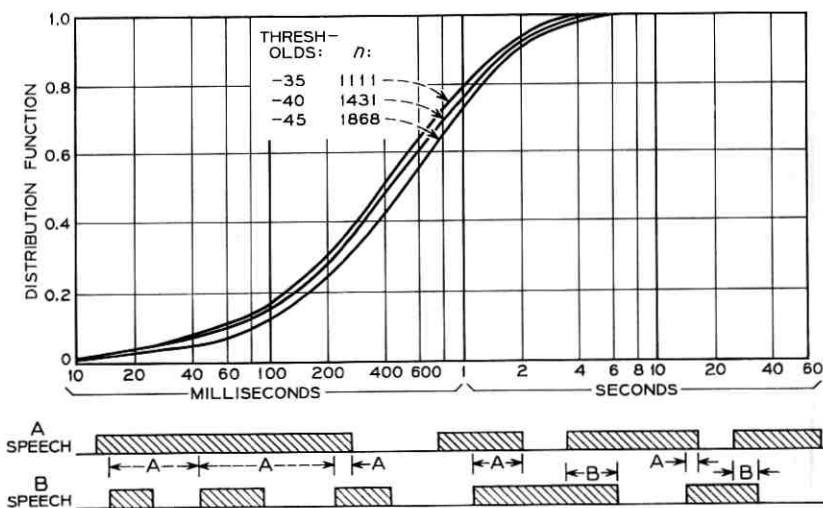


Fig. 10—Speech after interruption. Events from *A* and *B* have been combined.

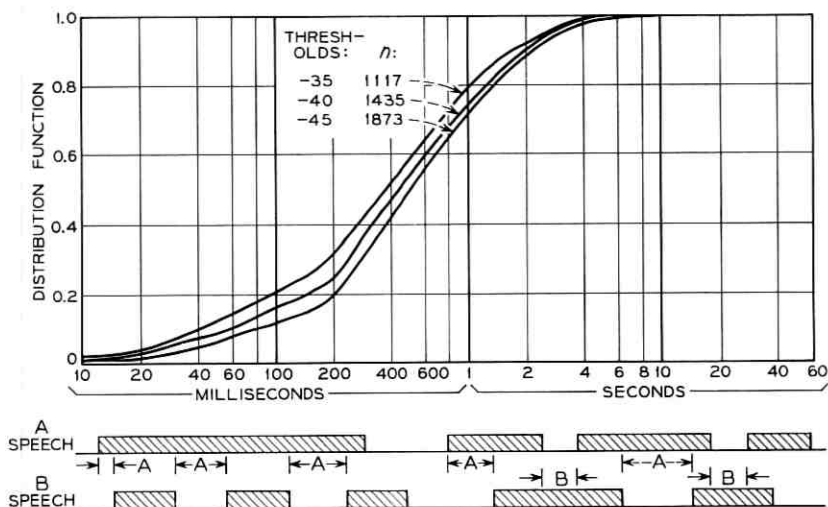


Fig. 11—Speech before interruption. Events from *A* and *B* have been combined.

of *B*'s talkspurt is entered here, unless *A* pauses and then again interrupts the same *B* talkspurt. The first "speech after interruption" would terminate upon *A*'s reinterruption, and a second speech after interruption would begin.

(*x*) Speech before interruption—if *A* interrupts *B*, *B*'s speech interval up to the interruption is entered here. If *A* then pauses at time  $t_1$  and reinterrupts at time  $t_2$ , (assuming *B* continues talking), a new *B* speech before interruption ( $t_2 - t_1$ ) is entered. If *A* continues talking and *B* pauses and then counter interrupts, the length of *B*'s pause is entered as *A*'s speech before interruption.

#### 4.4 Tabulated Events for the Entire Sample

Table III lists the mean, median, and number of events for talkspurts, pauses, and doubletalks of the entire 137.4-minute conversation sample. Notice that the talkspurts and pauses represent 274.8 minutes of speech, since the *A* and *B* speech samples can be separated and placed end to end.

#### 4.5 Means and Sigmas for Averages of Events

Table IV lists the means of the averages of the categorized events per person (or in some cases per conversation). For example, the

TABLE III — DURATIONS OF CERTAIN EVENTS FOR ENTIRE SAMPLE\*

Event	-45 dBm		No. of Events	-40 dBm		No. of Events	-35 dBm	
	Mean	Median		Mean	Median		Mean	Median
Talkspurt (274.8 min)	1.311	0.775	5486	1.125	0.675	5794	0.902	0.575
Pause (274.8 min)	1.695	0.725	5485	1.721	0.725	5792	1.664	0.675
Double talk (137.4 min)	0.296	0.213	1880	0.262	0.185	1442	0.235	0.165

\* 137.4 minutes of conversation, or 274.8 minutes of speech.

mean talkspurt length of 1.366 second for a  $-45$  dBm threshold is the average of 32 numbers, each in turn being the average talkspurt length for a particular speaker. The  $\sigma$  reported\* is the standard deviation of the 32 (or 16) averages among speakers (or conversations).

TABLE IV—MEANS AND STANDARD DEVIATIONS OF THE AVERAGES OF EVENTS\*

Event ( $k$ )	$-45$ dBm		$-40$ dBm		$-35$ dBm	
	Mean (seconds)	$\sigma$	Mean (seconds)	$\sigma$	Mean (seconds)	$\sigma$
Talkspurt (32) $n \sim 181$ †	1.366	0.442	1.197	0.444	0.980	0.425
Pause (32) $n \sim 181$	1.802	0.639	1.846	0.648	1.742	0.663
Double talk (16) $n \sim 90$	0.280	0.061	0.251	0.055	0.223	0.058
Mutual silence (16) $n \sim 271$	0.425	0.088	0.466	0.088	0.495	0.080
Alternation silence (32) $n \sim 58$	0.345	0.104	0.397	0.116	0.456	0.126
Pause in isolation (32) $n \sim 77$	0.488	0.093	0.502	0.092	0.512	0.091
Solitary talkspurt (32) $n \sim 106$	1.359	0.503	1.173	0.453	0.955	0.422
Interruption (32) $n \sim 45$	0.792	0.266	0.742	0.303	0.695	0.354
Speech after inter- ruption (32) $n \sim 45$	0.867	0.366	0.775	0.336	0.650	0.277
Speech before inter- ruption (32) $n \sim 45$	0.895	0.282	0.831	0.358	0.673	0.316

\* Per person ( $k = 32$ ) or per conversation ( $k = 16$ ).

† Values of  $n$  were obtained by dividing the total number of events for  $-40$  dBm threshold by  $k$ . These numbers thus give a rough idea of the frequency of these events per person (or conversation). These same values also apply to Table V.

#### 4.6 Means and Sigmas for Medians of Events

Table V lists the means of the *medians* of the categorized events per person (or conversation). For example, the "average of median" talkspurt length of 0.788 second for a  $-45$  dBm threshold is the average of 32 talkspurt medians, with 0.229 second as the standard deviation of the 32 medians among speakers.

\*  $\sigma = [(n/n - 1) \times (\text{sample variance})]^{1/2}$  through this paper.

4.7 *Male vs Female*

Table VI lists the means of the averages of the events per person or conversation, for the men and women separately. (Data on averages of the medians are available from the author.)

4.8 *Transitional Probabilities*

As we mentioned, some researchers have postulated first-order Markov processes to model speech patterns. A conversation, at any instant, can exist in one of four states depending on who is talking:

TABLE V—MEANS AND STANDARD DEVIATIONS OF THE  
MEDIAN OF EVENTS\*

Event ( <i>k</i> )	-45 dBm		-40 dBm		-35 dBm	
	Mean (seconds)	$\sigma$	Mean (seconds)	$\sigma$	Mean (seconds)	$\sigma$
Talkspurt (32)	0.788	0.229	0.756	0.250	0.652	0.307
Pause (32)	0.759	0.184	0.779	0.193	0.706	0.195
Double talk (16)	0.199	0.048	0.181	0.046	0.153	0.047
Mutual silence (16)	0.332	0.056	0.366	0.056	0.378	0.045
Alternation silence (32)	0.264	0.082	0.312	0.101	0.347	0.096
Pause in isolation (32)	0.397	0.091	0.389	0.079	0.384	0.069
Solitary talkspurt (32)	0.890	0.326	0.799	0.325	0.660	0.344
Interruption (32)	0.418	0.218	0.405	0.218	0.387	0.233
Speech after inter- ruption (32)	0.487	0.156	0.410	0.144	0.383	0.166
Speech before interruption (32)	0.503	0.160	0.439	0.151	0.346	0.148

\* Per person ( $k = 32$ ) or per conversation ( $k = 16$ ).

neither, *A*, *B*, or both. If the conversation is in state  $i$  ( $i = 1,2,3,4$ ) at some time  $t$ , it may be of interest to know the probability of being in state  $j$  ( $j = 1,2,3,4$ ) at  $t + \Delta t$ , possibly to establish a crude Markovian model for distributions of times in each state. Notice, however, that the simplest Markovian model will predict that each state will have an exponential distribution, which is a hypothesis not generally supported by the data. (For example, mutual silence is the event representing the first state, and a glance at Fig. 5 shows that this distribution is strongly colored by the 200 msec fill-in time.)

This paper is primarily a collection of data, and is not intended to pursue the problem of modeling conversational behavior. We shall therefore simply list the transition matrix for the -40 dBm threshold\*

\* Transition probabilities for the other thresholds may be obtained from the author.

TABLE VI—MEANS OF AVERAGES OF EVENTS

Event	Threshold (dBm)	Male	Female	Signif. Level*	M -40† F -45	M -35 F -40
Talkspurt	-45	1.503	1.229	—	—	—
	-40	1.393	1.000	0.01		
	-35	1.221	0.739	0.01		
Pause	-45	1.911	1.690	—	—	—
	-40	2.003	1.690	—		
	-35	1.885	1.598	—		
Double talk	-45	0.278	0.282	—	—	—
	-40	0.247	0.256	—		
	-35	0.235	0.211	—		
Mutual silence	-45	0.452	0.397	—	0.05	—
	-40	0.491	0.441	—		
	-35	0.506	0.484	—		
Alternation silence	-45	0.354	0.336	—	—	—
	-40	0.403	0.391	—		
	-35	0.448	0.464	—		
Pause in isolation	-45	0.523	0.453	0.05	0.05	0.05
	-40	0.533	0.471	—		
	-35	0.533	0.492	—		
Solitary talkspurt	-45	1.510	1.207	—	—	—
	-40	1.377	0.969	0.01		
	-35	1.204	0.706	0.01		
Interruption	-45	0.807	0.777	—	—	—
	-40	0.821	0.662	—		
	-35	0.811	0.578	—		
Speech after interruption	-45	0.963	0.770	—	—	—
	-40	0.840	0.710	—		
	-35	0.741	0.559	—		
Speech before interruption	-45	0.793	0.997	0.05	—	0.05
	-40	0.648	1.014	0.01		
	-35	0.484	0.862	0.01		

\* Compares events at a common threshold.

† Compares males at -40 dBm with females at -45 dBm threshold; similar for last column. All significance levels from *t*-test.

in Table VII. The table indicates transition probabilities for 5 msec time steps. For example, if both are talking, the probability is 0.98095 that they will still both be talking 5 msec later. The conversation will, therefore, leave the state with  $p = 1.0 - 0.98095 = 0.01905$ . If a Poisson termination process\* is assumed for terminating the event, the conversation would leave the state in 1 msec with  $p = 0.01905/5$ .

## V. OBSERVATIONS

Events of one subject that do not involve interaction with talkspurts of his partner include pauses in isolation and solitary talkspurts. Data on behavior during double talking should be contrasted

TABLE VII—TRANSITION PROBABILITIES OF CHANGING STATE\*

From To	Neither	A	B	Both
Neither	0.98940	0.00529	0.00530	0.00001
A	0.00387	0.99486	0.00001	0.00126
B	0.00367	0.0	0.99510	0.00123
Both	0.00005	0.00885	0.01015	0.98095

\* In a 5-msec Period for the -40 dBm Threshold Condition.

with data on these "isolated" events rather than, for example, the distribution of all talkspurts, since this distribution includes events during double talking.

The data are notably influenced by threshold changes. The author does not believe it is possible, from results reported here, to establish a single "correct" threshold. It is possible, however, to draw certain conclusions which are threshold independent (see (vi) and (vii) below, and Section 5.2.)

### 5.1 The Data

We know from the data that:

(i) As the threshold is raised (speech detector made less sensitive), events which measure periods of talking tend to decrease in length, since the longer events tend to be broken up into short ones. These

\* A good discussion of Poisson and Markovian processes may be found in Reference 8.

events include talkspurts, double talks, solitary talkspurts, interruptions, and speech before and after interruption.

(ii) As the threshold is raised, events which measure periods of silence tend to increase in length. These events include pauses, mutual silences, alternation silences, and pauses in isolation.

There are some individual speaker exceptions to these observations. For example, male No. 14 talkspurt averages are 1.683, 1.620, and 1.759 seconds for  $-45$ ,  $-40$ , and  $-35$  dBm thresholds, respectively. Two other male speakers exhibit such a reversal for talkspurts. In general, however, conclusions drawn from the gross data are true of most speakers or conversations.

(iii) The distribution functions of events resulting from periods of talking seem in general more strongly affected by threshold shifts than those resulting from silences. Compare, for example, talkspurts vs pauses, or solitary talkspurts vs pauses in isolation. The mutual silence distribution, however, seems strongly influenced by threshold changes.

(iv) For all events, the number of times they occur ( $n$ ) is notably influenced by the threshold. This is particularly true of pauses in isolation, whose distribution remains virtually unaffected while  $n$  changes from 1890 to 3322 for a 10 dB threshold shift.

(v) As the threshold is raised, the number of talkspurts tends to increase. This trend will obviously be reversed if the threshold becomes so high that only a few spurts of energy clear it. But for low thresholds, as threshold is raised, long talkspurts are apparently being broken up into shorter segments at a faster rate than that of low level talkspurts being left below the threshold.

(vi) For any particular threshold, the cumulative distributions of speech before and after interruption are practically identical, as seen from a comparison of Figs. 10 and 11.

(vii) Interruptions tend to be much shorter than solitary talkspurts, as would be expected because the interrupter might merely be trying to get attention rather than make a statement. Also, some interruptions are really not deliberate interruptions but rather acknowledgments, such as "uh huh" and "um." This effect may be seen, for example, at the  $-40$  dBm threshold for which 17 percent of the interruptions are less than 100 msec long, while only 9.5 percent of solitary talkspurts are less than 100 msec.

(viii) Many speech detectors operate with a hangover, rather than a fill-in, to bridge short gaps. By shifting the talkspurt distribution 200 msec to the right and the pause distribution 200 msec left, one

can determine the distributions for these events which would have resulted if a 200-msec hangover were used instead of fill-in. However, the "interaction event" (double talking, etc.) distributions will be changed in a manner which cannot be determined from our present data.

### 5.2 *Male vs Female Speech*

Table VI shows that when male and female speech is compared at the same threshold, four events show a statistically significant difference:\* talkspurt, pause in isolation, solitary talkspurt, and speech before interruption. With the exception of pause in isolation, which is significant only at  $-45$  dBm threshold, these are events resulting from talking rather than silence.

Some of the apparent difference in male and female speech may result from a difference in average levels. The average speech level for the females was 5.94 dB below the average male speech level (measured in apl). When male speech at  $-40$  dBm threshold is compared with female speech at  $-45$  dBm, and when male speech at  $-35$  dBm is compared with female speech at  $-40$  dBm, thus roughly compensating for the average 6 dB level difference, the significant differences previously observed tend to disappear. New events—pause in isolation, and possibly mutual silence and speech before interruption—become significant. It thus appears not possible to completely eradicate differences in male and female speech with a simple level adjustment, although a level difference does account for differences observed in certain events.

These conclusions are of particular interest in view of a recent study by Krauss and Bricker,<sup>9</sup> who made measurements of verbal interaction (measured from transcripts of the conversations) when pairs of men and pairs of women talked over a circuit containing voice-operated, fixed threshold devices. The verbal behavior of the two sexes was significantly different in certain tasks. One wonders if the devices operated differently on the male and female speech, as they did in the present study. This could be a contributing factor in bringing about the behavioral difference reported by Krauss and Bricker.

## VI. CONCLUSION

We hope that the publication of these data will encourage other researchers to make further observations leading toward a general

---

\* Differences are significant at  $\leq 0.05$  level.

model of the speech patterns occurring in conversations. We also hope that by emphasizing the events surrounding double talking and other speaker interaction, it may be possible to draw conclusions regarding difficulties in conversing on certain circuits that have voice-operated devices.

#### VII. ACKNOWLEDGMENTS

I am especially grateful to Mrs. Lynn Evans, who cheerfully spent considerable time making hand tallies and desk-calculator analyses of the computer printouts, and to C. J. Gspann, who set up the interface between the speech detector and computer.

#### REFERENCES

1. Brady, P. T. and Helder, G. K., Echo Suppressor Design in Telephone Communications, *B.S.T.J.*, *42*, November 1963, pp. 2893-2917.
2. Sondhi, M. M., An Adaptive Echo Canceller, *B.S.T.J.*, *46*, March 1967, pp. 497-511.
3. Jaffe, J., Cassotta, L., and Feldstein, S., Markovian Model of Time Patterns of Speech, *Science*, *144*, May 15, 1964, pp. 884-886.
4. Brady, P. T., Queueing and Interference among Messages in a Communication System with Transmission Delay, Ph.D. Thesis, NYU Department of Electrical Engineering, June 1966.
5. Brady, P. T., A Technique for Investigating On-Off Patterns of Speech, *B.S.T.J.*, *44*, January 1965, pp. 1-22.
6. Clemency, W. F. and Goodale, W. D., Jr., Functional Design of a Voice-Switched Speakerphone, *B.S.T.J.*, *40*, May 1961, pp. 649-668.
7. Brady, P. T., A Statistical Basis for Objective Measurement of Speech Levels," *B.S.T.J.*, *44*, September 1965, pp. 1453-1486.
8. Cox, D. R. and Smith, W. L., *Queues*, Methuen, London, 1961.
9. Krauss, R. M. and P. D. Bricker, Effects of Transmission Delay and Access Delay on the Efficiency of Verbal Communication, *J. Acoust. Soc. Amer.*, *41* No. 2, September 1966, pp. 286-292.



# Dielectric Loaded and Covered Rectangular Waveguide Phased Arrays

By V. GALINDO AND C. P. WU

(Manuscript received September 11, 1967)

*This study examines the effects of loading or covering a phased array with dielectric materials. It studies in detail the effect of dielectric geometry, dielectric constant, and sheath thickness on the wide angle array performance of an array of rectangular waveguides in the H and quasi-E plane modes of scan. We obtain numerical solutions of the integral equations describing an array covered with thick dielectric material. The results show that we can obtain a match over a wide scan angle for the array by appropriate use of dielectric geometries, and we discuss the advantages and disadvantages of several geometries.*

## I. INTRODUCTION

The advent of swift aircraft, missile warfare, and the need for modern radar to accomplish multifunction detection has given impetus for a considerable amount of research into phased-array antennas. Such arrays consist of a large group of small radiators in a grid, frequently a rectangular grid, and, most important, correlated in phase and amplitude. The radiated beam can be steered by an electronically-variable linear taper of the phase correlation among elements. (See Fig. 1).

Considerable knowledge of the behavior and problems of such arrays has been obtained in recent years by experimental and theoretical study of phased linear and parallel plate arrays. For example, it is well known that the coupling coefficients between any single excited element in the array and any terminated inactive element is uniquely determined by the inverse Fourier series transform of the reflection coefficient as a function of scan angle determined when all elements are excited.<sup>1</sup> Hence, by studying the array behavior for all possible linear tapers of phase, we can determine the behavior of the array, for any phase or amplitude distribution among the elements.

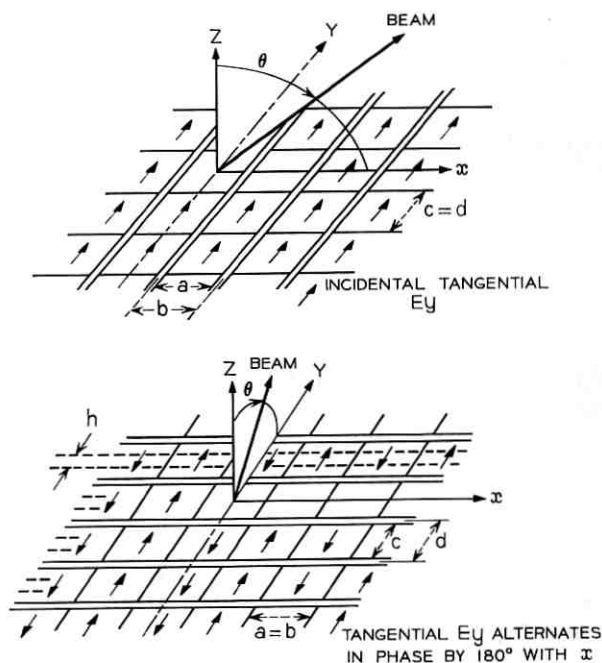


Fig. 1—Infinite array geometry. *Top*: H-plane scanning in X-Z plane, *Bottom*: Quasi-E plane scanning in Y-Z plane.

Of fundamental importance in designing such arrays is a knowledge, and control, of the mutual coupling (the coupling coefficients) between elements in an array. For arrays which scan over wide angles, this coupling very seriously affects the array, so substantial effort has been made to understand mutual coupling. Because the arrays of interest are very large and consist of very many elements, theoretical studies have generally assumed the arrays to be infinite in extent. The usefulness of this approximation for elements located near the center of a large array has been verified, and in fact, the approximation is frequently valid to within several elements from the edge.<sup>1</sup>

Because the arrays are generally very large, the coupling between greatly separated elements, the asymptotic coupling, is also of interest and has been theoretically studied.<sup>2,3</sup> In general, planar phased arrays with terminated elements behave like lossy surfaces and have an asymptotic  $1/r^2$  decay of coupling between elements separated by the distance  $r$  along the array surface.

Among other fundamental and interesting early developments is that the transmission coefficient of a phased array with all elements excited, as a function of scan angle, is directly related and proportional to the radiation pattern of a single-excited element in the array as a function of far-field observation angle.<sup>4</sup> As we mentioned, the two physical situations (all the elements excited with a linear phase taper and only one element excited) are uniquely related. Hence, an analytical formulation for only one or the other situation is necessary. Although most work has concentrated on the linear phase taper case, with the consequent application of periodicity conditions and Floquet's theorem,<sup>1, 5, 6</sup> some work has proceeded by directly attacking the case with only a single element excited.<sup>7</sup>

One of the most advantageous approaches to phased array problems has been through the use of high-speed computers and numerical solutions of the appropriate integral equations.<sup>5</sup> We use this approach in this study, which attempts to discover some problems and solutions associated with covering phased arrays with radomes. The principal problem is, of course, to maintain a good impedance match to the array over a wide scan angle when the phased array radome is included in the design. Now many antennas have radomes covering their moving mechanical parts and their interior electrical components. A planar phased array can be so protected by covering the array with a dielectric sheath or by loading it with a dielectric material. Hence our study concentrates on this type of cover.

Whereas ordinary radomes usually are designed to have the least effect on the antennas they cover, phased array covers often can be made to very substantially improve the wide angle scan performance of the array. In fact, Magill and Wheeler recently have shown that a dielectric sheath cover can greatly improve the wide angle match of the array.<sup>8</sup> However, their analysis was a transmission line analysis in the sense that it did not take into account the interaction of the evanescent modes, generated at the array interface, with the dielectric sheath.

More recently, Lee<sup>9</sup> has made an analysis restricted to an array of thin-walled parallel plates, wherein the interaction of a limited number of evanescent modes with the dielectric sheath is taken into account. His results bear out the possibility of improving the array match with a dielectric sheath.

By using a somewhat different and more powerful analytical approach, wherein the integral equations describing the array with a

dielectric covering are solved by an accurate numerical technique (basically Galerkin's method<sup>10</sup>), we may obtain a solution with few restrictions. The interaction of virtually all the modes at the array interface with one or more dielectric sheaths is accounted for with very little more difficulty than that entailed in the solution for the uncovered array. We made an extensive study of the rectangular array shown in Fig. 1 by this method for two modes of scan, the quasi-E and H planes of scan.<sup>5</sup> We use the term "quasi-E" because the adjacent columns of elements in the bottom part of Fig. 1 are out of phase by 180°.\* We assume that the waveguides in each case are excited in the dominant mode and we compute the parameter of particular interest, the reflection coefficient  $R$  of this mode, from the aperture field determined by the integral equations.

We divided the complete study into two parts. The first, considered in this paper, analyzes the effects of loading the waveguide with dielectric or covering the array with a very thick sheath where only one grating lobe, at most, is present in the sheath. Generally speaking, a thick sheath is used with only lower dielectric constant materials because with higher dielectric constants in a thick sheath a great and very frequency-sensitive mismatch arises. Furthermore, the presence of two grating lobes in the sheath gives rise to surface wave phenomenon. This is the subject of the second part of our study, which we have relegated to another part.<sup>11</sup> In that paper we plan to deal with thinner sheaths, multiple sheaths, and some anomalous surface wave effects that we have observed in arrays with dielectric covers.

## II. METHOD OF ANALYSIS

Fig. 2 shows the three dielectric geometries that we analyzed. In each case we assume a moderate fixed waveguide wall thickness<sup>5</sup> to exist in the plane of scan only. The top figure illustrates the "loaded" array with a symmetrical iris in the aperture (quasi-E scan only, Fig. 1). Fig. 2 also shows two other thick sheath covers. By "thick" we mean that there is very little interaction between the evanescent modes generated at the aperture plane ( $z = 0$ ) and the second dielectric boundary removed from the array interface ( $z = \pm d_s$ ). We may test the validity of this assumption by estimating the relative amplitudes of the evanescent to propagating modes at  $z = \pm d_s$  when the second boundary is not present. We made such a validity check with most

\* The waveguides are excited in this manner to reduce to a more easily numerically tractable one-dimensional integral equation the two-dimensional integral equations which result in the usual E-plane scan.

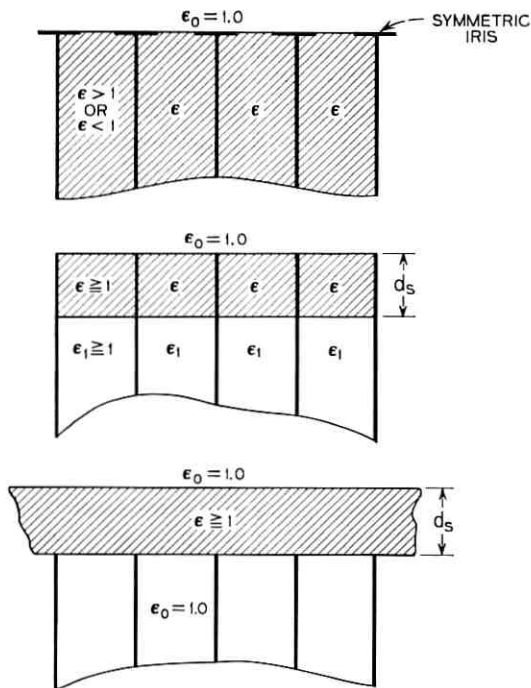


Fig. 2—Dielectric sheath geometry. *Top*: Dielectric loading. *Middle*: Sheath inside guides. *Bottom*: Sheath outside guides.

of the thick sheath results. Notice that with this assumption the input impedance or reflection coefficient is a periodic function of the distance  $d_s$ .

Actually the integral equations that are solved require only a slight modification to go from a "thick" approximation to a "total" accounting of the interaction of higher order modes with the dielectric interface removed from the aperture by  $d_s$ . The actual equations solved for the dielectric loaded case take the forms:<sup>5</sup>

$$2Y_0 e_{y_0}(y) = \int_{-h/2}^{h/2} \left[ \sum_0^{\infty} Y_n e_{y_n}(y) e_{y_n}(y') + \sum_{-\infty}^{\infty} Y'_m \psi_m(y) \psi_m^*(y') \right] E_y(y') dy' \quad (1)$$

for the unknown tangential electric field in the aperture in the quasi-E plane scan case, and

$$2Z_1 \varphi_1(x) = \int_{-b/2}^{b/2} \left[ \sum_1^{\infty} Z_n \varphi_n(x) \varphi_n(x') + \sum_{-\infty}^{\infty} Z'_m \psi_m(x) \psi_m^*(x') \right] H_x(x') dx' \quad (2)$$

for the unknown magnetic field over an entire cell ( $b \times d$ , see Fig. 1). The  $\varphi_n(x)$  and  $e_{v_n}(y)$  are appropriate interior orthonormal waveguide modes:

$$\begin{cases} \varphi_n = \sqrt{\frac{2}{a}} \begin{cases} \cos\left(\frac{n\pi}{a}x\right) & \text{for } (n = \text{odd}) \\ \sin\left(\frac{n\pi}{a}x\right) & \text{for } (n = \text{even}) \end{cases} & \text{in } |x| < \frac{a}{2} \\ \varphi_n = 0 & \text{in } \left(\frac{a}{2} < |x| < \frac{b}{2}\right) \end{cases} \quad (3)$$

and

$$\begin{cases} e_{v_n} = -\sqrt{\frac{\epsilon_n}{c}} \begin{cases} \cos\left(\frac{n\pi}{c}y\right) & \text{for } (n = \text{even}) \\ \sin\left(\frac{n\pi}{c}y\right) & \text{for } (n = \text{odd}) \end{cases} & \text{in } |y| \leq \frac{c}{2} \\ e_{v_n} = 0 & \text{in } \left(\frac{c}{2} < |y| < \frac{d}{2}\right), \quad \epsilon_n = \text{Neumann's constant} \end{cases} \quad (4)$$

The  $\psi_m(x)$  or  $\psi_m(y)$  are appropriate exterior orthonormal modes pertinent to the periodic structure and are obtained from an application of the Floquet theorem:

$$\begin{cases} \psi_m(x) = \sqrt{\frac{1}{b}} \exp j\left(\frac{2\pi m - kb \sin \theta}{b}\right)x \\ \psi_m(y) = \sqrt{\frac{1}{d}} \exp j\left(\frac{2\pi m - kd \sin \theta}{d}\right)y \end{cases} \quad k = \frac{2\pi}{\lambda_0} \quad (5)$$

By the laws of transmission of a plane wave through a plane dielectric boundary (Snell's law), the quantity ( $kb \sin \theta$ ) or ( $kd \sin \theta$ ) is unchanged by the presence of the dielectric. Hence the interior and exterior modes are independent of the dielectric constant. By using the  $h \leq c$  limits in (1) we also allow for the presence of a thin metallic iris directly at the aperture plane (see Fig. 1).

The incident electric field in (1) is given by  $e_{v_n}(y) \exp(-j\beta_n^e z)$  and the incident magnetic field in (2) by  $\varphi_n(x) \exp(-j\beta_n^h z)$ , where the interior modal propagation constants are given by

$$\begin{cases} \beta_n^e = \sqrt{\epsilon k^2 - \left(\frac{\pi}{b}\right)^2 - \left(\frac{n\pi}{c}\right)^2} & (\epsilon \text{ appropriate to the region}) \\ \beta_n^h = \sqrt{\epsilon k^2 - \left(\frac{n\pi}{a}\right)^2} \end{cases} \quad (6)$$

and the exterior propagation constants by

$$\begin{cases} \beta_m^{t*} = \sqrt{\epsilon k^2 - \left(\frac{\pi}{b}\right)^2 - \left(\frac{2\pi m - kd \sin \theta}{d}\right)^2} \\ \beta_m^{t^h} = \sqrt{\epsilon k^2 - \left(\frac{2\pi m - kb \sin \theta}{b}\right)^2} \end{cases} \quad (7)$$

Now the coefficients of the interior and exterior dyads in (1) and (2), the  $Y_n$ ,  $Y'_m$ ,  $Z_n$ , and  $Z'_m$ , take a form that is dependent on the dielectric sheath geometry. For the dielectric loaded case they become simply the modal admittances and impedances:<sup>5</sup>

$$\begin{aligned} \omega\mu Y_n &= \left[ \epsilon k^2 - \left(\frac{\pi}{b}\right)^2 \right] / \beta_n^*, & \omega\mu Y'_m &= \left[ \epsilon k^2 - \left(\frac{\pi}{b}\right)^2 \right] / \beta_m^{t*}, \\ Z_n &= \omega\mu / \beta_n^h, & Z'_m &= \omega\mu / \beta_m^{t^h}. \end{aligned} \quad (8)$$

For the dielectric sheath cases, with one or more sheaths, the  $Y_n$ ,  $Y'_m$ ,  $Z_n$ , and  $Z'_m$  become the modal admittances or impedances appropriately referred to the aperture plane ( $z = 0$ ). These modal admittances or impedances are obtainable by the usual transmission line equations. For example, suppose a single dielectric sheath inside the guides is considered (middle of Fig. 2) in the quasi-E plane scan case. Define

$$\begin{cases} \gamma_n = \beta_n^* \text{ inside the dielectric in the guide.} \\ \beta_n = \beta_n^* \text{ in the empty portion of the guide.} \\ Y_n = \text{admittance in the dielectric region.} \\ \mathcal{Y}_n = \text{admittance in the air region.} \end{cases} \quad (9)$$

Then the coefficients  $Y_n$  become

$$Y_n \rightarrow Y_n \left( \frac{\mathcal{Y}_n + jY_n \tan \gamma_n d}{j\mathcal{Y}_n \tan \gamma_n d + Y_n} \right), \quad (10)$$

while the exterior  $Y'_m$  coefficients remain unchanged (unless an exterior sheath is simultaneously included). The free term on the left becomes, if we postulate the same incident field as earlier,

$$2Y_0 e_{\nu_0} \rightarrow 2e^{j\beta_0 d} \left( \frac{\mathcal{Y}_0 Y_0 \sec \gamma_0 d}{j\mathcal{Y}_0 \tan \gamma_0 d + Y_0} \right) e_{\nu_0}. \quad (11)$$

Solving equations (1) and (2) by the Galerkin<sup>10</sup> (or Ritz) method means that (1) and (2) are approximated in an  $N$ -dimensional subspace\* of the complete Hilbert space.<sup>5</sup> One way of testing the accuracy of this approach is to choose two very dissimilar subspaces for approximation

\* Approximation in an  $N$ -dimensional subspace leads to a set of  $N$  linear equations to be solved by well-known matrix inversion methods.

and then compare the attained results. One subspace choice was that spanned by a set of  $N$  equally-spaced pulses<sup>3</sup> (that is, we sample the field at  $N$  points along the  $x$  or  $y$  axis). In this case,  $R$  is determined by averaging the coefficients of the pulses. Other bases used were the first  $N$  modes,  $e_{\nu_n}(y)$  and  $\psi_m(x)$ . In the case of  $e_{\nu_n}$ ,  $R$  is determined directly from only the coefficient of the  $e_{\nu_n}(y)$  term.

We made a number of additional checks on the solutions. We observed the convergence of the solutions with increasing  $N$ , and we verified the conservation of energy between incident, transmitted, and reflected waves. For certain angles of incidence we compared the results with those obtained previously by Marcuvitz and Lewin.<sup>12,13</sup> We also checked some of the results against values for  $R$  obtained experimentally. (See Ref. 5 for example.) We checked the thin dielectric sheath results (using the exact formula (10) for example) against thick dielectric sheath results (using the approximate formula (8) and subsequent application of the transmission line equations to the dominant mode).

In the thick sheath numerical results which follow, we restrict the results to include only the cases wherein at most a single propagating mode exists in any region where relative  $\epsilon$  is greater than one.

### III. DIELECTRIC LOADING RESULTS

We first consider the dielectric-loaded array (top of Fig. 2). In reality this may be viewed as an infinitely thick sheath with only one dielectric boundary interacting with the array interface ( $z = 0$ ). The phase of  $R$ , the reflection coefficient, and the amplitude of  $R$  are plotted as a function of scan angle ( $kb \sin \theta$  for the H-plane, and  $kd \sin \theta$  for the quasi-E plane), with  $\epsilon$  as a parameter. A moderate, but fixed, guide wall thickness in the plane of scan is assumed in all the data.

#### 3.1 H-Plane Results

Fig. 3 gives some typical results for the H-plane scan direction with the waveguides loaded with  $\epsilon = 0.9$  to  $\epsilon = 3.0$ . The change in  $R$  with  $\epsilon$  between curves is smooth. Between  $\epsilon = 0.9$  and  $\epsilon = 1.1$ , however, the change in  $|R|$  is great. This may be attributed to the fact that cutoff of the dominant waveguide mode occurs at  $\epsilon = 0.872$ .

We notice that for  $\epsilon \sim 1.3$ , the angular response is nearly flat, both in amplitude and phase. In fact, for all wavelengths examined there appears to be at least one value of  $\epsilon$  for which a nearly flat angular response for  $R$  is obtained. It should be noted that even if the magni-

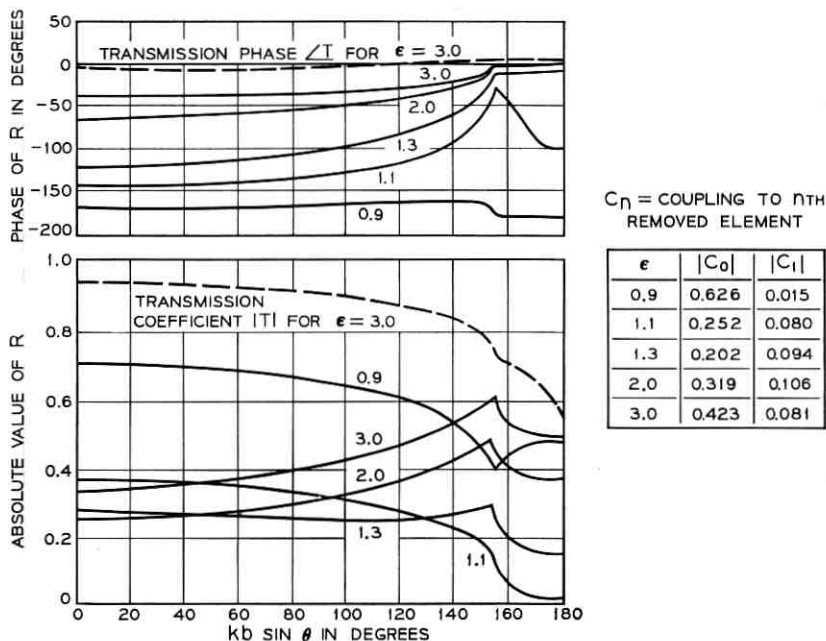


Fig. 3—Dielectric loading inside waveguides for H-plane scanning.  $a = 0.937b = 0.5354\lambda$ ,  $b = 0.5714\lambda$ .

tude of  $R$  were large, the flatness of the response in both amplitude and phase permits matching the array for all angles in the region of flat response, at least at one frequency.

The discontinuity in slope of these curves at  $kb \sin \theta = 2\pi(1 - \lambda/b)$  coincides with the onset of a grating lobe at that angle. Notice that the singularity in the derivative of the modulus of  $R$  ( $|R|$ ) lies on the right side of grating lobe incipience, but on the left side for the phase of  $R$ . This is the same as that found for thin walls<sup>1, 2</sup> and it is plausible that this will lead to the same asymptotic coupling.

The table in Fig. 3 shows the self-reflection coefficient  $C_0$  and the coupling to the adjacent element  $C_1$  when a single waveguide element is excited and the others merely terminated with a perfect match. The adjacent element coupling is found to be an order of magnitude smaller for the H-plane than for the quasi-E plane. For  $\epsilon = 3.0$ , some higher-order coupling coefficients for the H-plane case of Fig. 3 are:

$ C_0 $	$ C_1 $	$ C_2 $	$ C_3 $	$ C_4 $
0.423	0.081	0.032	0.017	0.013

Fig. 3 also shows the transmission phase and amplitude curves for  $\epsilon = 3.0$ . These curves are in fact the far field patterns when a single waveguide element is excited<sup>4</sup> (except that the maximum value for  $\theta$  is somewhat less than  $90^\circ$  since  $b/\lambda > \frac{1}{2}$ ). The very flat phase curve is an indication that the phase center for the singly excited element lies in the aperture plane.

For a wavelength further removed from the waveguide cutoff length, the variation of  $R$  between curves of constant  $\epsilon$  is considerably reduced. Fig. 4 gives some typical results for  $b/\lambda = 0.400$ . (The dielectric loading here permits an element spacing of less than  $\lambda/2$ .)

### 3.2 Quasi-E Plane Results

Fig. 5 gives typical quasi-E plane results, where  $R(\theta)$ ,  $|C_0|$ , and  $|C_1|$  are shown as a function of  $\epsilon$  from  $\epsilon = 0.8$  to  $\epsilon = 1.6$ . This range of  $\epsilon$  generally depicted all the important characteristics observed. Furthermore, a slightly greater value of  $\epsilon$  than  $\epsilon = 1.6$  would cause the waveguides to multimode (more than one mode propagates). Notice

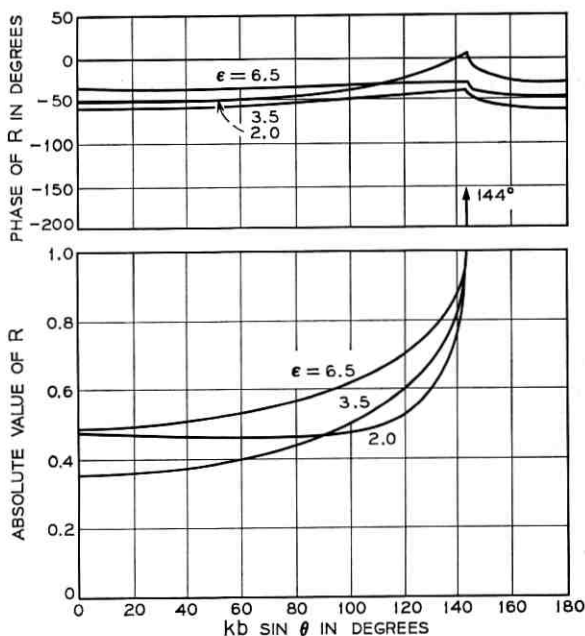


Fig. 4 — Dielectric loading inside waveguides for H-plane scanning (element spacing  $< \lambda/2$ ).  $\alpha = 0.937b = 0.3748\lambda$ ,  $b = 0.400\lambda$ .

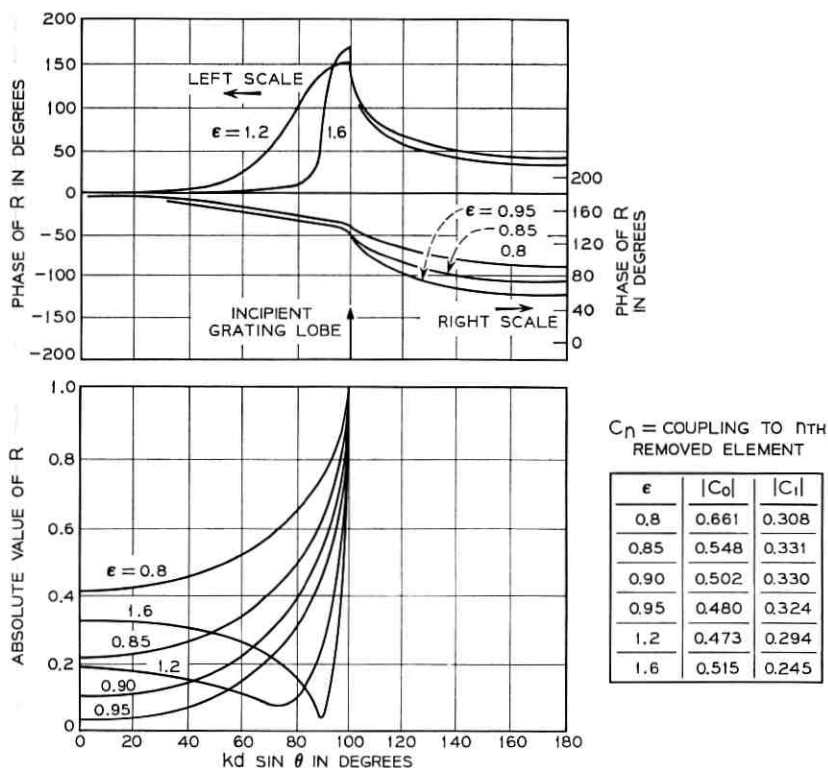


Fig. 5—Dielectric loading inside waveguides, for quasi-E plane scanning.  $a = b = d = 0.5714\lambda$ ,  $h = c = 0.937d = 0.5354\lambda$ .

in the table of coupling coefficients that the adjacent element coupling magnitudes are an order of magnitude greater than those for the H-plane scan case, independent of dielectric constant. This is also true for higher coupling coefficients for the case depicted in Fig. 5, as shown below:

$ C_0 $	$ C_1 $	$ C_2 $	$ C_3 $	$ C_4 $
0.515	0.245	0.153	0.102	0.075

This behavior is attributable to both element spacing and polarization. (By making  $b < \lambda/2$ , and with an appropriate dielectric loading, H-plane results very similar to these quasi-E plane results are obtainable. For example; see Fig. 4. The  $\lambda$  we refer to here is that which is appropriate at the aperture for  $z > 0$ .)

The curves of  $|R|$  in Fig. 5 show that total reflection occurs beyond a critical angle ( $\sim 100^\circ$ ). This occurs because the element spacing  $d$  is less than  $\lambda/[4 - (\lambda/b)^2]^{1/2}$ . Again, the infinite slopes for  $|R|$  and for the phase of  $R$ , which occur at this critical angle, exhibit the same behavior found in the thin wall analysis<sup>1,2</sup> when  $\epsilon = 1$ . Hence the same asymptotic behavior of coupling,  $\exp(-jkr)/r^{3/2}$ , may be expected for thick walled dielectric loaded arrays. (Here  $r$  is the distance between the excited and coupled element.)

A point of special interest in connection with these curves is the appearance of a resonance that occurs near the critical angle. A sharp dip in  $|R|$  occurs precisely at the same angle for which the slope of the phase of  $R$  curves has a maximum. Although the sharpness of the resonance increases gradually with  $\epsilon$ , it is interesting that there is no resonance for  $\epsilon < 1.0$ .

Fig. 6 illustrates the transmission phase and amplitude, or equivalently, the far field pattern of a singly excited element.

In Fig. 7 we illustrate the effect of a capacitive iris loading (that results when  $h < c$ ) together with dielectric loading. In this case we

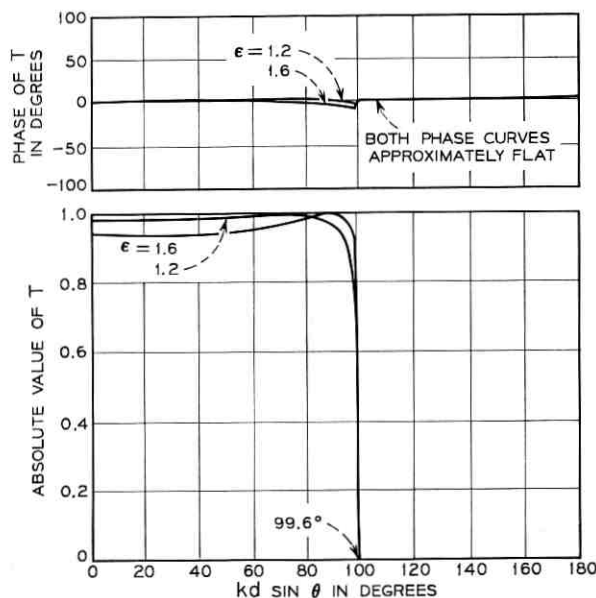


Fig. 6—Transmission coefficient for dielectric loading inside waveguides, with quasi-E plane scanning.  $a = b = d = 0.5714\lambda$ ,  $h = c = 0.937d = 0.5354\lambda$ .

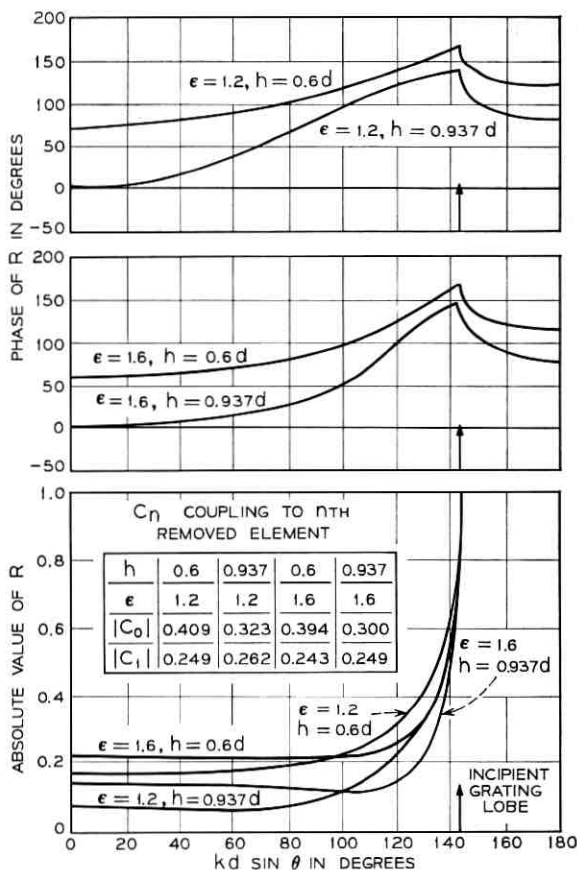


Fig. 7—Dielectric loaded waveguides and iris loaded apertures, for E-plane scanning.  $a = b = \infty$ ,  $d = 0.400\lambda$ ,  $h = 0.6d = 0.240\lambda$  and  $h = 0.937d = 0.3748\lambda$ ,  $c = 0.937d$  ( $h = 0.937d \Rightarrow$  fully open aperture;  $h < 0.937d \Rightarrow$  iris at aperture).

have let  $a = b \rightarrow \infty$  so that a true E-plane scan in a parallel plate array is considered. The effect of the iris tends to flatten the phase and amplitude responses, particularly the phase response, at the expense of a somewhat greater average  $|R|$ . The larger average  $|R|$  can, however, be uniformly reduced for all scan angles in a region of flat  $R(\theta)$  response.

The solutions of the integral equations (1) and (2) are actually complete solutions of the boundary value problem. The fields as well as the scattering matrix are determined. The variation of  $E_v$  in the

aperture as a function of scan angle ( $kd \sin \theta$ ) is sharper when the waveguides are loaded. Particularly interesting is the field change near the critical angle  $kd \sin \theta = \lambda/[4 - (\lambda/b)^2]^{\frac{1}{2}}$ , which has the value  $99.57^\circ$  for the results shown in Fig. 8. Since the relevant eigenvalue equation (See p. 157 of Ref. 4.) for  $[E_y(\theta) + E_y(-\theta)]$  has a Hermitian kernel\* for  $|kd \sin \theta| > 99.57^\circ$ , the phase of  $[E_y(\theta) + E_y(-\theta)]$  should be constant in this region. By observing the phase of the approximate field

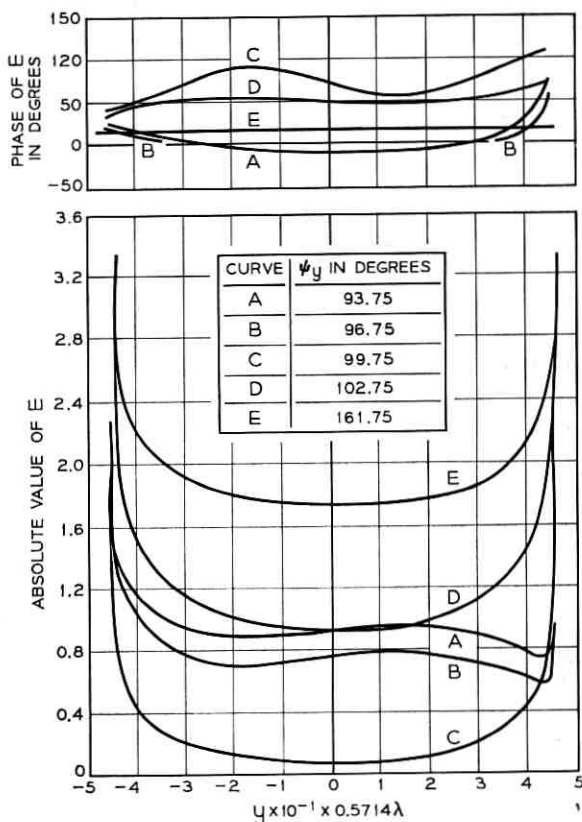


Fig. 8—Tangential electric field distribution,  $E_y(y)$ , in the aperture plane, for quasi-E plane scanning.  $\epsilon = 1.6$ ,  $a = b = d = 0.5714\lambda$ ,  $c = h = 0.937d = 0.5354\lambda$ ,  $\psi_y$  cutoff =  $99.57^\circ$ .

\* Since no power is radiated for  $|kd \sin \theta| > \lambda/[4 - (\lambda/b)^2]^{\frac{1}{2}}$  when the phasing is directed in the  $+\theta$  and  $-\theta$  directions simultaneously, the phased array behaves like a closed system, a cavity, and it is easy to show that a Hermitian kernel results. It is well known, then, that the eigenfunctions (the field solution here) of such a kernel have no varying phase.

solution at angles greater than the critical angle, we may obtain some evaluation of the errors in this solution. For most angles the errors are small. However, it is evident that errors in phase do occur for  $\theta$  near the critical angle and also for  $y$  near the singularity obtained for  $|E_v|$ . Nevertheless, since the computation of  $R$  is an averaged quantity over the range of  $y$ , these errors do not greatly affect the values obtained for  $R$ .

#### IV. DIELECTRIC SHEATH INSIDE WAVEGUIDES

When we add another dielectric boundary inside the waveguides, that is, when we place a dielectric sheath inside the guides, the results obtained for  $R$  are substantially different. This is true despite the fact that we will consider only thick sheaths, in the sense described earlier. The large change in  $R(\theta)$  behavior occurs because, even when a thick sheath is assumed, the second dielectric boundary is accounted for by a bilinear transmission line transformation which changes the input variation of  $R$  with  $\theta$ . (A linear transformation would leave  $R(\theta)$  functionally unchanged.)

In the following we will keep the dielectric constant fixed and plot  $R(\theta)$  versus  $kb \sin \theta$  with  $d_s$ , the sheath thickness, as a parameter. The phase of  $R$  will be referred to the aperture plane,  $z = 0$ , although  $R$  is the reflection coefficient for, or into, the region  $z < -d_s$ . The choice of  $\epsilon$  in any given figure was made so that the illustrated results were typical of a wider range of  $\epsilon$ . With the thick sheath approximation, the results will repeat every half guide wavelength, so that  $d_s$  is varied over only one half wavelength. The minimum  $d_s$  for which the thick approximation is valid is determined by the relative decay of the first evanescent mode in the distance  $d_s$ . This decay factor,  $df$ , is presented with each curve. It is found, generally, that  $df \gtrsim 0.1$  is sufficient for the thick sheath approximation to be valid. This result is usually satisfied for some  $d_s \gtrsim \lambda_g/2$ . Of course, by adding a sufficient number of multiples of a half guide wavelength to  $d_s$ , the results must become valid to any accuracy desired.

##### 4.1 *H-Plane Scan Results*

In Fig. 9 we have illustrated some typical results with  $\epsilon = 2.0$ . For any given  $\epsilon$  we have found that there exists a thickness,  $d_s$ , for which both the amplitude and phase of the reflection coefficient is flat over the generally useful region of scan angle (region in which only one lobe radiates). However, as the dielectric constant is increased, the

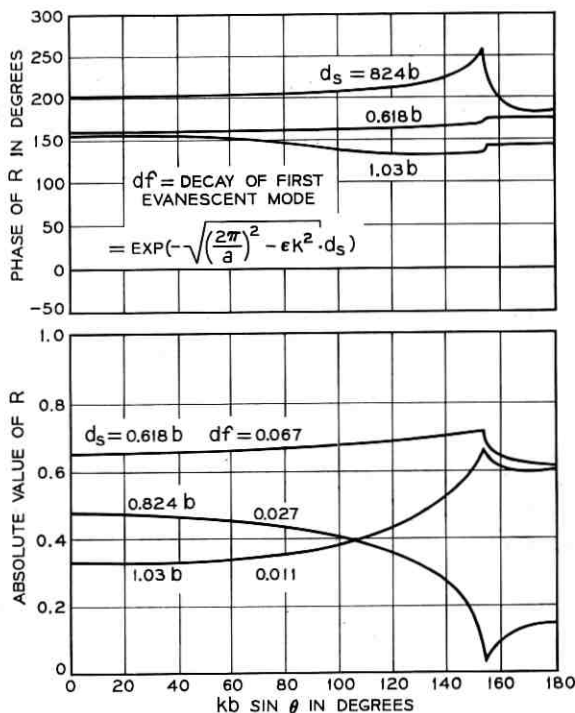


Fig 9—Dielectric sheath inside waveguides, for H-plane scanning.  $\epsilon = 2.0$ ,  $\epsilon_1 = 1.0$ ,  $a = 0.937b = 0.5354\lambda$ ,  $b = 0.5714\lambda$ .

frequency sensitivity of the angular response is increased. This is manifested, basically, by an increased spread between the curves shown. Furthermore, since the nearly flat curve also is found to have the maximum amplitude of  $R$  ( $d_s = 0.618b$  in Fig. 9), the necessity of matching out a larger  $|R|$ , when  $\epsilon$  is greater, further aggravates the frequency sensitivity problem that occurs with increasing  $\epsilon$ . The results in Fig. 10, when compared with those in Fig. 9, show the effect of increasing  $\epsilon$ .

#### 4.2 Quasi-E Plane Scan Results

Qualitatively similar results are obtained in the quasi-E plane scan case as illustrated in Figs. 11 and 12. The increasing dielectric constant, illustrated by comparing the results in Figs. 11 and 12 ( $\epsilon = 1.2$  and  $\epsilon = 1.6$ , respectively), causes a greater spread between curves and, consequently, a greater frequency sensitivity.

In addition, we again notice a sharp resonance here (increasingly sharper with greater  $\epsilon$ ), just as we noticed when only a single dielectric boundary was present. The primary difference between these results and those for a single dielectric boundary is that we may keep the dielectric constant fixed here and vary the thickness,  $d_s$ , to obtain a flat response. This is done, however, with the cost of increased frequency sensitivity.

#### V. DIELECTRIC SHEATH OUTSIDE WAVEGUIDES

We notice that very similar results are obtained in the quasi-E plane scan independent of whether the second dielectric boundary is placed inside or outside the waveguides; that is, independent of whether there is a dielectric sheath inside or outside the waveguides. Fig. 13 illustrates a typical result. In this figure the value of  $\epsilon$  is held fixed while the sheath thickness (see the bottom figure of Fig. 2) is varied from curve to curve.

Notice first that when the interaction between the second dielectric

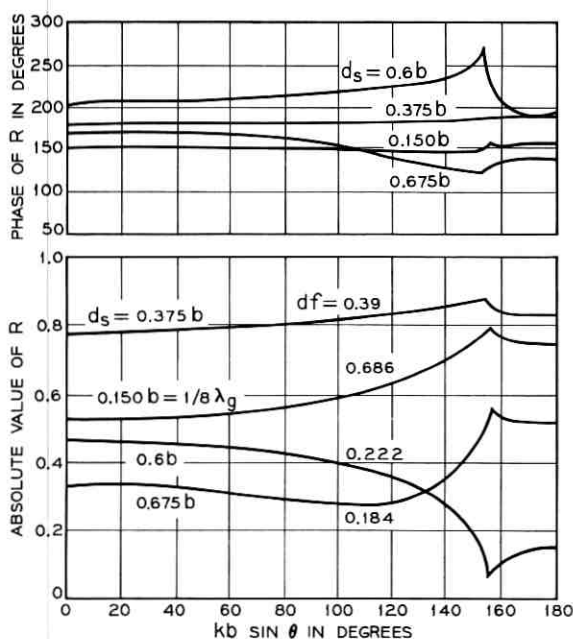


Fig. 10—Dielectric sheath inside waveguides, for H-plane scanning.  $\epsilon = 3.0$ ,  $\epsilon_1 = 1.0$ ,  $a = 0.937b = 0.5354\lambda$ ,  $b = 0.5714\lambda$ .

boundary, at  $z = +d_s$ , and the array face is accounted for, with all the evanescent modes, then the results shown by the circles and triangles are obtained. The results agree very well with those results in which higher order mode interaction with the second dielectric boundary is neglected, that is, the sheath satisfies the earlier specified thickness criteria.

Fig. 14 shows a useful way of estimating what value of  $d_s$  will be properly "thick". Notice first that the rate of decay of higher order modes away from the array face is a function of scan angle in the exterior sheath case. Hence, a single value cannot be used as a decay factor for all  $\theta$ . In Fig. 14, however, the actual ratios of the first and second evanescent mode amplitudes to the propagating modes is

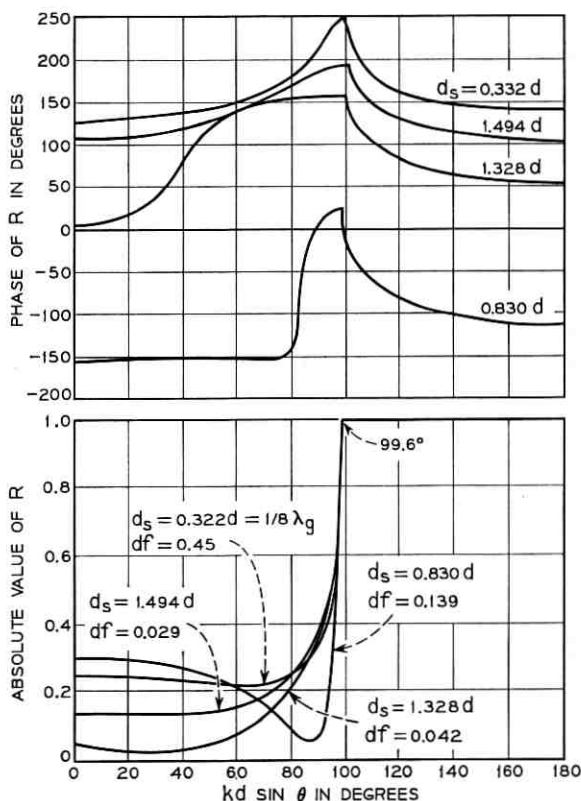


Fig. 11—Dielectric sheath inside waveguides, for quasi-E plane scanning.  $\epsilon = 1.2$ ,  $\epsilon_1 = 1.0$ ,  $a = b = d = 0.5714\lambda$ ,  $c = h = 0.937d = 0.5354\lambda$ .

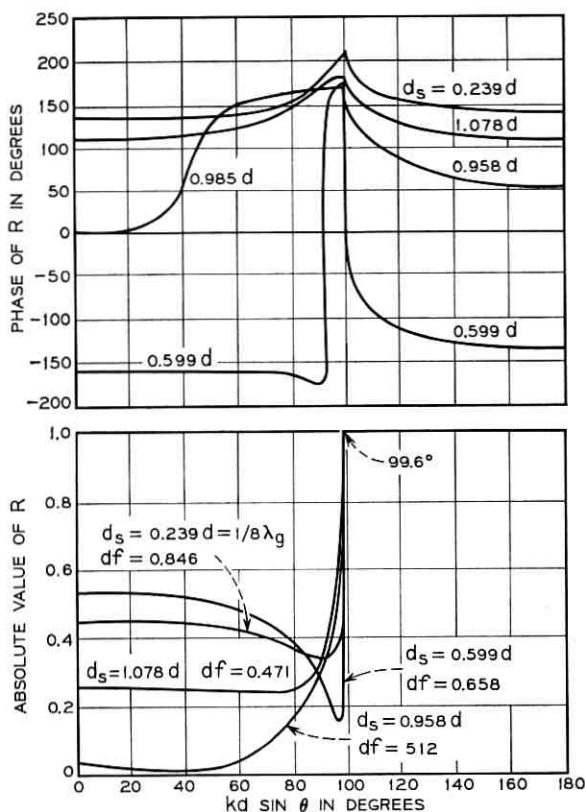


Fig. 12—Dielectric sheath inside waveguides, for quasi-E plane scanning.  $\epsilon = 1.6$ ,  $\epsilon_1 = 1.0$ ,  $a = b = d = 0.5714\lambda$ ,  $c = h = 0.937d = 0.5354\lambda$ .

plotted versus  $kd \sin \theta$ . Again we see that if  $RD1$  and  $RD2$  (see Fig. 14 for definitions) are less than about 0.1, then the particular  $d_s$  is thick.

A "thick"  $d_s$  means that, for a given scan angle, the results for  $R(\theta)$  will repeat periodically so that

$$R\left(\theta, d_s + n \frac{\lambda_{z,z}}{2}\right) = R(\theta, d_s)$$

for all  $n > 0$ . The question remains whether  $\lambda_{z,z} = 2\pi/\beta_0^*$  (see equation (7)) varies rapidly with  $kd \sin \theta$ . This may be answered by examining the grating lobe structures in the dielectric sheath as compared with that in free space, as shown in the inset in Fig. 13. This structure is obtained

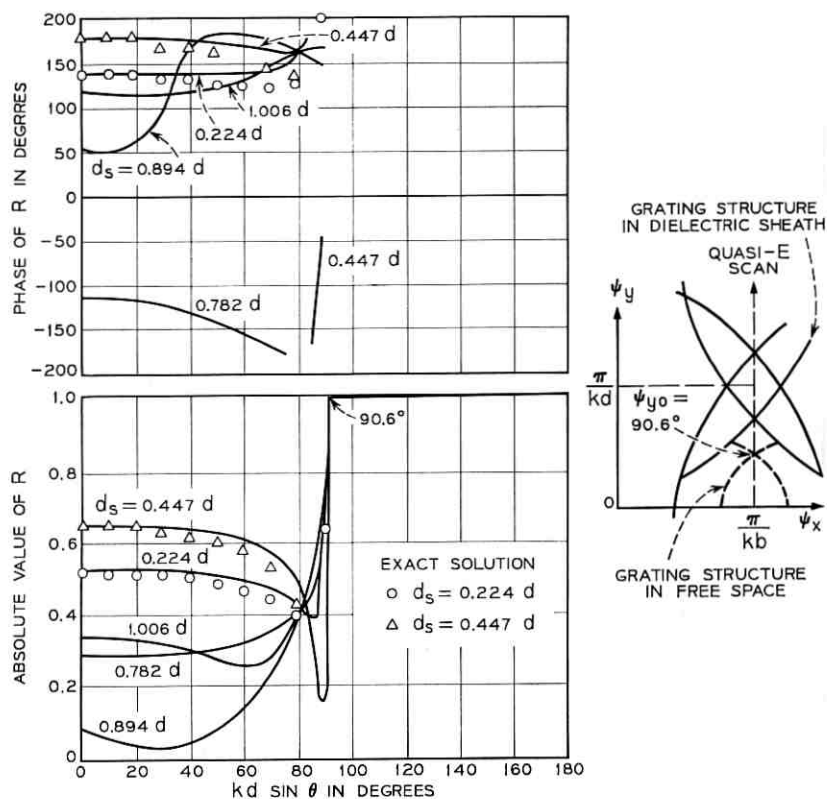


Fig. 13—Dielectric sheath outside waveguides, for quasi-E plane scanning.  $\epsilon = 1.818$ ,  $a = b = d = 0.5596\lambda$ ,  $c = h = 0.937d = 0.5243\lambda$ .

by setting

$$\text{and } \begin{cases} \beta'_{m_s} = 0 = \sqrt{\epsilon k^2 - \left(\frac{\pi}{b}\right)^2 - \left(\frac{2\pi m - \psi_y}{d}\right)^2} & (\psi_y \equiv kd \sin \theta) \\ \beta'_{m_o} = 0 = \sqrt{k^2 - \left(\frac{\pi}{b}\right)^2 - \left(\frac{2\pi m - \psi_y}{d}\right)^2} \end{cases} \quad (12)$$

(Actually (12) defines the intersections shown in the Fig. 13 inset. The total grating lobe structure requires setting the two-dimensional  $z$ -directed propagation constants to zero.) Now the  $z$ -directed wavelength in the sheath is given by

$$\lambda_{z_s} = \frac{2\pi}{\beta'_{0_s}}$$

which is a slowly-varying function of  $\theta$  in that part of the grating lobe structure bounded by the dashed lines in the Fig. 13 inset. Only this region is useful, because the propagating wave in the dielectric is totally reflected at  $(kd \sin \theta)^2 \geq k^2 - (\pi/b)^2$  ( $\psi_v > 90.6^\circ$ ). Hence the pole in  $\lambda_{z\epsilon}$  doesn't affect the variation of  $\lambda_{z\epsilon}$ , and  $\lambda_{z\epsilon}$  varies very little with  $\theta$ , from  $\psi_v = 0$  to  $\psi_v^2 = (k^2 - (\pi/b)^2)$ , providing that

$$\frac{\sqrt{\epsilon - 1}}{\sqrt{\epsilon - \left(\frac{\lambda_0}{2b}\right)^2}} \sim 1. \quad (13)$$

We should mention that the quasi-E plane results for the sheath inside and outside the waveguides are similar, primarily because of the element spacing that causes total reflection to occur at the defined critical angle. When the element spacing is changed, very markedly different results can be obtained. The results depicted in Fig. 15 for the H-plane are typical of this.

In examining the grating lobe diagram in the inset of Fig. 15 we notice that, in the shaded region, *two waves* propagate in the dielectric sheath whereas only *one wave* propagates in free space. This is a potentially very useful operating region for the phased array because

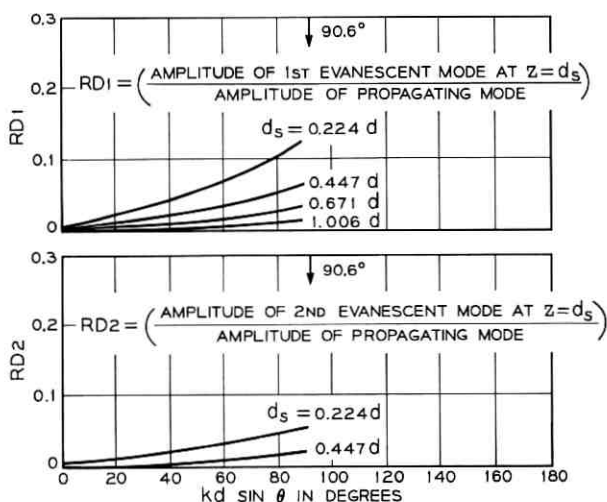


Fig. 14—Validity check of transmission line approximations, for quasi-E plane scanning with a dielectric sheath outside waveguides.  $\epsilon = 1.818$ ,  $a = b = d = 0.5596\lambda$ ,  $c = h = 0.937d = 0.5243\lambda$ .

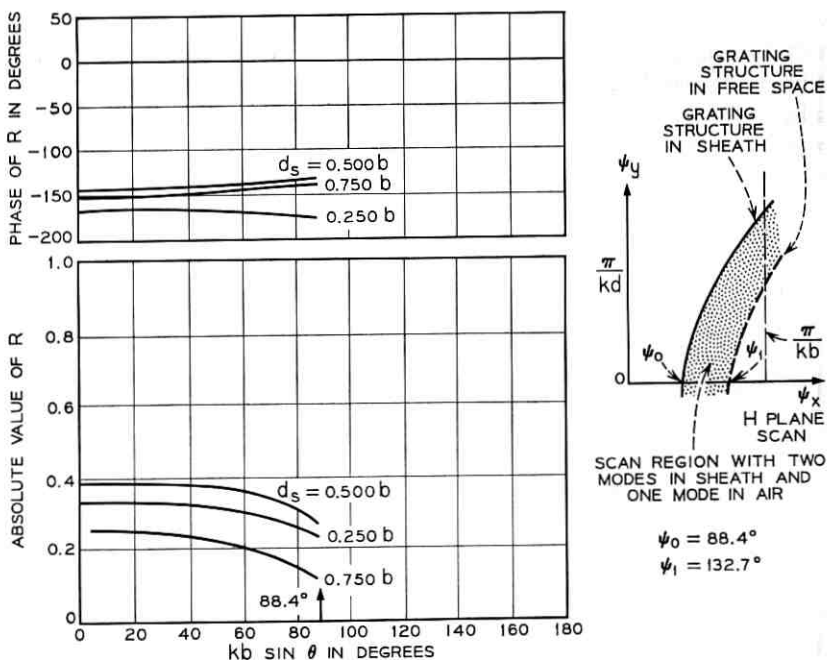


Fig. 15—Dielectric sheath outside waveguides, for H-plane scanning.  $\epsilon = 1.429$ ,  $a = 0.937b = 0.5915\lambda$ ,  $b = 0.6313\lambda$ .

only one beam will be radiated. However, we find that interference between the two propagating waves in the dielectric causes some very interesting anomalous results associated with what might be described as unattenuated surface waves. This effect is markedly different from that which may occur for a sheath inside the guides (although as a function of frequency or sheath thickness, as opposed to scan angle, similar results may occur). Further discussion on this subject is deferred to another paper.<sup>11</sup>

The results in Fig. 15 for the  $|R|$  and the phase of  $R$  are shown in the scan angle region in which only one wave, at most, propagates in the sheath. In this angular region the results are also very different than those for the interior sheath in that the response is comparatively flat for a wide range of sheath thicknesses.

## VI. CONCLUSIONS

In summary we may state that dielectric loading or covering has a very substantial effect on the array performance to the extent that an

array and dielectric cover should be designed as an integral unit instead of being designed for minimal effect or match correction. Nevertheless, the additional parameters available in the design of an array with a dielectric cover can be used to match the array over a wide angular and frequency region.

No particular method of loading or covering appears to be universally superior except that when only one dielectric boundary is present (Fig. 2, top), the wide angle match appears to be less frequency sensitive than when a sheath or two boundaries are present. Furthermore, with thick sheaths, the maximum permissible value of  $\epsilon$  is small before serious matching problems occur (a large  $|R|$  together with a flat  $R[\theta]$ ). Finally, by placing the sheath inside the waveguides instead of outside, certain anomalous reflection phenomena, associated with the exterior sheath grating lobe structure and surface waves, can be avoided.<sup>11</sup>

Although we did not give analytic proof, the numerical results do indicate that the asymptotic behavior of the coupling coefficients<sup>2</sup> is not altered by the presence of the dielectric materials.

#### REFERENCES

1. Wu, C. P. and Galindo, V., Properties of a Phased Array of Rectangular Waveguides with Thin Walls, *IEEE Trans. on Antennas and Propagation*, *AP-14*, No. 2, 1966, pp. 163-172.
2. Galindo, V. and Wu, C. P., Asymptotic Behavior of the Coupling Coefficients for an Infinite Array of Thin-Walled Rectangular Waveguides, *IEEE Trans. on Antennas and Propagation*, *AP-14*, No. 2, March 1966, pp. 248-9.
3. Galindo, V. and Wu, C. P., On the Asymptotic Decay of Coupling for Infinite Phased Arrays, paper presented at International Union of Radio Science, Washington, D. C., April 1966. (To be published.)
4. Galindo, V. and Wu, C. P., The Relation Between the Far-Zone Pattern of the Singly Excited Element and the Transmission Coefficient of the Principal Lobe in an Infinite Array, *IEEE Trans. on Antennas and Propagation*, *AP-14*, No. 3, March 1966, pp. 397-398.
5. Galindo, V. and Wu, C. P., Numerical Solutions for an Infinite Phased Array of Rectangular Waveguides with Thick Walls, *IEEE Trans. on Antennas and Propagation*, *AP-14*, 1966, pp. 149-158.
6. Galindo, V. and Wu, C. P., Integral Equations and Variational Expressions for Arbitrary Scanning of Regular Infinite Arrays, *IEEE Trans. on Antennas and Propagation*, *AP-14*, No. 3, May 1966, pp. 392-394.
7. Galindo, V. and Wu, C. P., A Variation Expression for the Dominant Mode Coupling Coefficients Between The Elements in an Infinite Array, *IEEE Trans. on Antennas and Propagation*, *AP-14*, No. 5, September 1966, pp. 637-639.
8. Magill, E. G. and Wheeler, H. A., Wide Angle Impedance Matching of a Planar Array Antenna by a Dielectric Sheet, *IEEE Trans. on Antennas and Propagation*, *AP-14*, 1966, pp. 49-53.
9. Lee, S. W., Impedance Matching of an Infinite Phased Array by Dielectric Sheets, *IEEE Elec. Letters*, *2*, No. 10, October 1966, pp. 366-368.

10. Kantorovich, L. V. and Krylov, V. I., *Approximate Methods of Higher Analysis*, Interscience Publishers, New York, 1958.
11. Wu, C. P. and Galindo, V., Surface-Wave Effects on Dielectric Sheathed Phased Arrays of Rectangular Wave-Guides, B.S.T.J. 47, No. 1, January 1968, pp. 117-142 (next article in this issue).
12. *Waveguide Handbook*, N. Marcuvitz, ed., MIT Radiation Lab. Series, 10, McGraw-Hill Book Company, Inc., New York, 1951.
13. Lewin, L., *Advanced Theory of Waveguides*, Iliffe and Sons, Ltd., London, 1951.

# Surface-Wave Effects on Dielectric Sheathed Phased Arrays of Rectangular Waveguides

By C. P. WU AND V. GALINDO

(Manuscript received September 12, 1967)

*A further study of the effects of dielectric slabs on the radiation characteristics of an infinite array of rectangular waveguides has been carried out. It is found that, in addition to causing substantial and sometimes beneficial changes in the array performance, the presence of dielectric slabs can give rise to sharp resonant peaks in the reflection coefficient at certain scan angles. The occurrence of such resonant peaks at which total reflection occurs is contingent upon the presence of space harmonics which have surface-wavelike field distribution. Extensive data for both the H and E planes of scan, when the array is covered with a single slab, have been obtained and are presented here. This paper discusses the influence of the dielectric constant, slab thickness, and waveguide wall thickness on the resonant peak location, and points out the relationship between the resonance phenomenon and the surface wave propagation over a corrugated surface. It also presents some further results for the thin sheath and their extension to multiple sheaths.*

## I. INTRODUCTION

We presented the radiation properties of a dielectric-loaded rectangular waveguide array in some detail in a previous paper<sup>1</sup> for two planes of scanning: the H plane and a quasi-E plane. (See Fig. 1.) We discussed the effects of a thick dielectric sheath placed inside or outside the array aperture. We concluded that the presence of a dielectric material can cause a substantial change in the array performance, so that dielectric material should be considered an integral part of the array when it is designed. Moreover, we demonstrated that the effects of a dielectric may be used to improve the match performance of an array, perhaps at the cost of a larger frequency sensitivity, by a judicious choice of the added physical parameters.

This paper deals with some different aspects of the problem based

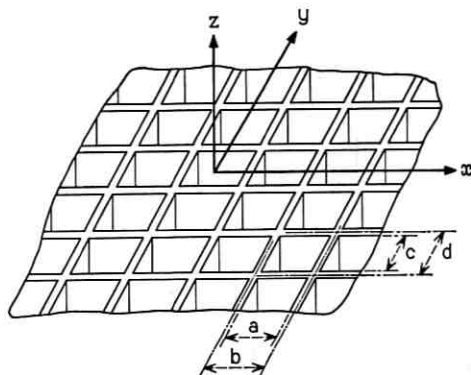


Fig. 1 — An infinite array of rectangular waveguides.

on an extensive further analysis. We completely removed the restrictions placed on the parameters in the previous work in order to analyze the full effects of a dielectric medium. In particular, since dielectric slabs can support surface waves, we direct special attention toward investigating the possibility of anomalous array behavior when dielectric slabs are used to cover the array. Indeed, a resonance phenomenon is found to exist due to the presence of trapped- (or surface-) wave type space harmonics at the air-dielectric interface. One important effect of such space harmonics is to cause the appearance of sharp resonant peaks in the reflection coefficient at certain scan angles. The peaks attain, for all practical purposes, values of unity. We present results for a dielectric slab of arbitrary thickness placed over an array, thereby, removing the previous restriction to thick slabs. We also discuss radiation through a stratified medium.

## II. ANALYSIS

The approach we use in this work, as in previous ones,<sup>1,2</sup> is based on an integral equation having either the aperture electric or the aperture magnetic field as the unknown function. One of the advantages of such an approach is that the integral equation may be easily and *rigorously* derived without any limitations from the physical parameters of the problems, and the approach is readily adaptable to a more general class of problems such as, for example, an array covered by a stratified dielectric medium. Although the basic procedures for formulating the integral equation have been discussed else-

where,<sup>2, 11</sup> in order to facilitate a further discussion of the formulation and to make this paper more or less self-contained, we present a brief derivation here and point out the modifications necessary for an extension to a more general situation of stratified media.

### 2.1 Integral Equation Formulation of the Problem

The procedure in the integral equation method is first to expand the fields into the appropriate normal modes in the various regions and then to match the boundary conditions across the interfaces. Consider, for example, an infinite array of parallel plates, covered with a single dielectric slab and scanned in the H plane as shown in Fig. 2. It is convenient in this case to divide the space into three regions, the region inside the waveguides, the region inside the dielectric slab, and the free space region. However, as will become evident shortly, it turns out that the geometry of the problem is such that it suffices to partition the space into two regions, inside and outside the waveguides.

The orthonormal modal functions and the modal impedances pertinent to the waveguide region are the usual ones given by

$$\varphi_n(x) = \begin{cases} \sqrt{\frac{2}{a}} \cos\left(\frac{n\pi}{a}x\right) & (n = \text{odd}) \\ \sqrt{\frac{2}{a}} \sin\left(\frac{n\pi}{a}x\right) & (n = \text{even}) \end{cases} \quad \text{for } |x| \leq \frac{a}{2}$$

$$0 \quad \frac{a}{2} \leq |x| \leq \frac{b}{2}$$

and

$$Z_n = \omega\mu/\alpha_n$$

where

$$\alpha_n = \sqrt{k^2\epsilon_1 - \left(\frac{n\pi}{a}\right)^2}$$

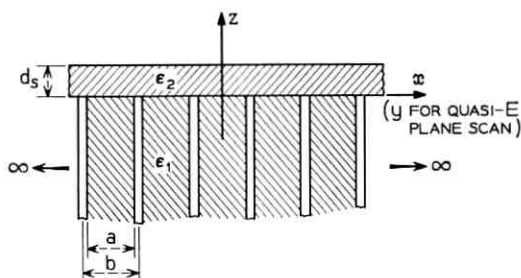


Fig. 2 — A parallel plate array covered by a dielectric sheath.

are the  $z$ -directed propagation constants for a waveguide filled with a dielectric of dielectric constant  $\epsilon_1$ .

By using the Floquet theorem, it can be easily shown that the dielectric slab and free space regions have identical modal functions, owing to the requirement that the tangential fields must be continuous at all points across the dielectric-free space interface. The normalized modal functions take the usual form:

$$\psi_m(x) = \sqrt{\frac{1}{b}} e^{j((2m\pi/b) + T_x)x}, \quad m = 0, \pm 1, \dots$$

where  $T_x$  is the phase shift per unit length. The modal impedances for these two regions are different, however. They are given respectively by

$$Z_m^D = \omega\mu/\beta_m, \quad \beta_m = \sqrt{k^2\epsilon_2 - \left(\frac{2m\pi}{b} + T_x\right)^2}$$

for the dielectric region,  $0 \leq z \leq d_s$ , and

$$Z_m^0 = \omega\mu/\gamma_m, \quad \gamma_m = \sqrt{k^2 - \left(\frac{2m\pi}{b} + T_x\right)^2}$$

for the free space,  $d_s < z$ .

When the fields in the various regions are expanded into the normal modes under the situation in which the waveguides are excited in the fundamental mode of unit amplitude, we have

$$\mathcal{H}_x(x, z) = \begin{cases} (e^{j\alpha_1 z} + Re^{-j\alpha_1 z})\varphi_1(x) + \sum_{n=2}^{\infty} I_n \varphi_n(x) e^{-j\alpha_n z} & z \leq 0 \\ \sum_{m=-\infty}^{\infty} (I_m^+ e^{j\beta_m z} + I_m^- e^{-j\beta_m z}) \psi_m(x) & 0 \leq z \leq d_s \\ \sum_{m=-\infty}^{\infty} I_m' \psi_m(x) e^{j\gamma_m(z-d_s)} & d_s \leq z \end{cases} \quad (1)$$

$$\mathcal{E}_y(x, y) = \begin{cases} -Z_1(e^{j\alpha_1 z} - Re^{-j\alpha_1 z})\varphi_1(x) + \sum_{n=2}^{\infty} Z_n I_n \varphi_n(x) e^{-j\alpha_n z} & z \leq 0 \\ -\sum_{m=-\infty}^{\infty} Z_m^D (I_m^+ e^{j\beta_m z} - I_m^- e^{-j\beta_m z}) \psi_m(x) & 0 \leq z \leq d_s \\ -\sum_{m=-\infty}^{\infty} Z_m I_m' \psi_m(x) e^{j\gamma_m(z-d_s)} & d_s \leq z \end{cases}$$

A time convention of  $\exp(-j\omega t)$  is assumed and suppressed for brevity throughout this paper. The  $I$ 's are the unknown modal coefficients. Waves of all modes travelling in both the positive and negative  $z$  directions are included in the fields for  $0 \leq z \leq d_s$ , because this region is situated between two interfaces. Likewise, the fields for  $z \leq 0$  contain waves travelling in the negative  $z$  direction due to the scattering at the array aperture.

We find, by applying the boundary conditions at  $z = 0$ , that

$$\begin{aligned} H_x(x) &= \mathcal{H}_x(x, 0) = (1 + R)\varphi_1(x) + \sum_{n=2}^{\infty} I_n \varphi_n(x) \\ &= \sum_{m=-\infty}^{\infty} (I_m^+ + I_m^-) \psi_m(x) \end{aligned} \quad (2)$$

$$\begin{aligned} E_y(x) &= \mathcal{E}_y(x, 0) = -Z_1(1 - R)\varphi_1(x) + \sum_{n=2}^{\infty} Z_n I_n \varphi_n(x) \\ &= - \sum_{m=-\infty}^{\infty} Z_m^D (I_m^+ - I_m^-) \psi_m(x). \end{aligned}$$

Hence, on account of the orthonormality among the modal functions, it follows that

$$(1 + R) = \int_{-b/2}^{b/2} \varphi_1(x) H_x(x) dx, \quad I_n = \int_{-b/2}^{b/2} \varphi_n(x) H_x(x) dx, \quad n \geq 2 \quad (3)$$

$$I_m^+ + I_m^- = \int_{-b/2}^{b/2} \psi_m^*(x) H_x(x) dx.$$

Similarly, from the boundary conditions at the interface  $z = d_s$ ,

$$\mathcal{H}_x(x, d_s) = \sum_{m=-\infty}^{\infty} (I_m^+ e^{i\beta_m d_s} + I_m^- e^{-i\beta_m d_s}) \psi_m(x) = \sum_{m=-\infty}^{\infty} I'_m \psi_m(x) \quad (4)$$

$$\begin{aligned} \mathcal{E}_y(x, d_s) &= - \sum_{m=-\infty}^{\infty} Z_m^D (I_m^+ e^{i\beta_m d_s} - I_m^- e^{-i\beta_m d_s}) \psi_m(x) \\ &= - \sum_{m=-\infty}^{\infty} Z_m^0 I'_m \psi_m(x). \end{aligned}$$

By observing that the right and left sides of (4) are the field expansions with respect to the same set of modal functions, one may immediately write

$$\begin{aligned} I_m^+ e^{i\beta_m d_s} + I_m^- e^{-i\beta_m d_s} &= I'_m \\ Z_m^D (I_m^+ e^{i\beta_m d_s} - I_m^- e^{-i\beta_m d_s}) &= Z_m^0 I'_m. \end{aligned} \quad (5)$$

Equations (5) show that the air-dielectric interface at  $z = d_s$  is a simple one in that the  $m^{\text{th}}$  order mode in the dielectric region couples

only into the same order mode in the free space region and vice versa. The implication of this result is that the fields at the air-dielectric interface are completely determined when the fields at the array aperture are obtained. Therefore, it is necessary only to solve for the aperture field alone. With this in mind, we may then make use of (2), (3) and (5) to derive an integral equation having only the aperture magnetic field as the unknown function. Thus,

$$2Z_{1\varphi_1}(x) = \int_{-b/2}^{b/2} \left\{ \sum_{n=1}^{\infty} Z_n \varphi_n(x) \varphi_n(x') + \sum_{m=-\infty}^{\infty} Z'_m \psi_m(x) \psi_m^*(x') \right\} H_x(x') dx' \quad (6)$$

where

$$Z'_m = Z_m^D \frac{Z_m^0 - jZ_m^D \tan \beta_m d_s}{Z_m^D - jZ_m^0 \tan \beta_m d_s} \quad (7)$$

It is clear from expression (7) that the equivalent impedances  $Z'_m$  for the  $m^{\text{th}}$  order modes are the familiar input impedance of a transmission line, which has a characteristic impedance  $Z_m^D$ , propagation constant  $\beta_m$ , and length  $d_s$ , and is terminated in a load impedance  $Z_m^0$ . Notice also that only quantities pertaining to the  $m^{\text{th}}$  space harmonic appear in (7). All these facts suggest that the space exterior to the waveguides may be treated as a single region from the onset, as observed earlier, provided that the effects of the dielectric slab are taken into account through the use of appropriate modal impedances. Moreover, the integral equation given by (6) is readily extended to a more general situation in which the array is covered or loaded with stratified dielectric media (or both covered and loaded). Only the modal impedances need to be modified for this purpose.

As an example, suppose we wish to study the properties of an array covered by a stratified medium as Fig. 3 shows. Equation (6) still is a valid integral equation to use. In this case, the  $Z_n$  are the usual waveguide modal impedances, whereas the  $Z'_m$  are the modal impedances as seen at the array aperture of the  $N$  layer stratified dielectric medium, which may be calculated by standard techniques.<sup>3</sup>

The integral equation appropriate to the quasi-E plane of scan may be derived in a similar manner. In a quasi-E plane of scan, the scanning takes place in the plane of the electric field while there is a sinusoidal field variation in the direction normal to the plane of scanning.\*

\*Such a mode of scanning results from a planar array of rectangular waveguides, which is scanned in the E plane direction with a fixed scan angle of  $180^\circ$  applied in the H plane direction. This special scan case is considered for the sake of simplifying the problem. See Ref. 4.

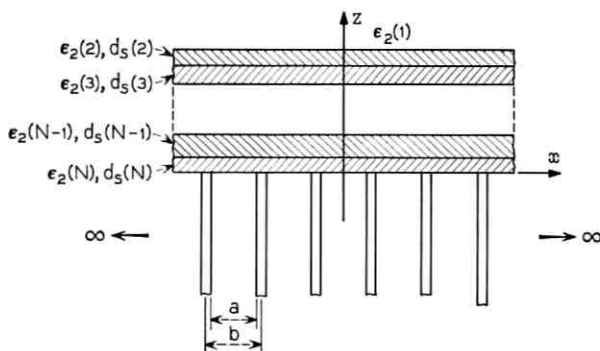


Fig. 3—Radiation of an array through  $N$  dielectric sheaths.

The exterior modal functions for the quasi-E plane scan are the same as those for H plane scan, according to the Floquet theorem, but the wave modes which the waveguides support are different. The orthonormal modal functions for this case are

$$\omega_n(y) = \begin{cases} -\sqrt{\frac{\epsilon_n}{c}} \begin{cases} \cos\left(\frac{n\pi}{c}y\right), & n = \text{even} \\ \sin\left(\frac{n\pi}{c}y\right), & n = \text{odd} \end{cases} & \text{for } y \leq \frac{c}{2} \\ 0 & \text{for } \frac{c}{2} \leq y \leq \frac{d}{2} \end{cases}$$

Here we have used  $c$  for the internal waveguide width and  $d$  for the element spacing. A sinusoidal variation of  $\sin[(\pi/b)x]$ , which applies to all tangential field components, is omitted for brevity.

The integral equation with the aperture electric field as the unknown is given by

$$2Y_0\omega_0(y) = \int_{-c/2}^{c/2} \left\{ \sum_{n=0}^{\infty} Y_n\omega_n(y)\omega_n(y') + \sum_{-\infty}^{\infty} Y'_m\psi_m(y)\psi_m^*(y') \right\} E_y(y') dy',$$

where the

$$Y_n = \left[ k^2\epsilon_1 - \left(\frac{\pi}{b}\right)^2 \right] / \omega\mu\alpha_n$$

are the interior modal admittances and the  $Y'_m$  are the exterior modal admittances with the presence of dielectric slab(s) appropriately taken into account.

## 2.2 Method of Solution

The method used in solving the integral equations is basically that of Galerkin,<sup>5,6</sup> the method of moments. Briefly, in this method, the

first step is to expand the unknown function as a linear combination of  $N$  linearly independent functions. Substitution of the representation into the original integral equation leads to an approximate equation. The difference between the left and right sides of the approximate equation is then required to be orthogonal to the set of functions individually, thus yielding a set of  $N$  equations in  $N$  unknowns. The resulting set of equations may then be inverted with the help of an electronic computer.

There are different sets of functions one may choose to use in this approach. Although the choice, aside from consideration of computer time and convenience, seems to be largely a matter of personal preference, it is desirable to incorporate as much prior knowledge about the problem as possible. We have used the set of first  $N$  modal functions to obtain most of the results reported here. This step is tantamount to assuming the higher order modal coefficients to be zero. For example, to solve (6), we set

$$H_x(x) \approx \sum_{m=-M}^M \tilde{I}'_m \psi_m(x), \quad \tilde{I}'_m = 0 \quad |m| > M. \quad (8)$$

Substituting (8) into (6) leads to

$$2Z_1 \varphi_1(x) - \sum_{m=-M}^M \left\{ \sum_{n=1}^{\infty} Z_n C_{nm} \varphi_n(x) + Z'_m \psi_m(x) \right\} \tilde{I}'_m \approx 0, \quad (9)$$

where

$$C_{nm} = \int_{-b/2}^{b/2} \varphi_n(x) \psi_m(x) dx.$$

The expression (9) is then required to be orthogonal to the set of functions  $\psi_l^*(x)$ ,  $l = 0, \pm 1, \dots, \pm M$ , individually, thus yielding

$$\sum_{m=-M}^M \left\{ \sum_{n=1}^{\infty} Z_n C_{nm} C_{nl}^* + Z'_m \delta_{ml} \right\} \tilde{I}'_m = 2Z_1 C_{1l}^* \quad l = 0, \pm 1, \dots, \pm M. \quad (10)$$

The set of equations (10) may be solved by a standard technique. The reflection coefficient  $R$  is then obtainable from

$$(1 + R) = I_1 \approx \sum_{m=-M}^M C_{1m} \tilde{I}'_m. \quad (11)$$

Since it appears that there is no convenient scheme for estimating the error in the type of problem being considered here, the following procedures have been used to ascertain the accuracy of the results. They include:

- (i) Observing the "convergence" of the solution by increasing  $N$ , the number of functions used to represent the unknown aperture field.
- (ii) Using different sets of functions, such as the set of piecewise constant or pulse functions for the approximation.
- (iii) Comparing the results with known solutions obtained by different methods where applicable.<sup>4, 7, 8</sup>
- (iv) Applying the variational principle to check the adequacy of the algorithm used in the numerical procedure.
- (v) Checking how well energy is conserved.

### III. RESULTS

In the previous report,<sup>1</sup> we placed the emphasis on the results for the situations where the waveguides are either completely filled with a dielectric material or loaded with a dielectric slab. We also discussed some preliminary results for covering the array with a dielectric sheath. We obtained that data for a range of parameters such that, at most, one propagating mode could exist inside the dielectric region, and only relatively thick slabs were considered. Such a choice of the parameters was necessary in order that an approximation based on the transmission line theory could be applied.

The results presented here are concerned largely with the effects of dielectric sheaths covering the array. In particular, we concentrate on the situation in which more than one wave can propagate inside the dielectric region so that there will be trapped- (or surface-) wave-like space harmonics at the air-dielectric interface. Although in principle it is still possible in such cases to apply a *generalized* transmission line approximation, this approach might not be very convenient in practice. The modification required for generalization depends on the number of modes which can propagate inside the dielectric, and this number is, in turn, dependent on the dielectric constant being used. Moreover, the minimum slab thickness necessary for a valid approximate calculation might sometimes become so large that it would exclude a useful range of practical interest. Therefore, it is desirable to proceed with the solution of the appropriate integral equations without introducing any intermediate steps. Thus, the effects of the air-dielectric interface at  $z = d_s$  on *all* the modes generated at the array aperture may be fully taken into account. By doing so, we are also able to obtain data for comparison with those calculated by using the transmission line theory, and thus gain a

general feeling for the accuracy of this type of approximation. Some results of such a comparison are presented in Ref. 1.

### 3.1 General Remarks

The effect of an ordinary dielectric ( $\epsilon > 1$ ) on wave propagation is to slow down the phase velocity, or equivalently to shorten the wavelength. Hence, when a dielectric slab is placed over a phased array, two apparent element spacings (in terms of the wavelength) have to be considered: one inside the dielectric medium and the other in the free space; the former always greater than the latter. A difference in the element spacings as seen in the two regions results in different scan angles for the appearance or disappearance of grating lobes in the respective regions. Consequently, when the fields are expanded into normal modes according to the Floquet theorem, there will be a range of scan angles over which the number of propagating modes inside the dielectric is larger than that in free space. A mode is said to be propagating when the corresponding  $z$ -directed propagation constant is real. In a linear array, this propagation constant is given by

$$\beta_m = \sqrt{k^2 \epsilon - \left( \frac{2m\pi}{b} + T_z \right)^2},$$

with an appropriate  $\epsilon$  for each region. It is easy to show that for  $m < b/\lambda_e < (m + 1/2)$ , where  $m$  is an integer and  $\lambda_e$  is the wavelength of a plane wave in a medium with dielectric constant  $\epsilon$ , the number of propagating modes will change from  $(2m + 1)$  for  $0 \leq T_z b < 2\pi(b/\lambda_e - m)$  to  $(2m)$  for  $2\pi(b/\lambda_e - m) \leq T_z b \leq \pi$ . On the other hand, when  $(m + 1/2) < b/\lambda_e < (m + 1)$ , the number of propagating modes will increase by one from  $(2m + 1)$  to  $(2m + 2)$ , when the scan angle passes from  $0 < T_z b < 2\pi(m + 1 - b/\lambda_e)$  to  $2\pi(m + 1 - b/\lambda_e) < T_z b < \pi$ .

The wave modes which are propagating inside the dielectric and are evanescent in free space have the same field distribution as that of a surface wave. Such wave modes have profound effects on the radiation characteristics of a phased array as we will see in the examples. It is important to emphasize that a single wave mode of this type alone is *not* sufficient to satisfy the boundary conditions. In other words, all the modes are required to constitute a correct solution.

### 3.2 H-Plane Scan Results

Figs. 4 and 5 give the reflection coefficients as a function of scan for an infinite array of rectangular waveguides covered with a single

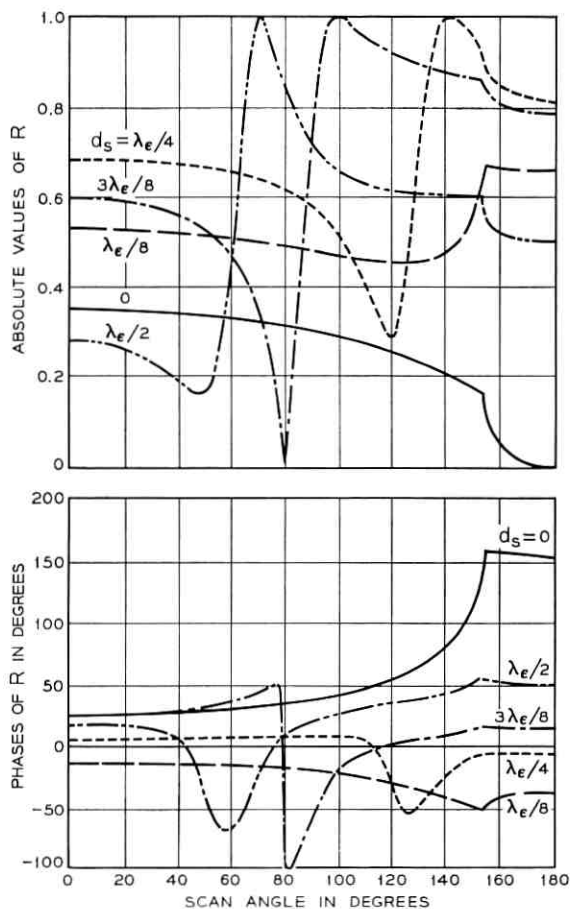


Fig. 4—Reflection coefficient  $R$  vs scan angle  $T_x b$  for H plane scan with  $a/\lambda = b/\lambda = 0.5714$ , and  $\epsilon = 3.0625$ .

dielectric sheath and scanned in the H plane. The results are obtained for the following parameters:  $b/\lambda = a/\lambda = 0.5714$ ,  $\epsilon = 3.0625$  with the thickness of the dielectric slab  $d_s$  varied over one  $\lambda_e$  at an increment of  $\lambda_e/8$ , where  $\lambda_e$  is the wavelength of a plane wave in the dielectric medium. Notice that the element spacing is measured in terms of the free space wavelength  $\lambda$ , for  $b/\lambda$  is the quantity which determines the number of radiated beams at a certain scan angle. With the given arrangement, the element spacing is such that the array radiates one beam for  $0 \leq T_x b \leq 2\pi(1 - b/\lambda) = 154^\circ$ , and two beams when  $2\pi(1 - b/\lambda) \leq T_x b \leq$

180°. The dielectric constant of the slab makes the apparent element spacing in the medium to be  $b/\lambda_e = 1$ . Thus, there are always two propagating modes inside the dielectric slab for all scan angles. As a result, we have in  $0 \leq T_z b \leq 2\pi(1 - b/\lambda)$  a mode which exhibits a surface-wavelike behavior by being propagated inside the dielectric and evanescent in free space. The effect of such a mode is to cause the appearance of sharp resonant peaks in the reflection coefficient at certain scan angles as is evident from the graphs.

Based on the results presented here and some further calculations at different wavelengths, we may make the following general observations:

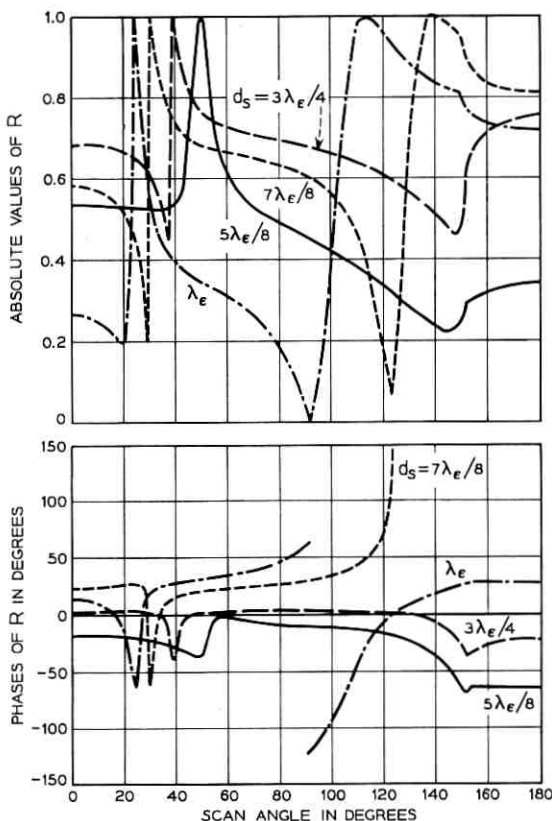


Fig. 5—Reflection coefficient  $R$  vs scan angle  $T_z b$  for H plane scan with  $a/\lambda = b/\lambda = 0.5714$ , and  $\epsilon = 3.0625$ .

- (i) When the thickness of the dielectric slab is relatively small, no resonant peak occurs.
- (ii) When the thickness is increased beyond a critical value, usually in the neighborhood of  $3\lambda_\epsilon/16$ , a resonant peak starts to appear at a scan angle close to the value  $2\pi(1-b/\lambda)$ , and the peak is usually preceded by a dip.
- (iii) Increasing the slab thickness causes the peak to move toward the broadside direction and the peak becomes sharper.
- (iv) A further increase in the slab thickness makes more than one peak appear.
- (v) The peaks attain, for all practical purposes, values of unity.

The dielectric constant used in obtaining the results for Figs. 4 and 5 was chosen to have a value  $\epsilon = (\lambda/b)^2$ . This creates a situation where one space harmonic possesses a surface-wavelike field distribution in  $0 \leq T_z b \leq 2\pi(1 - b/\lambda)$ . It is possible for a resonant peak to appear at any scan angle within this range. If a smaller dielectric constant had been used, the range of scanning over which a resonant peak might appear would be reduced accordingly. On the other hand, a larger value of dielectric constant would give rise to more than one surface-wavelike space harmonic, and it is possible for resonant peaks to appear with dielectric slab of thickness even smaller than  $3\lambda_\epsilon/16$ .

Recall that when we use a dielectric slab of small dielectric constant and large slab thickness, the transmission line approximation may be effectively applied to yield useful results.<sup>1</sup> The reflection coefficients calculated under such conditions are periodic functions of the slab thickness; hence, the calculations only need be performed over a period, that is, a half guided wavelength. If the dielectric constant is large so as to permit more than one propagating mode inside the dielectric, however, the periodic property is no longer present, and separate calculations have to be carried out for different slab thicknesses.

Fig. 6 is typical of the transmission coefficients calculated for  $b/\lambda = a/\lambda = 0.5714$ ,  $\epsilon = 3.0625$  and  $d_s = \lambda_\epsilon/2$ . These transmission coefficients are referred to the air-dielectric interface  $z = d_s$ . The figure shows both the transmission coefficients for the zero<sup>th</sup> order mode (corresponding to the main beam) and the first space harmonic (corresponding to a grating lobe). These coefficients are defined so that the sum of the reflection coefficient squared and the square of the transmission coefficient(s) equals one. Thus, if  $T_0$  and  $T_1$  denote the

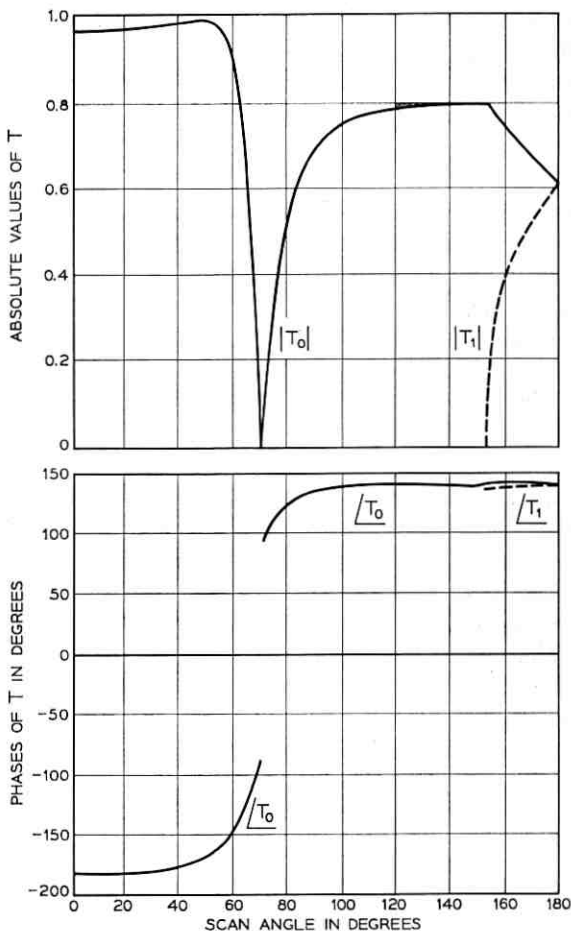


Fig. 6—Transmission coefficients  $T$  vs scan angle  $T_x b$  for H plane scan with  $a/\lambda = b/\lambda = 0.5714$ ,  $\epsilon = 3.0625$ ,  $d_x = 0.5\lambda$ .

transmission coefficients of the main beam and the grating lobe respectively, then

$$|R|^2 + |T_0|^2 = 1 \quad \text{for } 0 \leq T_x b \leq 2\pi\left(1 - \frac{b}{\lambda}\right)$$

$$|R|^2 + |T_0|^2 + |T_1|^2 = 1 \quad \text{for } 2\pi\left(1 - \frac{b}{\lambda}\right) \leq T_x b \leq \pi.$$

Clearly,  $T_1$  has significance as a transmission coefficient only in the scan range  $2\pi(1 - b/\lambda) \leq T_x b \leq \pi$ .

The graph of  $|T_0|$  shows a sharp dip at the scan angle of  $T_x = 70^\circ$ , at which the reflection coefficient attains its peak value of one. Notice that the phase of  $T_0$  exhibits a discontinuity of  $180^\circ$  at this scan angle. This is so because both the real and imaginary parts of  $T_0$  go through zero and then change sign as the beam is scanned past this scan angle. This appears to indicate that  $|T_0|$  does go to zero rather than approach zero, or equivalently, that  $|R|$  actually attains the value one. The significance of the difference between  $|R|$  approaching one and  $|R|$  actually attaining one lies in whether the match of an array can be improved by network compensation. Moreover, there is an intimate connection between the fact that  $|R| = 1$  and the surface wave propagation along a plane corrugated structure. We discuss this in detail in Section IV).

Another point which might be of interest is that  $T_0$  is the radiation pattern in the angular range  $0 \leq \theta \leq \sin^{-1}(\lambda/2b)$ , when a single element is excited with the rest of the elements terminated in the characteristic impedances.<sup>9</sup> The radiation pattern for the remaining angular range  $\sin^{-1}(\lambda/2b) \leq \theta \leq \pi/2$  may be obtained from the curve of  $T_1$  in the scan range  $2\pi(1 - b/\lambda) \leq T_x b \leq \pi$ , reflected with respect to the  $T_x b = \pi$  axis.

### 3.3 E Plane Scan Results

The incident wave in the E plane scan is a TEM wave with the electric field polarized in the direction normal to the waveguide walls. Figs. 7 and 8 give the results for both the amplitudes and phases of the reflection coefficients as a function of scan. The set of parameters used for obtaining these results is:  $d/\lambda = 0.5714$ ,  $c/d = 0.85$ . The array is covered with a single layer of dielectric material flush with the array aperture. A dielectric constant of  $\epsilon = 3.0625$  is chosen for the same reason as for the H plane, namely to have one surface wavelike space harmonic present over as wide a scan angle as possible. Relatively thick waveguide walls are used in this case in order that the waveguides support only the dominant TEM mode, because the element spacing is larger than  $\lambda/2$ .

From the numerical data we may observe that, in the absence of a dielectric material, the reflection coefficient is relatively flat over a large range of scan angles, except in the vicinity of the grating lobe formation angle (in this case  $T_x d = 154^\circ$ ), at which we find a sharp

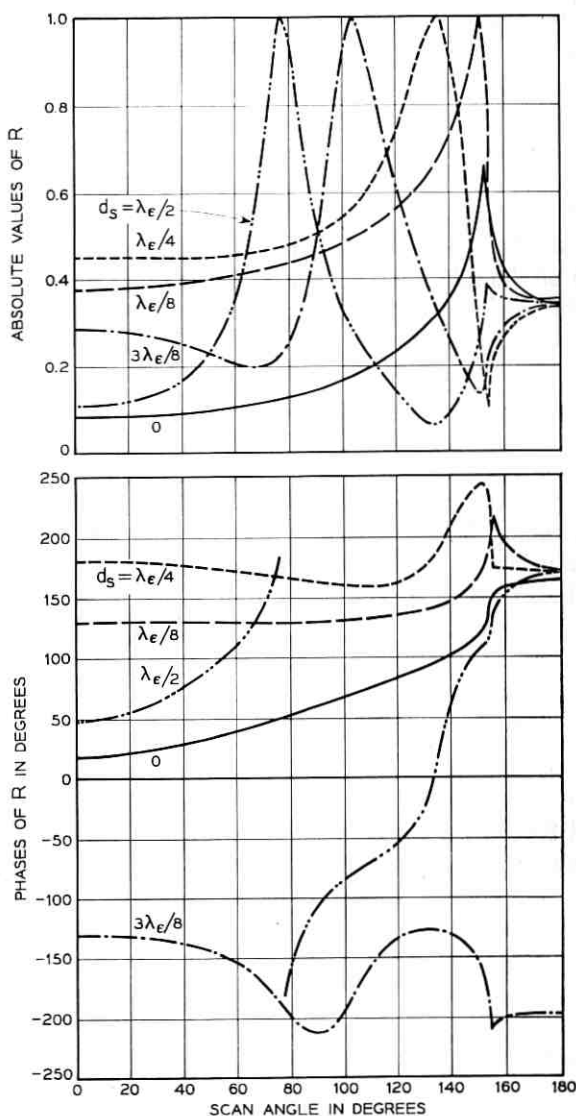


Fig. 7—Reflection coefficient  $R$  vs scan angle  $T_v d$  for E plane scan with  $d/\lambda = 0.5714$ ,  $c/d = 0.85$  and  $\epsilon = 3.0625$ .

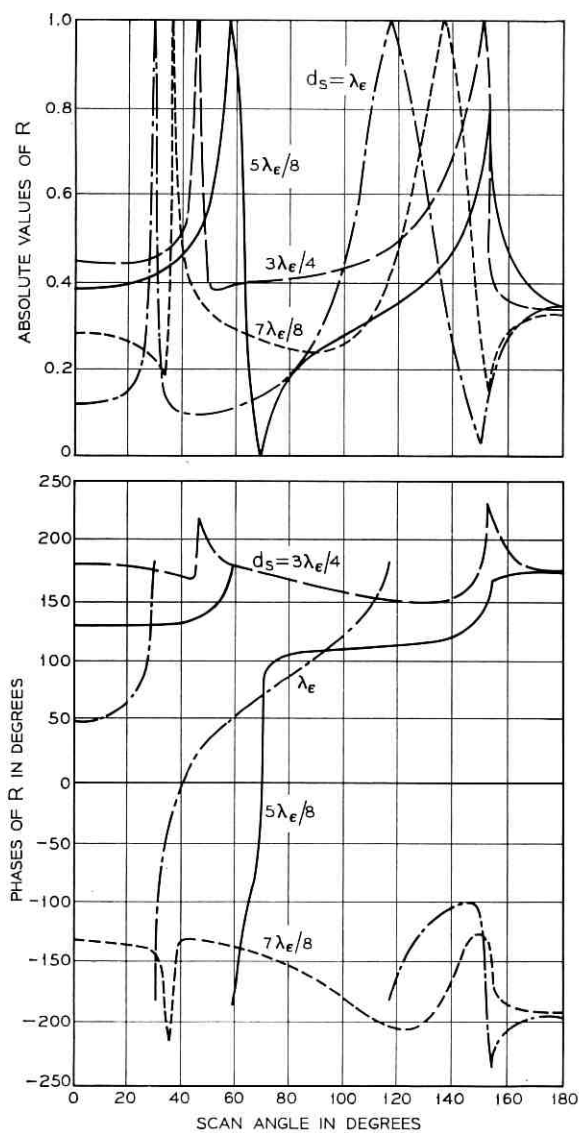


Fig. 8—Reflection coefficient  $R$  vs scan angle  $T, d$  for E plane scan with  $d/\lambda = 0.5714$ ,  $c/d = 0.85$  and  $\epsilon = 3.0625$ .

peak. This is in marked contrast with the H plane scan case (see Fig. 4). The peak value does not reach one, however. When a dielectric sheath of thickness  $\lambda_e/8$  is used to cover the array, the effect is to raise the level of reflection almost uniformly over all the scan angles. In particular, the peak which occurs at the grating lobe formation angle is seen to reach a value of unity. Although not presented here, the results for thinner dielectric sheaths show similar tendencies with the exception that the peak values are not necessarily unity. While the position for the appearance of the resonant peaks remains practically unchanged when the dielectric slab is relatively thin, it does start to shift toward the broadside direction as the thickness is increased beyond a critical value of about  $\lambda_e/4$ . A further thickening of the dielectric sheath eventually leads to the emergence of multiple resonant peaks.

### 3.4 Quasi-E Plane Scan Results

A quasi-E plane scan is a scan in which the fields have a sinusoidal variation in the direction perpendicular to the plane of scanning.<sup>4</sup> The reason for considering such a scan condition is that it enables us to simplify a vector three dimensional problem for a planar array to a scalar two dimensional one.

The  $z$ -directed propagation constants of the exterior modes for this case are given by

$$\beta_m = \sqrt{k^2 \epsilon - \left(\frac{\pi}{b}\right)^2 - \left(\frac{2m\pi}{d} + T_v\right)^2}.$$

From this expression, it is easy to show that when  $m < d\sqrt{\epsilon - (\lambda/2b)^2}/\lambda < (m + 1/2)$ , there will be  $(2m + 1)$  modes propagating for

$$0 \leq T_v d \leq 2\pi[d\sqrt{\epsilon - (\lambda/2b)^2}/\lambda - m]$$

and  $2m$  modes for

$$2\pi[d\sqrt{\epsilon - (\lambda/2b)^2}/\lambda - m] \leq T_v d \leq \pi.$$

If  $(m + 1/2) < d\sqrt{\epsilon - (\lambda/2b)^2}/\lambda < (m + 1)$ , on the other hand, the number of propagating modes will increase from  $(2m + 1)$  to  $(2m + 2)$  as the scan angle is steered through the angle of transition  $T_v d = 2\pi[m + 1 - d\sqrt{\epsilon - (\lambda/2b)^2}/\lambda]$ .

With the parameters of the array chosen to be  $a/\lambda = b/\lambda = 0.5714$ ,  $c/d = 0.937$ , the array radiates one beam in  $0 \leq T_v d \leq T_{v,c} d = (2\pi d/\lambda) \cdot [1 - (\lambda/2a)^2]^{1/2}$ , and no beam in  $T_{v,c} d \leq T_v d \leq \pi$ . Fig. 9 shows some

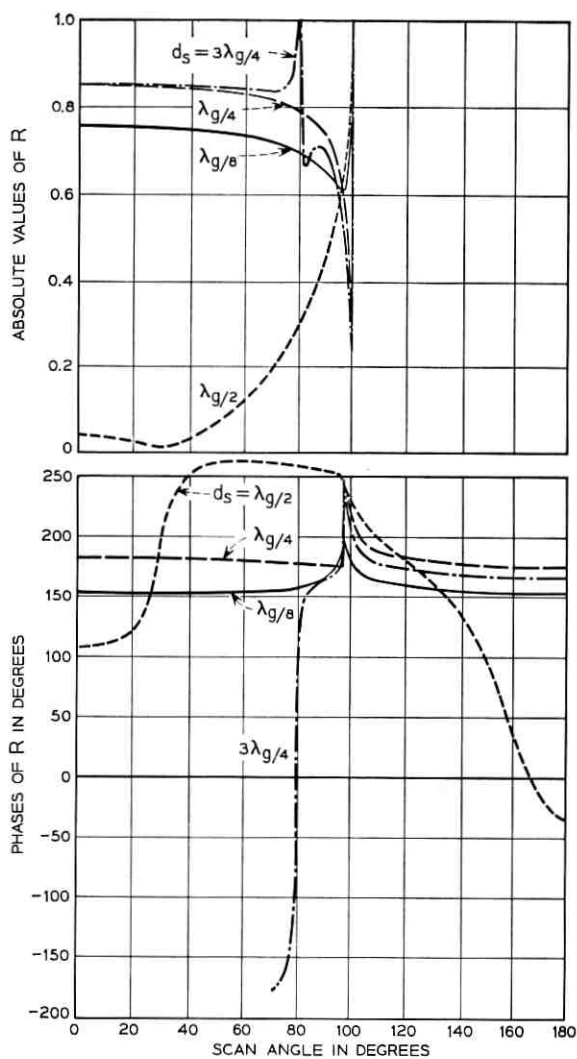


Fig. 9— Reflection coefficient  $R$  vs scan angle  $T_v d$  for quasi-E plane scan with  $b/\lambda = d/\lambda = 0.5714$ ,  $c/d = 0.937$ ,  $\epsilon = 3.825$ .

results of the reflection coefficient for this array when it is covered by a dielectric sheath with dielectric constant 3.835. The choice of this relatively large value of dielectric constant is again dictated by the interest in making as large a range of scan angle as possible for a mode in the region outside the waveguides to have surface wavelike behavior.

From the results for both the  $H$  plane and  $E$  plane scans as we already discussed, it might be anticipated that a resonant peak would be encountered with a relatively thin dielectric slab. The actual calculation, however, shows that this is not so. In fact, the reflection coefficient starts to show sharp peaks only when the slab thickness exceeds  $3\lambda_e/4$ , where

$$\lambda_e = \lambda_e / \sqrt{1 - (\lambda_e/2b)^2}.$$

Moreover, even when a resonant peak is present, the reflection coefficient as a function of scan is usually quite flat except near the scan angle at which the resonant peak appears.

### 3.5 *Effects of the Size of the Radiating Aperture*

So far, we have presented results for the situation where the element spacing and the dielectric constant were kept constant while the thickness of the dielectric sheath was varied. We studied the effects of the sheath thickness on the location of the resonant peak in some detail under these conditions.

Now let us look at some data showing the effect of the waveguide wall thickness. Fig. 10 shows both the amplitude and phase of the reflection coefficient as functions of the scan angle for an array which is scanned in the  $E$  plane and is covered by a single dielectric sheath. We obtained the results with fixed values for the element spacing  $b/\lambda = 0.5714$ , a dielectric constant of the sheath  $\epsilon = 3.0625$ , and its thickness  $d_s = 0.5 \lambda_e$ . However, the waveguide wall thickness (or equivalently, the size of the radiating aperture) is varied over a wide range. It is evident from the graphs in Fig. 10 that the size of the radiating aperture has substantial effects on the reflection coefficient. The scan angle for the appearance of the resonant peak is shifted toward the broadside direction as the aperture decreases. Similar shift in the scan angle for the resonant peak has also been observed in the case of the  $H$  plane scan. Moreover, loading the waveguides with a dielectric material also causes similar effects. It is apparent that the resonance phenomenon is strongly dependent on the aperture impedance which is a function of the array parameters.

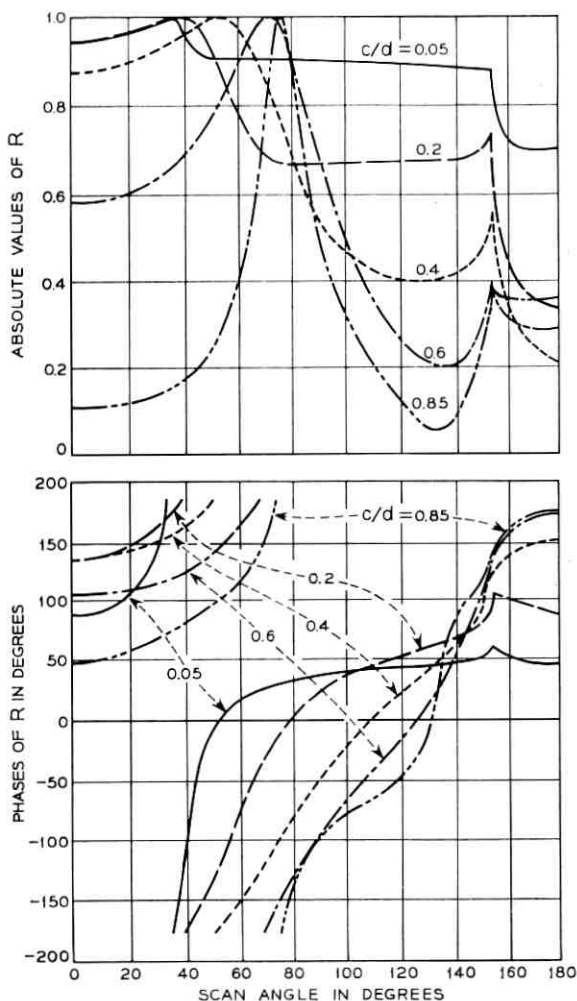


Fig. 10—Effects of radiating aperture size (E plane scan,  $d/\lambda = 0.5714$ ,  $\epsilon = 3.0625$ ,  $d_s = 0.5\lambda_c$ ).

### 3.6 Thin Sheath Results

The results presented earlier indicate that when a dielectric slab thicker than  $\lambda_\epsilon/4$  is used to cover an array, an important effect is manifested by the appearance of sharp resonant peaks in the reflection coefficient. Such resonances may be avoided if thin dielectric

sheaths are used. A thin dielectric sheath covered array for H plane scanning has these dimensions:  $a/\lambda = b/\lambda = 0.5714$ , and the dielectric slab has a fixed thickness  $d_s = \lambda/16$ . We obtained the results for dielectric constants ranging from 1.25 to 3. As the graphs in Fig. 11 show, even though it does not cause "resonance," a thin dielectric slab does have a considerable effect on the array match characteristics. This is true even when the dielectric constant is close to one. In fact, in the example shown here for  $\epsilon = 1.25$ , the reflection coefficient seems to have a larger variation than that of an uncovered array. However, by varying the dielectric constant, and perhaps also the thickness of the slab (as long as the slab is thin), it is possible to obtain a suitable combination of these two parameters and thus achieve a flat response in both amplitude and phase of the reflection coefficient at a single frequency. Such a possibility has been demonstrated previously.<sup>1</sup> The significance of this possibility is that a thin dielectric slab may be used as an effective means for the wide angle match of an array over a narrow frequency band.

#### IV. DISCUSSIONS AND CONCLUSIONS

We have shown the effects of a dielectric slab on the radiation characteristics of a phased array. One outstanding feature of the substantial changes which the dielectric slab brings to array performance is the appearance of resonance peaks in the reflection coefficient of the array at certain scan angles. This phenomenon is caused by surface-wavelike space harmonics at the interface between the dielectric and free space.

When the fields in the free space region are expanded into a generalized Fourier series according to the Floquet theorem, each space harmonic may be viewed as homogeneous or inhomogeneous plane waves, depending on whether it is propagating or evanescent. In the absence of a secondary boundary at  $z = d_s$  introduced by the dielectric slab, the plane waves generated at the array aperture either propagate away from it if they are homogeneous, or decay away if inhomogeneous.

When an air-dielectric interface is introduced at  $z = d_s$ , it causes each space harmonic generated at the aperture to be reflected and refracted upon encountering the interface as it travels away from the aperture. Naturally, only wave modes of the propagating type are significantly affected, because those of the evanescent type are usually rapidly attenuated away from the aperture. Furthermore,

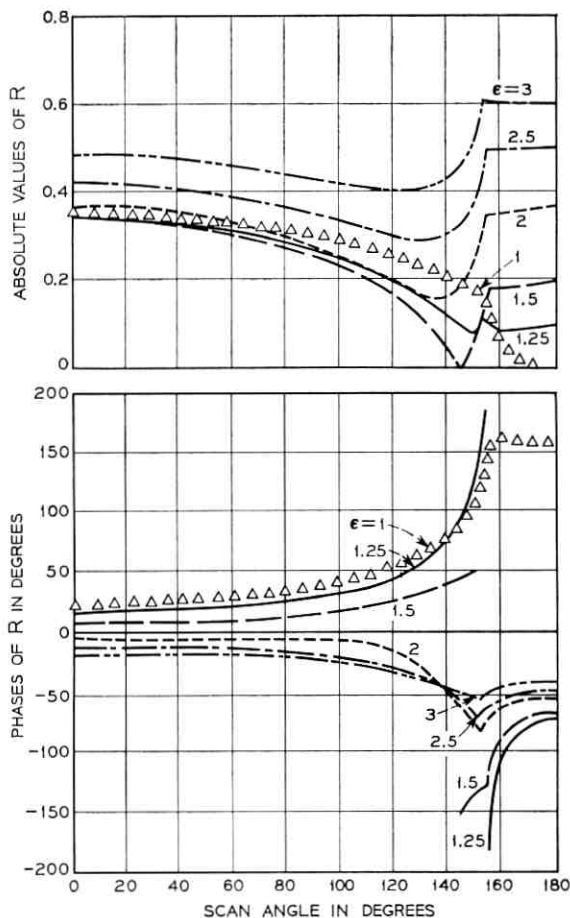


Fig. 11— Reflection coefficient  $R$  vs scan angle  $T_s b$  for an array covered with a thin dielectric slab (H plane scan,  $a/\lambda = b/\lambda = 0.5714$ ,  $d_s = \lambda/16$ ).

modes which exhibit a surface-wavelike field distribution suffer total reflection at the interface. The energy reflected from the interface is returned to the aperture as a wave incident to the array from the exterior region, and is scattered there.

In the presence of a dielectric sheath, there usually exists a range of scan angles over which there are two or more propagating modes inside the dielectric while only one propagating mode is present in the free space region. Under such circumstances, the two propagating

modes inside the dielectric interact as they are multiply-scattered at the array aperture. The degree of interaction depends on the various array parameters as well as the scan angle. It is then possible that, given a suitable set of parameters, the multiple scatterings between the two interfaces might lead to a situation in which a large reflection is generated at certain scan angles. The numerical examples in Section III indicate that the reflections can be so high as to reach unity for all practical purposes. In fact, it has been inferred from the numerical results for the transmission coefficient that the reflection can indeed reach the value one exactly.

#### 4.1 Relation with a Corrugated Structure

The fact that the modulus of the reflection coefficient can attain exactly the value of unity assumes some special significance. For when this happens, inside the waveguides at a distance away from the array aperture such that all the evanescent modes are sufficiently attenuated, the incident and reflected waves combine to form a pure standing wave. This implies that the tangential electric and magnetic fields alternatively go through zero at one half guide wavelength intervals. Specifically, by writing  $R = e^{j\varphi}$ , the resultant tangential electric field under these conditions may be expressed as

$$\mathcal{E}_y(x, z) = -2jz_1 e^{i\varphi/2} \sin(\alpha_1 z - \varphi/2).$$

Hence, for  $z = -L_n$  such that  $(\alpha_1 L_n + \varphi/2) = n\pi$ , or equivalently  $L_n = (n\pi - \varphi/2)/\alpha_1$ , the tangential electric field vanishes. As a consequence, electric conductors may be introduced at these positions without disturbing the field distributions of the entire system. When this is done, however, the array is then transformed into a corrugated structure which is completely isolated from the source region. The solution for the aperture fields obtained under these situations may then be regarded as the solution of a surface wave which propagates along a corrugated structure.

There are two aspects of this conclusion which deserve further comments. A corrugated surface has long been known as a structure which is capable of supporting surface waves. The characteristics of such a system are that it supports only the TM type surface wave, relative to the direction of propagation, in the absence of a dielectric material and that the period of corrugation be less than a half free space wavelength in order for the wave to propagate. Moreover, there is some requirement in regard to the depth of the corrugation for the surface to be properly reactive.

The introduction of a dielectric sheath above the array aperture or corrugated surface produces two significant effects. One is to enable a surface wave to propagate in the TE mode, corresponding to the case of H plane scan, as well as in the TM mode. The other is that the surface wave propagation is possible even though the period of corrugation is larger than a half free-space wavelength. It is important to observe that when the corrugation period is larger than a half wavelength, the zero<sup>th</sup> space harmonic of the fields outside the corrugation is a propagating mode. Therefore, it is necessary for the modal coefficient of this mode to be identically zero in order for the fields to conform to that of a surface wave. The results presented in this calculation indicate that indeed this is the case.

#### 4.2 Determination of the Location of the Resonant Peak

The scan angles at which resonant peaks appear may be determined accurately by the transverse resonant method when the radiating aperture is small. This situation applies readily to the case of the E plan scan. In this method, the sum of impedances looking towards the positive and negative  $z$  directions at some reference plane is set equal to zero, thus yielding a characteristic equation. It is convenient to use the array aperture as the reference plane. When the radiation aperture is small in comparison to the size of a periodic cell, the "average" impedance looking toward the array side is almost zero. The impedance looking away from the aperture may be approximated by that of the lowest order mode, in this case the  $(-1)$ st space harmonics. The impedance of this mode is given by

$$Z'_{-1} = Z_{-1}^D \frac{Z_{-1}^0 - jZ_{-1}^D \tan \beta_{-1}d_s}{Z_{-1}^D - jZ_{-1}^0 \tan \beta_{-1}d_s}.$$

By setting this expression to zero and using the appropriate modal impedances, we find

$$\epsilon\gamma_{-1} = j\beta_{-1} \tan \beta_{-1}d_s .$$

When this equation is used to determine the scan angle for the appearance of the resonant peak, it is found that excellent agreement with actual calculation is obtainable for aperture size up to 10 percent of the size of the periodic cell. For larger aperture sizes, the agreement gradually becomes poorer. This is because the impedance looking toward the waveguide side no longer remains negligibly small. It appears at this time that an accurate determination of the scan angle for resonant peaks under such conditions is best carried out by

solving the boundary value problem directly. Fortunately, this is a relatively easy task nowadays with the help of high speed electronic computers.

#### 4.3 Array Match

The numerical results obtained so far have revealed that the occurrence of sharp resonant peaks is associated with rather thick dielectric sheaths, and such resonance may be avoided by using thin sheaths. Thus, dielectric covering of an array is still a useful tool for the protection of the array from its environment. More importantly, the scan (or incident angle) dependent reflectivity of dielectric slabs may be utilized to advantage in improving the match performance of an array. The feasibility of this desirable feature has been demonstrated by extensive data presented herein and in [1]. It has also been suggested by other workers.<sup>8, 10</sup> Although, based on the calculated results, the improvement in array match by a thin dielectric sheath is obtainable at the expense of a higher frequency sensitivity, it seems possible to achieve a broadband compensation by using multiple thin sheaths. Further work is being carried out along this line, and the results will be reported at a later date.

#### REFERENCES

1. Galindo, V. and Wu, C. P., Dielectric Loaded and Covered Rectangular Waveguide Phased Arrays, presented at International Symposium on Antennas and Propagation, Palo Alto, California, December 1966.
2. Galindo, V. and Wu, C. P., Numerical Solutions for an Infinite Phased Array of Rectangular Waveguides with Thick Walls, IEEE Trans. Antennas and Propagation, AP-14, March 1966, pp. 149-158.
3. See, for example, J. R. Wait, *Electromagnetic Waves in Stratified Media*, The Macmillan Co., New York, 1962, Chapter 2.
4. Wu, C. P. and Galindo, V., Properties of a Phased Array of Rectangular Waveguides with Thin Walls, IEEE Trans. Antennas and Propagation, AP-14, March 1966, pp. 163-172.
5. Hildebrand, F. B., *Methods of Applied Mathematics*, Prentice-Hall, Inc., New York, 1954, pp. 451-452.
6. Kantorovitch, L. V. and Krylov, V. I., *Approximate Methods of Higher Analysis*, Interscience Publishers, New York, 1958.
7. *Waveguide Handbook*, N. Marcuvitz, ed., Radiation Laboratory, Series 10, McGraw-Hill Book Co., New York, 1950.
8. Lee, S. W., Impedance Matching of an Infinite Phased Array by Dielectric Sheets, Electronics Letters, 2, October 1966, pp. 366-368.
9. Galindo, V. and Wu, C. P., The Relation Between the Far-Zone Pattern of the Singly Excited Element and the Transmission Coefficient of the Principal Lobe in an Infinite Array, IEEE Trans. Antennas and Propagation, AP-14, May 1966, pp. 397-398.
10. Magill, E. G. and Wheeler, H. A., Wide Angle Impedance Matching of a Planar Array Antenna by a Dielectric Sheet, IEEE Trans. Antennas and Propagation, AP-14, January 1966, pp. 49-53.
11. Collin, R. E., *Field Theory of Guided Waves*, McGraw-Hill Book Co., New York, 1960, Chapter 8.

# Sequence-State Coding for Digital Transmission

By P. A. FRANASZEK

(Manuscript received May 9, 1967)

*A systematic approach to the analysis and construction of channel codes for digital baseband transmission is presented. The structure of the codes is dominated by the set of requirements imposed by channel characteristics and system operation. These requirements may be translated into symbol sequence properties which, in turn, specify a set of permissible sequence states. State-dependent coding of both fixed and variable length is a direct result. Properties of such codes are discussed and two examples are presented.*

## I. INTRODUCTION

### 1.1 General

Binary information to be transmitted over a baseband digital system must typically be encoded into a sequence of symbols suitable for transmission through the channel. The structure of such codes is dominated by the set of requirements imposed by considerations such as channel characteristics and system operation. Several codes designed for baseband transmission have been discussed in the literature,<sup>1, 2, 3</sup> but the analysis of such coding has received little attention. This paper presents a systematic approach to the description and construction of codes for such application. The symbol sequence to be generated by the code is viewed as the output of a sequential machine with a set of permissible states derived from the imposed requirements. State-dependent codes, both of fixed and of variable length, are a direct result. Various properties of such codes are discussed, and two examples are presented.

An advantage of using a sequence-state point of view is the ease with which it may be adapted to computer analyses, which are feasible due to the typically short word length of such codes (usually less

than eight symbols), and useful because normal design procedure often entails the construction of a number of codes, derived from different sequence requirements, in order to compare properties.

### 1.2 System Requirements

A block diagram of a baseband digital transmission system is shown in Fig. 1. Binary signals are encoded into a sequence of pulses (symbols) which are transmitted over a channel with regularly spaced re-constructive repeaters.<sup>4</sup> Typically, a number of factors strongly influence the choice of a channel code. Examples are:

(i) The symbol sequence is often required to furnish timing information to the repeaters.

(ii) The channel may impose restrictions on the spectral shape of the sequence. Most such systems, for example, have a transmission null at dc. This implies that long strings of symbols of one polarity cannot be tolerated.

(iii) Provisions for monitoring the channel error rate during normal operation may be necessary.

(iv) Pulse sequence requirements must be satisfied independently of the source statistics.

Requirements such as the above may usually be translated into limitations on the length of strings of like symbols, specifications of sets of allowable transitions between symbols (such as when a + 2 pulse must be followed by a - 2 pulse to avoid timing jitter due to asymmetries), and bounds on the variation of the running digital sum. The latter is defined as

$$\xi(T) = \sum_{t=T_0}^T a_t ,$$

where  $\{a_t\}$  are the weights assigned to the channel symbols and  $T_0$  is an arbitrary but fixed time.

The objective of the code designer is to specify a code which meets the imposed conditions while obtaining maximum information capacity (average number of bits per channel symbol) or alternatively to optimize sequence properties.

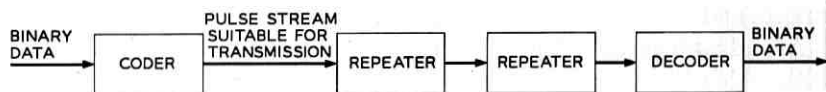


Fig. 1 — Block diagram of a baseband digital transmission system.

### 1.3 Permissible Sequences

A code may be defined as a mapping from the binary input information to the ensemble of symbol sequences which satisfy the imposed criteria. The allowable symbol sequences can, in turn, be specified by a set of permissible states  $\{s_i\}$  for each point, describing such quantities as the present value of the running digital sum, the preceding number of symbols of a given type, etc. In addition to the  $\{s_i\}$ , it is convenient to define a set of allowable words  $\{w_j\}$ , which take the sequence through a succession of allowable states, one for each symbol in the word. A necessary condition for  $w_j$  to be permissible is that there exists at least one state  $s_r$  such that the states resulting from the use of  $w_j$  at  $s_r$  are all allowable. In addition, the words to be used in the code may be restricted to a subset of  $\{w_j\}$  which satisfies requirements not specified by a particular choice of states, such as various error-correcting properties. The latter restriction will not be treated in this paper.

It is assumed in this paper that each code word carries an integral number of information bits, and that the ratio of bits per symbol remains constant over each word. The latter assumption is a sufficient condition for synchronous transmission.

## II. FIXED LENGTH CODE STRUCTURE

### 2.1 General

The simplest codes of the above type are those of fixed length, which may be defined as mappings from the set of input binary words of length  $\log_2 L$  to the set of allowable words  $\{w_j\}$  of length  $N$ . These mappings are generally state-dependent. That is, the choice of a code word may be a function of the state occupied by the sequence.

It is convenient to introduce a number of definitions.

*Definition:*  $W(s_i)$  is the set of words (alphabet) of length  $N$  which take the symbol sequence from state  $s_i$  through a succession of allowable states.

The fact that each word  $w_j$  must carry  $\alpha = \log_2 L$  information bits implies that words used in a code must terminate in states for which  $W(s)$  contains a minimum of  $2^\alpha$  words.

*Definition:* The principal states  $\{S_m\}$  of the channel sequence are those states for which  $W\{S_m\}$  contains at least  $2^\alpha$  words each of which takes the sequence to another principal state.

The existence of a set of principal states is a necessary and suf-

ficient condition for the existence of a code. It is possible to implement computer search routines for finding such states. The appendix contains a description of a search method which was used as an aid on constructing the two codes in Section 5.2.

A given code actually occupies a subset  $\{\sigma_n\}$  of the principal states at the end of code words. Let  $W^*(\sigma_n) \subset W(\sigma_n)$  be the words actually used for coding when the sequence occupies the state  $\sigma_n$ .

*Definition:*  $\sigma_n$  and  $\sigma_k$  are in the same *alphabet class*  $R_q$  if and only if  $W^*(\sigma_n) = W^*(\sigma_k)$ .

The above relation partitions the set of terminal states into alphabet classes  $R_q$ ,  $q = 1, 2, \dots, Q$ . A set of words  $W^*(R_q)$  is associated with each such class. Each  $W^*(R_q)$  contain  $2^a$  words which are used when the sequence occupies one of the terminal states in the class  $R_q$  (i.e., each word in  $W^*(R_q)$ ,  $q = 1, 2, \dots, Q$  is associated with one binary input word  $b_e$ ). It is advantageous to minimize the number of alphabet classes in order to simplify the coding and decoding circuits.

The coder tracks the state of the symbol sequence, and at the end of each word, codes the next binary word  $b_e$  into a word chosen from the alphabet corresponding to the state occupied by the output sequence. For example, the Paired Selected Ternary<sup>1</sup> code book consists of two alphabets, which contain words of zero or positive weight and zero or negative weight, respectively. The coder switches to a different alphabet after use of a word with non-zero weight.

## 2.2 State-Independent Decoding

The class of codes defined in Section 2.1 may be uniquely decoded provided the state of the symbol sequence is known. Frequently, however, it is not feasible for the decoder to distinguish which member of a given subset of states the sequence occupies at the end of a code word. For example, the states may be functions of the instantaneous symbol sequence sum. Here a single error in detection may result in an unbounded string of decoding errors. In addition, implementation of state-dependent decoding requires circuits to track the sequence state. Thus, state-independent decoding may often be necessary.

Decoding independently of the state is possible if and only if one binary word  $b_e$  corresponds to each code word  $w_i \in \{w_i\}$ . That is, the state-dependent mapping of  $\{b_e\}$  into  $\{w_i\}$  must have a unique inverse. If decoding is to be independent of the state within a given subset of the terminal states, the above mapping must have a unique inverse within this subset.

Given a group of terminal states  $\{\sigma_q\}$ ,  $q = 1, 2, \dots, Q$ , and their associated alphabets  $W^*(\sigma_q)$  [each containing  $2^a$  words], it is desirable to determine whether it is possible to code so that decoding is independent of  $q$ . The following are necessary and sufficient conditions for the above:

*Condition 1: A sufficient, but not necessary, condition for the existence of an assignment of binary words to the members of  $W^*(\sigma_t)$   $q = 1, 2, \dots, Q$  so that decoding is independent of  $t$  is that for any integers  $u, v$  such that  $1 \leq u < v \leq Q$*

$$w_r \in W^*(\sigma_u) \cap W^*(\sigma_v) \rightarrow w_r \in W^*(\sigma_{u+v}).$$

*Proof:* Suppose that a binary word  $b_r$  has been assigned to  $w_r$  in the alphabet  $W^*(\sigma_u)$ . Then it is possible to give  $w_r$  the same binary assignment in  $W^*(\sigma_{u+1}) \dots W^*(\sigma_v)$ . The lack of necessity of the above condition may be demonstrated by a renumbering of the alphabets.

*Condition 2: A necessary and sufficient condition for the possibility of assigning binary words to the members of  $W^*(\sigma_\theta)$ ,  $\theta = 1, 2, \dots, \Theta$  so that decoding is independent of  $\theta$  is that for  $1 \leq u \leq v \leq x \leq \Theta$  and for each*

$$w_r \in W^*(\sigma_u) \cap W^*(\sigma_x)$$

*such that*

$$w_r \notin W^*(\sigma_v)$$

*there exists a  $w_p \in W^*(\sigma_v)$  such that there exists no  $\sigma_m$ ,  $1 \leq m \leq \Theta$ , for which  $w_r, w_p \in W^*(\sigma_m)$ .*

*Proof:* Sufficiency follows from condition 1 by requiring that  $w_p$  and  $w_r$  be equivalent (in the sense that they are assigned the same binary word).

The necessity of the condition follows from the fact that if

$$w_r \notin W^*(\sigma_v)$$

then some other word  $w_p \in W^*(\sigma_v)$  must be assigned the binary word assigned to  $w_r$  in the  $u$ th alphabet. But if  $w_p, w_r \in W^*(\sigma_m)$ ,  $1 \leq m \leq T$ , state-independent decoding is precluded.

It is obvious from the above conditions that state-independent decoding is always possible when there are only two alphabets (as in Paired Selected Ternary<sup>1</sup>). An example of a group of alphabets which do not admit state-independent decoding is shown in Table I.

### 2.3 Framing

The received symbol sequence must be correctly partitioned into blocks of words length  $N$  before decoding. This may be done by ob-

serving whether the received words coincide with the words utilized in a code, by tracking the sequence state to determine whether ends of the received words coincide with sequence terminal states, or by looking for the presence of nonallowable sequences of permissible words.

### III. VARIABLE LENGTH CODES

#### 3.1 General

Attempts to increase fixed length state-dependent code efficiency with constraints on pulse sequence properties result in increased word length, and thus in rapidly mounting coder and decoder complexity, reframe times and sensitivity to detection errors. Hence, variable length codes, which may combine the advantages of short and long word lengths, are frequently advantageous.

Consider a sequence of symbols generated by a fixed length code of word length  $N$ . The sequence by definition occupies a principal state at the end of each word. Often, however, a principal state will be entered in the middle of a word. This offers the possibility of using the word fragment to convey information, and of starting any of at least  $2^a$  words from this point (by definition of a principal state). The result, subject to a number of restrictions outlined below, is a variable length code.

Variable length codes offer the possibility of using short words more frequently than those of longer lengths. This often permits a marked decrease in coder and decoder complexity relative to a fixed length code of like efficiency and sequence properties, since the number of stored words may be far smaller. For example, VL43 (described below), a three alphabet variable length code, uses a total of 56 words,

TABLE I—A SET OF ALPHABETS WHICH DO NOT ADMIT STATE-INDEPENDENT DECODING.

$W^{*}(\sigma_1)$	$W^{*}(\sigma_2)$	$W^{*}(\sigma_3)$	$W^{*}(\sigma_4)$
$w_1$	$w_1$		
$w_2$		$w_2$	
$w_3$			$w_3$
		$w_4$	$w_4$
$w_5$	$w_5$	$w_5$	$w_5$
	$w_6$	$w_6$	$w_6$
	$w_7$		

binary words:  $b_1, b_2, b_3, b_4$

compared to the 256 required for a single alphabet of a fixed length code of equal efficiency and sequence properties.

### 3.2 Variable Length Code Structure

The structure of variable length codes required to satisfy sets of sequence requirements is quite similar to that of fixed length codes. A number of special features, however, arise from the presence of words of different lengths.

The requirement of synchronous transmission, coupled with the assumption that each word carries an integer number of information bits, implies that the word lengths in a given code are integer multiples of a *basic word length*  $N$ , where  $N$  is the smallest integer for which the bit per symbol ratio  $\alpha/N$  is that of two integers (i.e., if the bit per symbol ratio is 1.5, the basic word length is 2). The proof of this statement follows from the fact that the word length  $K_i N$  must be such that the number of bits per word  $K_i \alpha$  is an integer [this paper covers the transmission of binary data]. Suppose that  $K_i = n + b$ , where  $n$  is an integer and  $0 < b < 1$ . Then  $b\alpha$  and  $bN$  must also be integers, which violates the definition of  $N$ .

The set of allowable words may be written as  $\{w_{ij}\}$ ,  $i = 1, 2, \dots, M$ , where  $w_{ij}$  is the  $j$ th word of length  $iN$ .

*Definition:*  $W_i(s_i)$  is the set of words of length  $iN$ ,  $i = 1, 2, \dots, M$ , which may be used in the permissible state  $s_i$  without violating the sequence requirements.

$$W(s_i) = \bigcup_{i=1}^M W_i(s_i).$$

A set of principal states may be defined for a symbol sequence associated with a variable length code in a manner analogous to that of Section II.

*Definition:* The principal states  $\{S_i\}$  are those allowable states for which  $W(S_i)$  contains sufficient words terminating in principal states to maintain an information rate of  $\alpha$  bits per  $N$  symbols.

The number of words of length  $iN$ ,  $i = 1, 2, \dots, M$  required to maintain a bit rate of  $\alpha$  bits per  $N$  symbols is given by

$$L_1[W(s_i)] + L_2[W(s_i)]2^{-\alpha} + \dots + L_M[W(s_i)]2^{-(M-1)\alpha} = 2^\alpha,$$

where  $L_i[W(s_i)]$  is the number of words in  $W_i(s_i)$ . Equation (1) clearly indicates the advantage of using as many short words as possible.

The terminal states  $\{\sigma_m\}$  are as defined in Section II. Similarly,  $W^*(\sigma_m)$  and  $W(\sigma_m)$  are those members of  $W_i(\sigma_m)$  and  $W(\sigma_m)$ , respectively, which are actually used in the code; two terminal states  $\sigma_m$  and  $\sigma_p$  are in the same alphabet class if and only if  $W^*(\sigma_m) = W^*(\sigma_p)$ .

It is clear that

$$w_{ji} \neq P_i(w_{kr})$$

for all  $w_{ji}, w_{kr} \in W^*(\sigma_s)$  and  $w_{ji} \neq w_{kr}$ .  $P_i(w_{kr})$  denotes the first  $iN$  symbols of the word  $w_{kr}$ . The above condition follows from the fact that  $w_{ji} \in W(S_s)$  implies that  $w_{ji}$ , when used in the state  $S_s$ , takes the sequence to another principal state.

### 3.3 State-Independent Decoding

State-independent decoding of a variable-length code is desirable for the same reasons as for one of fixed length. The criterion for such decoding is the same as for a fixed length code — the state-dependent mapping from the binary words  $\{b_e\}$  to the words to be transmitted in the channel must have a unique inverse. Two considerations which affect the complexity of this mapping are the presence of words of length  $iN$ ,  $i = 1, 2, \dots, M$  and the existence of words which consist of concatenations of two or more shorter words. Such word combinations will be called *concatenated* words. It follows from Section 3.2 that a concatenated word and its prefix cannot occupy the same alphabet. From Section 3.2, it can be concluded that a concatenated word of length  $iN$  is a legitimate word in a given alphabet if no terminal state is reached with the  $KN$ th symbol for  $0 < K < i$ . A requirement for state-independent decoding is that the binary words assigned to a concatenated word be concatenations of the binary words assigned to the words of which the concatenated word is composed. Section 5.2 contains an example of a variable-length code which satisfies these criteria.

### 3.4 Framing

The process of framing (at the decoder) a symbol sequence generated by a variable-length code may be divided into two parts: partitioning the sequence into blocks of length  $N$  (the basic word length), and properly grouping these blocks into words of length  $iN$ ,  $i = 1, 2, \dots, M$ . Framing may be performed in much the same manner as for a fixed-length code. A misframe condition may be detected by noting the presence of nonpermissible words, word sequences which

do not occur in the code, and/or the occupation of a nonterminal state at the end of a word.

It is often possible to substantially simplify the framing process by ensuring that secondary misframing (the condition that results from improper grouping of blocks of length  $N$  into words) is self-terminating. This restricts the need for framing to blocks of length  $N$  (the basic word length), and frequently results in superior framing performance compared to a fixed length code of equal efficiency and sequence properties.

Consider a state-independent decoder which stores all word prefixes of length  $iN$ ,  $i = 1, 2, \dots, M-1$ , and which operates in the following manner: If the first  $fN$  symbols that are received form a prefix of a legitimate word, the decoder considers the first  $(f+1)N$  symbols. Otherwise the first  $fN$  symbols are decoded into an arbitrary binary word of length  $f\alpha$ . The concatenated words are treated as strings of the shorter words of which they are composed.

A sufficient condition for secondary misframing to be self-terminating in the above decoder is that (excluding concatenated words)

$$E_r[w_{ki}] \neq P_r[w_{m\epsilon}]$$

for all  $r, k, i, m, \epsilon$  such that  $\epsilon > r$  and  $i > r$ .  $E_r[w_{ki}]$  denotes the last  $rN$  symbols of the word  $w_{ki}$ . This ensures that the secondary misframing condition terminates with the ending of the word  $w_{ki}$ .

#### IV. PERFORMANCE MONITORING

It is often necessary to monitor the level of channel performance without interrupting service. Codes with bounded sequence sums readily lend themselves to this objective, especially in the low noise environment typical of telephone communications systems. This is because an error is quite likely to eventually cause the sequence sum to exceed the imposed bounds. Alternatively, the behavior of the digital sequence at the bound can be observed. For example, not more than one consecutive zero (null pulse) might be permitted at extreme sequence sum values, while strings of length  $N > 1$  may occur at intermediate sums. Here, the detection of a string of zeros at an extreme sequence sum value indicates that an error has occurred in detection. An advantage of these methods<sup>1</sup> is that error monitoring can be performed without framing.

Standard methods of error monitoring (or error detection) can also be incorporated in a code of this form. A possibility is the require-

ment that the words have even digital sums, or more generally that the terminal states  $\{\sigma_j\}$  be separated by a minimum "distance."

#### V. CODE CONSTRUCTION

The foregoing sections have described a number of features of state-dependent codes. Steps in the construction of a code in this class are outlined below.

(i) Specification of the required channel symbol sequence properties.

(ii) Translation of the requirements into a set of acceptable states.

(iii) Search for the permissible words in each allowable state. Search for the principal states. The above can be done either by hand or by a computer search routine such as that described in the appendix.

(iv) Terminal states and code words are chosen for (if necessary) state-independent decoding, to optimize spectral properties, error monitoring and framing statistics. This usually requires much tedious computation.

It may occur that a given set of sequence requirements are such that a set of principal states does not exist for codes of word length  $N$ , but that a length of  $MN$  yields an acceptable code. In this case, a variable length code of basic word length  $N$  with maximum length  $MN$  might be a possibility. It is advantageous to use as many words of length  $N$  as possible, and to utilize the longer lengths to achieve a sufficient number of words in each terminal state.

#### VI. EXAMPLES

The following two ternary codes, one of fixed length and one of variable length, are examples of results of the above procedures. These codes were designed for possible use in a future high-speed baseband digital communication system.<sup>5</sup> The symbols to be transmitted on the line consist of positive, negative and null pulses. The main objectives in the design of these codes was to restrict the variations in the running digital sum of the pulse stream (with positive, negative, and null pulses assigned values of +1, -1, and 0 respectively) to avoid dc buildup in the channel, and to have as many transitions between symbols as possible in order to provide energy for self-timing in the repeaters.<sup>4</sup>

The information capacity of each code is four bits for every three symbols. The allowable states are described in terms of the running digital sum. Words were chosen from those permissible in each state so as to maximize the number of transitions between symbols. The search routine described in the appendix was used as an aid in code construction.

### 6.1 *A Fixed Length Selected Ternary Code*

The MS43 selected ternary code (Table II) is an example of a fixed length, three alphabet code of word length three. The digital sequence sum varies over six levels, which are arbitrarily labeled zero to five. These six levels are the allowable states. Terminal states occur only at values of one to four inclusive. There are three alphabet classes.  $R_1$  and  $R_3$  correspond to terminal states with sequence sums of one and four respectively, while  $R_2$  corresponds to a sum of either two or three. The choice of MS43 words is such that strings of zeros and symbols of like sign are limited to lengths of four and five respectively.

Coding is performed as a function of the terminal state. For example, if 00110100 is to be coded when the value of the sequence sum is +1, the first four bits are coded as 0-+ and the second as 0++. It can easily be seen from Table II that decoding is independent of the state.

### 6.2 *A Variable Length Selected Ternary Code*

The VL43 code [Table III] is an example of a three alphabet selected ternary code of variable length. The basic word length is three and the maximum length six. The bit per symbol ratio is 4/3, as in MS43. Secondary misframing is self-terminating and decoding is state-independent. The variable length feature permits a decrease in the variation of the running digital sum from six to five levels, and a significant increase in density of transitions. There are three terminal states ( $\sigma_1, \sigma_2, \sigma_3$ ) each with its own alphabet.  $W^*(\sigma_2)$  contains only words of length three.  $W^*(\sigma_1)$  and  $W^*(\sigma_3)$  each contain 16 words of length six (each carrying eight bits) and 15 words of length three. Both  $W^*(\sigma_1)$  and  $W^*(\sigma_3)$  contain concatenated words.

Coding is performed in much the same manner as for MS43. For example, if 110000010000 is to be coded when the state is  $\sigma_2$ , the first four bits are coded as --+, after which the state is  $\sigma_1$ . The next eight bits are coded into a six symbol word, -+-+--.

TABLE II—MS43 CODE BOOK

Binary Equivalent	$R_1$	$R_2$	$R_3$
0000	+++	-+-	-+-
0001	+ +0	00-	00-
0010	+0+	0-0	0-0
0100	0++	-00	-00
1000	+ - +	+ - +	- - -
0011	0 - +	0 - +	0 - +
0101	-0+	-0+	-0+
1001	00+	00+	- - 0
1010	0+0	0+0	-0-
1100	+00	+00	0 - -
0110	-+0	-+0	-+0
1110	+ - 0	+ - 0	+ - 0
1101	+0-	+0-	+0-
1011	0+-	0+-	0+-
0111	-++	-++	- - +
1111	++-	++-	+ - -

## VII. CONCLUSION

This paper has presented a description of a number of properties of multilevel coding for synchronous baseband transmission. The dominant feature of such coding is the set of pulse sequence requirements imposed by channel characteristics and system operation. It was shown that multialphabet and variable length codes are a natural consequence of attempting to attain high efficiency with codes of this type.

## VIII. ACKNOWLEDGMENTS

The author is indebted to Miss N. K. Shellenberger for programming support, and to J. M. Sipress for many valuable discussions.

## APPENDIX

*A Search Routine for the Principal States of a Ternary Sequence*

This appendix describes a search routine to find the principal states and associated code words from a given ensemble of ternary sequences. The codes are of fixed word length  $N$  and the symbol sequence is required to have the following properties:

(i) The maximum number of different levels which can be assumed by the running digital sum (with positive, zero and negative pulses assigned values of  $+1$ ,  $0$ , and  $-1$ , respectively) is  $2Q + 1$ .

(ii) The maximum number of consecutive zeros is  $R$ .

TABLE III—VL43 CODE BOOK

Binary Equivalent	Alphabet for Coder State		
	$W^*(\sigma_1)$	$W^*(\sigma_2)$	$W^*(\sigma_3)$
0000	+ - +	+ - +	- + -
0001		- + -	- 0 -
0010	0 + 0	0 + 0	- 0 -
0100	+ 0 0	+ - -	+ - -
1000	0 0 +	0 0 +	- - 0
0011	0 + -	0 + -	0 + -
0101	+ 0 -	+ 0 -	+ 0 -
1001	+ + 0	0 0 -	0 0 -
1010	+ 0 +	0 - 0	0 - 0
1100	0 + +	- - +	- - +
0110	+ - 0	+ - 0	+ - 0
1110	- + 0	- + 0	- + 0
1101	- 0 +	- 0 +	- 0 +
1011	0 - +	0 - +	0 - +
0111	+ + -	+ + -	0 - -
1111	- + +	- + +	- 0 0

Binary Equivalent	$W^*(\sigma_1)$ Alphabet	Binary Equivalent	$W^*(\sigma_3)$ Alphabet
00010000	- + - + - +	00000000	- - - + - +
00010001	+ + + - + -	00000001	+ + + - + -
00010010	- + - 0 + 0	00000010	+ - + - 0 -
00010100	- + - + 0 0	00000100	0 0 0 + - -
00011000	- + - 0 0 +	00001000	+ - + - - 0
00010011	+ + + - 0 -	00000011	- - - + 0 +
00010101	+ + + - - 0	00000101	- - - + + 0
00011001	- + - + + 0	00001001	+ - + 0 0 -
00011010	- + - + 0 +	00001010	+ - + 0 - 0
00011100	- + - 0 + +	00001100	+ - + - - +
00010110	0 0 0 + + -	00000110	0 0 0 + - 0
00011110	0 0 0 - + 0	00001110	0 0 0 - - +
00011101	+ + + - - +	00001101	- - - + + -
00011011	+ + + - 0 0	00001011	- - - + 0 0
00010111	- + - + + -	00000111	+ - + 0 - -
00011111	0 0 0 - + +	00001111	+ - + - 0 0

(iii) The maximum number of consecutive pulses of like sign is  $P \leq 2Q$ .

The first step is a search for the set  $\{w\}$  of words of length  $N$  which satisfy the above conditions.

Let  $w_i = a_1 a_2 \dots a_{N_i}$ , with  $a_i = -1, 0$  or  $+1$ . It is then required that

$$-Q \leq \sum_{i=1}^r a_{i,j} \leq +Q$$

for all  $r, \rho$  such that

$$1 \leq r \leq N$$

$$1 \leq \rho \leq r,$$

where  $N$  is the fixed word length. Moreover, if

$$a_{i,j} = a_{i+1,j} = \dots = a_{i+p-1,j} = \pm 1$$

then

$$a_{i+p,j} \neq a_{i,j}.$$

Also, if

$$a_{i,j} = a_{i+1,j} = a_{i+r-1,j} = 0$$

then

$$a_{i+r,j} \neq 0.$$

Next, a set of allowable states  $s(t,u,v)$  is defined, where  $t$  denotes the value of the running digital sum of the pulse sequence,  $u$  the preceding number of zeroes and  $v > 0$  ( $v < 0$ ) the number of preceding positive (negative) pulses. It is required that

$$-Q \leq t \leq Q, \quad 0 \leq u \leq R, \quad -P \leq v \leq P.$$

The words  $\{w\}$ , when used in a particular state  $s(t,u,v)$  take the sequence through  $N$  states. A word  $w_j$  is permissible in  $s(t,u,v)$  if and only if the  $N$  resulting states are allowable. Each word in  $\{w\}$  is tested to determine the states in which it is permissible. The result is that a set of words  $\{w\}_{t,u,v}$  is associated with each state  $s(t,u,v)$ .

When the above procedure is completed, the program searches for the principal states. States which contain less than  $2^a$  words are discarded. Then, for each remaining state  $s(t,u,v)$ , those words in  $\{w\}_{t,u,v}$  are eliminated which terminate in a state which has been discarded. If  $\{w\}_{t,u,v}$  contains fewer than  $2^a$  words after this operation,  $s(t,u,v)$  is eliminated. This procedure is continued until either no states remain or the routine runs through a complete cycle of states without eliminating any words or states. In the latter case, the remaining states are the principal states,  $\{\sigma_q\}$ , and the remaining words are  $\{W(\sigma_q)\}$ .

## REFERENCES

1. Sipress, J. M., A New Class of Selected Ternary Pulse Transmission Plans for Digital Transmission Lines, *IEEE Trans. Commun. Tech., COM-13*, No. 3, September, 1965, pp. 366-372.
2. Davis, C. G., An Experimental Pulse Code Modulation System for Short-Haul Trunks, *B.S.T.J.*, 41, January, 1962, pp. 1-24.
3. Aaron, M. R., PCM Transmission in the Exchange Plant, *B.S.T.J.*, 41, January, 1962, pp. 99-142.
4. Mayo, J. S., A Bipolar Repeater for Pulse Code Modulation Signals, *B.S.T.J.*, 41, January, 1962, pp. 25-97.
5. Dorros, I., Sipress, J. M., and Waldhauer, F. D., An Experimental 224 Mb/s Digital Repeated Line, *B.S.T.J.*, 45, No. 7, September, 1966.



## Contributors to this issue

PAUL T. BRADY, B.E.E., 1958, Rensselaer Polytechnic Institute; M.S.E.E., 1960, Massachusetts Institute of Technology; Ph.D., 1966, New York University; Bell Telephone Laboratories, 1961—. He has worked in statistical modeling of on-off speech patterns and of speech level distributions, and in studying two-way transmission of speech and data on circuits containing transmission delay.

P. A. FRANASZEK, Sc.B., 1962, Brown University; M.A., 1964, Ph.D., 1965, Princeton University. Bell Telephone Laboratories, 1965—. Mr. Franaszek has been concerned with the analysis of digital data transmission problems. Member, Sigma Xi, Tau Beta Pi, AAAS.

VICTOR GALINDO, B.S. (E.E.), 1954, New York University; M.S. (E.E.), 1962, and Ph.D. (E.E.), 1964, University of California, Berkeley; Hughes Aircraft Company, 1954-1957, 1958-1960; M.I.T. Lincoln Laboratory, 1957-1958; Bell Telephone Laboratories, 1964—. Mr. Galindo has been engaged in applying electromagnetic theory to studies of microwave transmission devices, antennas, and phased arrays. Member, Eta Kappa Nu, Tau Beta Pi, IEEE.

MARCO A. MURRAY-LASSO, M.S., E.E., 1962, and Sc.D., E.E., 1965, both from Massachusetts Institute of Technology; Bell Telephone Laboratories, 1965—. Dr. Murray-Lasso has done theoretical research in communication system components, computer studies involving predicting the behavior of directional couplers, and design work on control and data reduction systems. Member, IEEE, Sigma Xi, Association of University Professors of Mexico, and Association of Mechanical Electrical Engineers of Mexico.

LAWRENCE R. RABINER, S.B. and S.M., 1964, and Ph.D., in electrical engineering, 1967, all from the Massachusetts Institute of Technology. From 1962 through 1964 he participated in the cooperative plan in electrical engineering at Bell Telephone Laboratories, Whippany and Murray Hill, New Jersey. He worked on digital circuitry, military communications problems, and problems in binaural hearing. He joined the staff of Bell Laboratories in 1967 and has been engaged

in speech communications research. Member, Eta Kappa Nu, Sigma Xi, Tau Beta Pi, Acoustical Society of America, and IEEE.

HAN-CHIU WANG, B.S.E.E., 1955, Cheng-kung University, Taiwan, China; M.S.E.E., 1960, University of Notre Dame; Ph.D., 1965, Polytechnic Institute of Brooklyn; Chinese Government Radio Adm., 1956-1958; Polytechnic Institute of Brooklyn, 1964-1965; Bell Telephone Laboratories, 1965—. He is currently engaged in developing microwave components for radio relay systems.

C. P. WU, B.S., 1956, National Taiwan University; M.S., 1959, and Ph.D., 1962, Ohio State University; Bell Telephone Laboratories, 1962—. Mr. Wu was an assistant instructor at the National Taiwan University, 1956-57. He has done research in electromagnetic radiation in anisotropic media. His present work includes phased array antennas and electromagnetic scattering. Member, IEEE, Sigma Xi.